PHYSIOLOGICAL CONTROL OF AN IMPLANTABLE ROTARY BLOOD PUMP

MAHDI MANSOURI

THESIS SUBMITTED IN FULFILMENT OF THE REQUIREMENTS FOR THE DEGREE OF DOCTOR OF PHILOSOPHY

FACULTY OF ENGINEERING
UNIVERSITY OF MALAYA
KUALA LUMPUR

2016

UNIVERSITY OF MALAYA
ORIGINAL LITERARY WORK DECLARATION

Name of Candidate: Mahdi Mansouri

Matric No: KHA120148

Name of Degree: Doctor of Philosophy

Title of Thesis: Physiological control of an implantable rotary blood pump

Field of Study: Electrical Control Engineering-Rotary Blood Pumps

I do solemnly and sincerely declare that:

(1) I am the sole author/writer of this Work;
(2) This Work is original;
(3) Any use of any work in which copyright exists was done by way of fair dealing and for permitted purposes and any excerpt or extract from, or reference to or reproduction of any copyright work has been disclosed expressly and sufficiently and the title of the Work and its authorship have been acknowledged in this Work;
(4) I do not have any actual knowledge nor do I ought reasonably to know that the making of this work constitutes an infringement of any copyright work;
(5) I hereby assign all and every rights in the copyright to this Work to the University of Malaya ("UM"), who henceforth shall be owner of the copyright in this Work and that any reproduction or use in any form or by any means whatsoever is prohibited without the written consent of UM having been first had and obtained;
(6) I am fully aware that if in the course of making this Work I have infringed any copyright whether intentionally or otherwise, I may be subject to legal action or any other action as may be determined by UM.

Candidate's Signature Date: 16/03/2016

Subscribed and solemnly declared before,

Witness's Signature Date: 16/03/2016

Name:

Designation:

ABSTRACT

Left ventricular assist devices (LVADs) are mechanical pumps that their usage expanded from bridging to recovery to bridging to decision, and destination therapy. A physiologically responsive pump control strategy, which automatically adjusts variations in the metabolic demands, is tremendously needed to maximize the quality of the implant recipients' life. The aim of this dissertation is providing a robust physiological based controller, which could resist against all possible distortion during its working life.

At the first step, the performance of a number of previously proposed physiologically responsive controllers were comparably evaluated. The study proved applying a constant (static) controlling method could not provide the pump best controlling performance level, and indicates the demand of an adaptive (dynamic) controller, which will satisfy all physiological requisites. The results also suggested putting the focus on preload sensitivity of the ventricular myocardium. Such issue is an essential requirement for the Frank-Starling mechanism by which the left ventricular end-diastolic pressure (PLVED) controls the force of contraction of the left ventricle (LV) in proportion to the blood flow received from the right heart and pulmonary circulation.

At the next step a preload-based Starling-like controller for Implantable rotary blood pumps (IRBPs) using PLVED as the feedback variable was evaluated in a validated numerical model. The controller emulated the response of the natural LV to changes in PLVED. It was reported the performance of the preload-based Starling-like controller in comparison with recently designed pulsatility controller and constant speed operation. In handling the transition from a baseline state to test states, which included vigorous exercise, blood loss and a major reduction in the LV contractility (LVC), the preload controller outperformed pulsatility control and constant speed operation in all three test scenarios.

The study third objection was realizing preload-based using a controlling technique that reinforced the system to rapidly reach the target pump flow within eight heartbeats, else suction might occur. The technique must be also robust against noises contaminated the feedback signal. Accordingly, this study also attentively examined the transient and steady state response of two different preload-based control implementations in the numerical model. The implementations were tested under both ideal (noise free) and noisy conditions at baseline to vigorous exercise as well as blood loss transitions. Proportional-integral-derivative (PID) and sliding mode controller (SMC) were the chosen controlling techniques, selected due to their popularity and robustness reputation. While at the noise free condition system measured PLVED was directly fed to the controller, the author contaminated the feedback signal with different levels of Gaussian white noises to realize the noisy condition. The results showed no significant difference between the two preload-based control implementations under ideal condition during all testing scenarios. Proceeding the tests showed that both PID and SMC delivered almost comparable performance at signal to noise ratio (SNR) of 15dB, although by increasing the noise level to 7dB PID finally failed at blood loss scenario and severely penetrated in the suction, indicated by persistent negative PLVED. On the contrary, SMC is the control strategy that not only could tolerate all the noise levels and never fell into the suction region, but also could maintain a reasonable level of hemodynamic parameters deviations comparably.

The last objective of this study was to develop an in-vitro evaluation protocol for control system utilizing a mock circulation loop (MCL) exploiting the same scenarios used in the second objective. The test showed that the devised scenarios were useful for evaluation of preload-based control. Observing the results showed the preload controller could again outperform the constant speed operational in all three scenarios, provided the impetus for further animal trials.

ABSTRAK

Peranti pembantu ventrikel kiri (LVADs) merupakan pam mekanikal yang penggunaannya berkembang daripada merapatkan pemulihan kepada merapatkan keputusan,. Satu strategi kawalan pam responsif amat fisiologi, yang menyesuaikan perubahan sekara automatik permintaan metabolik, adalah diperlukan untuk memaksimumkan kualiti hidup penerima inplan. Tujuan kajian ini adalah menyediakan satu pengawal berasaskan fisiologi yang kukuh, yang dapat menahan terhadap semua penyelewengan yang mungkin berlaku sepanjang penggunaannya.

Sebagai langkah pertama, prestasi dalam beberapa pengawal fisiologi responsif yang dicadangkan sebelum ini telah dibanding nilai. Perbezaan dari segi prestasi jelas menunjukkan bahawa pelaksanaan pengawalan kaedah tetap (statik) tidak dapat memberi tahap prestasi pengawalan yang terbaik kepada pam dan menunjukkan kepentingan pengawal adaptif (dinamik) amat diperlukan untuk memenuhi segala syarat fisiologi. Juga daripada keputusan yang dikumpulkan, sensitiviti prabeban terhadap miokardium ventrikle haruslah diberikan tumpuan utama. Hal ini berkenaan dengan mekanisme Frank-Starling yang menyatakan daya pengecutan ventrikle kiri (LV) adalah bergatungan kepada tekanan ventrikle kiri akhir *diastolic* (PLVED) supaya keseimbangan aliran darah antara sistem *pulmonary* dan sistem sistemic dapat dicapai.

Pada langkah seterusnya pengawal Starling berasaskan perabeban-untuk pam darah berputar implan (IRBPs) menggunakan PLVED sebagai pembolehubah maklum balas yang telah dinilai dalam model pengiraan yang disahkan. Pengawal ini mencontahi tindakbalas LV semula jadi kepada perubahan dalam PLVED. Dilaporkan prestasi pengawal Starling seperti berasaskan prabeban-berbanding dengan pengawal pulsatility direka baru-baru ini dan operasi kelajuan tetap. Dalam mengendalikan peralihan dari keadaan asas untuk menguji keadaan, termasuk sukan berat, kehilangan darah dan

keutanaan pengurangan dalam contractility LV (LVC), pengawal prabeban yang mengatasi kawalan pulsatility dan operasi kelajuan tetap dalam ketiga-tiga senario ujian.

Kajian bantahan ketiga menggunakan teknik kawalan yang mengukuhkan sistem untuk mencapai aliran pam sasaran lagi dengan pesat dalam tempoh lapan degupan jantung, kalau sedutan tidak mungkin berlaku memeriksa dengan teliti. Teknik ini mesti juga teguh terhadap hingar yang mencemarkan isyarat maklum balas. Oleh itu, kajian ini juga memeriksa dengan teliti keadaan fana dan mantap dalam dua aplikasi kawalan berasaskan prabeban-berbeza dalam model berangka. Pelaksanaan yang telah diuji di bawah keadaan ideal (hingar bebas) dan keadaan bising pada garis dasar untuk latihal fisikan berat serta peralihan kehilangan darah. *Proportional-Integral-Derivative* (PID) dan *Sliding Mode Controller* (SMC) adalah teknik pengawalan yang dipilih, dipilih kerana kepopularan dan reputasi keteguhan. Manakala dalam sistem keadaan hingarbebas PLVED yang diukur telah disuapkan terus pengawal, pengarang mencemarkan isyarat maklum balas dengan hingar putih *Gauss* bertabah untuk merealisasikan keadaan bising. Keputusan kajian menunjukkan tiada perbezaan yang ketara antara kedua-dua implentasi kawalan berasaskan prabeban di bawah keadaan yang ideal semasa semua senario ujian.

Prosiding ujian menunjukkan bahawa kedua-dua PID dan SMC mencapai prestasi yang setanding dengan nisbah isyarat hingar (SNR) sebanyak 15dB, walaupun dengan meningkatkan tahap hingar kepada 7dB PID akhirnya gagal dengan senario kehilangan darah dan menembusi dalam sedutan, tertunjuk dengan PLVED negative yang berteruan. Sebaliknya, SMC adalah strategi kawalan yang bukan sahaja boleh bertolak ansur dengan semua peringkat bunyi dan tidak pernah jatuh ke rantau sedutan, tetapi juga boleh mengekalkan penyisihan parameter hemodinamik tahap yang padah munasabah.

Objektif terakhir kajian ini adalah untuk maeciptakan satu penilaian protokol in-vitro untuk sistem kawalan menggunakan gelung peredaran olok-olok (MCL) menggunakan

senario yang sama digunakan dalam objektif kedua. Keputusan tersebut tertakluk kepada prabeban dan afterload perubahan sama seperti yang diperhatikan dalam model berangka. Keputusan menunjukkan pengawal prabeban boleh mengatasi kelajuan malar operasi dalam semua tiga senario, dengan syarat dorongan untuk ujian haiwan selanjutnya.

ACKNOWLEDGEMENT

I would like to express my sincere gratitude to my beloved wife, Elham, for her continuous support. I appreciate all the motivation and enthusiasm she has given to me. I would not have accomplished this thesis without her help and encouragement.

I thank my supervisors, Dr. Lim Einly and Prof. Dr. Rini Akmeliawati, for their immense knowledge. I also thank my advisors, Prof. Robert F. Salamonsen and Dr. Shaun D. Gregory, for their kind support. Their guidance helped me throughout my research, and I could not have imagined having better advisors and mentors for my PhD study. I would like to thank Prof. Nigel H. Lovell for his encouragement and insightful comments.

I thank my fellow lab-mates in the Asian Cardiac Engineering Lab, Faculty of Engineering, University of Malaya, and Innovative Cardiovascular Engineering and Technology Lab, The Prince Charles Hospital, Brisbane, Queensland, Australia, for the stimulating discussions and all the fun we have had in the last three years.

TABLE OF CONTENTS

LIST OF FIGURES

LIST OF TABLES

LIST OF SYMBOLS AND ABBREVIATIONS

A(t)	Target value in mean absolute error
AO	Aorta
ARX	Autoregressive exogenous
at	After transition
AV	Aortic valve
bt	Before transition
CF	Continuous flow
C_{Ln}	Control line
C_{Lv} (mmHg/s)	LV end systolic elastance
CO (L/min)	Cardiac output
$\overline{CO}$ (L/min)	Mean cardiac output
CP	Cardiopulmonary
CV	Cardiovascular
CVP (mmHg)	Mean central venous pressure
CVS	Cardiovascular system
D	Diode
DSMC	Discrete sliding mode control

$\overline{dP}$ (mmHg)	Constant average pressure difference between the aorta and the left atrium
$\overline{dP_{pump}}$ (mmHg)	Constant average differential pump pressure
E (mmHg/mL)	Elastance
e[k]	The model noise components
$e_l(t)$	Time varying elastance function
EDPVR	End-diastolic pressure-volume relationship
E_i	Elastance in compartment i
E_{lv} (mmHg/mL)	Left ventricular elastance
$E_{max,lv}$ (mmHg/mL)	Left ventricular end systolic elastance
E_{rv} (mmHg/mL)	Right ventricular contractility
ESPVR	End-systolic pressure-volume relationship
FSLC	Frank-Starling-like control
GPI	Gradient of pulsatility index
H_{CVS} (mmHg)	Differential pressure between the left ventricle and the aorta
HF	Heart failure
HIP	Hydrostatic indifference point
H-Q	Pump differential pressure versus pump flow

HR (bmp)	Heart rate
HUT	Head-up tilt
IRBP	Implantable Rotary Blood Pump
I_s	Number of intervals over which the actual pump speed exceeds the suction speed
K	Preload-based equation scaling factor
K_{cl}	Tracking control state-feedback gain matrix
K_I	Integral gain
K_D	Derivative gain
K_P	Proportional gain
L ($Kg.m^{-4}$)	Inertance
LA	Left atrium
LAP (mmHg)	Left atrial pressure
L_{in} ($Kg.m^{-4}$)	Inlet cannula inertance
LL_x	Lower limit bound of variable x
L_{out} ($Kg.m^{-4}$)	Outlet cannula inertance
LTI	Linear time varying
LVP (mmHg)	Left ventricular pressure

LV	Left ventricle
LVAD	Left ventricle assist device
MAE	Mean absolute error
MAP (mmHg)	Mean arterial pressure
MCL	Mock circulation loop
NM	Numerical model
NSD	Normalized square deviation
$NSD_x(t)$	Normalized square deviation of variable of x(t)
P (mmHg)	Pressure
PA	Pulmonary peripheral vessels
PI (L/min)	pulsatility index
PID	Proportional-integral and derivative
PI_{QP} (L/min)	Pump flow pulsatility index
P_{la} (mmHg)	Left atrial pressure
$\overline{P_{la}}$ (mmHg)	Mean left atrial pressure
PLVED (mmHg)	Left ventricle end diastolic pressure
$\overline{PLVED}$ (mmHg)	Mean left ventricle end diastolic pressure
$\widehat{PLVED}$ (mmHg)	Estimated left ventricle end diastolic pressure

$PLVED_m$ (mmHg)	Mean left ventricle end diastolic pressure, used in in-vitro section
P_{pa} (mmHg)	Pulmonary arterial pressure
$\overline{P_{Pa}}$ (mmHg)	Mean pulmonary arterial pressure
P_S (L/min/mmHg)	Preload sensitivity
P_{sa} (mmHg)	Systemic arterial pressure
$\overline{P_{sa}}$ (mmHg)	Mean systemic arterial pressure
$P_{thor,1}$ (mmHg)	Intrathoracic pressure 1
$P_{thor,1}$ (mmHg)	Intrathoracic pressure 2
P_u (mmHg)	Pulmonary veins
P_V (mmHg)	Valve pressure
PWM (V)	Pulse width modulation
$\overline{PWM}$ (V)	Mean pulse width modulation
Q_{av} (L/min)	Aortic valve flow
$\overline{Q_{av}}$ (L/min)	Mena aortic valve flow
Q_i (L/min)	Blood flow in compartment i
Q_P (L/min)	Pump flow
$\overline{Q_P}$ (L/min)	Mean pump flow

$\widehat{\overline{Q_P}}$ (L/min)	Estimated averaged pump flow
$\overline{Q_{P_{Ref}}}$ (L/min)	Desired mean pump flow
Q_v (L/min)	Blood flow through the valve
R (mmHg.s/mL)	Resistance
RA	Right atrium
RAP (mmHg)	Right atrial pressure
$ratio_{PI}$	Constant ratio between mean pump flow and pump flow pulsatility
R_{in} (mmHg.s/mL)	Inlet cannula resistance
RMSHD	Root mean squared hemodynamic deviation
R_{out} (mmHg.s/mL)	Outlet cannula resistance
R_{suc} (mmHg.s/mL)	Suction resistance
RV	Right ventricle
S	Constant switching vector of sliding mode control
s[k]	Sliding mode control switching function
SA	Systemic peripheral vessels
S_l	Complex number frequency
SHD	Squared hemodynamic deviation

SMC	Sliding mode control
SNR (dB)	Signal-to-noise ratio
SV	Systemic veins
SVC	Systemic venous compliance
SVR (mmHg.s/mL)	Systemic vascular resistance
T (s)	Sampling period
T_d (s)	Simulation duration
u[k]	Sliding mode control output
u_{fi}[k]	Final controller output, fed to sliding mode control
UL_x	Upper limit value of variable x
u_{sf}[k]	State feed-back control output
VAD	Ventricular assist device
VC	Vena cava
V_i (mL)	Blood volume in compartment i
V_t (mL)	Total blood volume
WHO	World health organization
Y(t)	Actual value in mean absolute error
y_x	Actual value of variable x

$y_x(t)$	Actual value of variable x(t)
B	Desensitized reflex response
β_s	Sliding mode control disturbance bound
β_{HR}	Desensitized effector response (except heart rate)
Δt_i	The i^{th} interval over which the actual pump speed exceeds the suction speed
δA	System parameter variation
ϵ	Sliding mode control reaching velocity
η	Measure shows how deep, on average, the pump speed progresses into the suction region
ρ	Percentage of total simulation time during which suction occurs
τ	Sliding mode control converging exponential
τ_i (s)	Broreflex model time constants
ω (rpm)	Blood pump speed
$\bar{\omega}$ (rpm)	Mean blood pump speed
ω_s (rpm)	The speed at which suction occurs
$\overline{\omega_{SP}}$ (rpm)	Mean blood pump speed set-point

CHAPTER 1: INTRODUCTION

1.1 Research Motivation

The latest world health organization (WHO) report disclosed that heart failure (HF) is the leading cause of death in Malaysia, killing 22,700 people, or 22% of total deaths in 2011 only (World Health Organization, 2015). This disease affects a wide range of population, including the youngsters and the elderly. The severity of the disease ranges from mild to severe, which requires immediate surgery and transplantation in many instances. In addition, it also devours a huge portion of public health budget annually.

Left ventricular assist devices (LVADs) are mechanical pumps that now enjoy a clinically accepted role in supporting the failing heart in a number of scenarios, including destination therapy, bridge to recovery and bridge to transplantation. Implantable rotary blood pumps (IRBPs) are continuous flow ventricular assist devices (VADs) that have become increasingly popular due to the negligible blood trauma along with their light weight and small size, which facilitate their usage for in-home patient care (D. Timms, 2011). Currently, most commercially available IRBPs still function at a fixed speed predetermined by the physicians, which is insensitive to changes in the metabolic requirements of the patients and preload (the end diastolic volume that stretches the right or left ventricle of the heart to its greatest dimensions) (Salamonsen, Mason, & Ayre, 2011). Such insensitivity increases the risk of over-pumping, causing left ventricular (LV) suction, or under-pumping, which can cause pulmonary congestion, renal insufficiency and other problems (Salamonsen et al., 2013).

These deficiencies have driven the development of more than 30 different physiological control methods to match pump output to physiological requirements (A.-H. H. AlOmari et al., 2013). Despite the extensive efforts, none of these controllers have gained clinical acceptance in commercial devices due to their lack of confidence by clinicians

(Salamonsen et al., 2012). For example, Choi, Boston, and Antaki (2007) proposed a fuzzy logic controller that utilized the pulsatility ratio of the pump flow and (dp_{pump}) a control index. The controller regulated the pump speed regarding a reference pulsatility ratio under different operational states. The major limitation of Choi and any other controller that is based on pump pulsatility is a strong dependency established on the controller and pump operating point. Pump pulsatility (flow, current, pressure gradient, or speed) is a consequence of left ventricular (LV) contraction whereas LV preload is one of the determinants of LV contraction. With severe LV failure, as is the case for all LVAD recipients, the LV does not have the ability to induce major changes in pulsatility. Therefore, the dynamic range of the pulsatility index is small, and consequently its ability as a control input is limited. In the extreme case where LV contractility is zero, pulsatility control is not feasible

Preload sensitivity of the ventricular myocardium is an essential requirement for the Frank-Starling mechanism by which the left ventricular end-diastolic pressure (PLVED) controls the force of contraction of the left ventricle (LV) in proportion to the blood flow received from the right heart and pulmonary circulation. Therefore, it would seem logical that LV preload be selected as the feedback variable of choice in physiological control systems designed for IRBPs. However, this has not happened seemingly because developing a controller with fast response that can reach the pump flow set point within ten seconds (Salamonsen et al., 2012) is a real challenge in any physiological control system, considering a slow response may result in suction after hemorrhage or changes in posture. Additionally, one of the main concerns relating to preload control implementation regards measuring LV pressure. Currently available implantable pressure transducers are rendered virtually unusable due to a range of problems; particularly, the noise (disturbance) that generally affects the signal measured in ventricular pulsatility waveform (Lin, Lowe, & Al-Jumaily, 2014). Therefore, the purpose of this dissertation

is to propose a robust preload-based physiological controller that could adapt to the body requirement during various hemodynamic perturbations in the presence of external noise, and without falling into critical conditions such as suction or pulmonary congestion.

1.2 Objectives

The objectives of this dissertation are as follows:

i. The first objective of this dissertation is to evaluate the performance of a number of previous proposed physiologically responsive controllers based on constant set-point controlling methods using a validated numerical model. This includes constant speed, constant flow PI, constant average pressure difference between the aorta and the left atrium ($\overline{dP}$), constant average differential pump pressure ($\overline{dP_{pump}}$), constant ratio between mean pump flow and pump flow pulsatility ($ratio_{PI}$) or linear Starling-like control, and constant left atrial pressure (P_{la}) control.

ii. The second objective of this dissertation is to develop a preload-based Frank-Starling control method, which emulates the Frank-Starling mechanism of the native heart. The preload-based control regulates pump flow using left ventricular end diastolic pressure (PLVED) as the feedback signal. The performance of the proposed preload-based control was assessed in comparison with the constant speed operation and the pulsatility index control. The study was carried out using a sophisticated and experimentally validated computer model of the human circulation and the VentrAssist^{TM} LVAD.

iii. The third objective of this dissertation is to develop a sliding mode controller (SMC) to drive the preload-based control method through various hemodynamic transitions, and compared the transient and steady state performance of the SMC with a proportional-integral-derivative (PID) controller using the dynamic cardiovascular (CV) numerical model. The hypothesis is that the preload-based SMC is superior to the PID controller with regards to speed of response and robustness to noisy feedback signals.

iv. The final objective of this dissertation is to implement the preload-based controller in vitro using a mock circulatory loop (MCL) to characterize the flow sensitivity of the controllers to preload, and to compare its performance with the constant speed controller. Three different test scenarios were implemented, which include moderate exercise, 70^0 head-up-tilt (HUT), and a major reduction in LV contractility (LVC).

1.3 Thesis layout

This thesis is organized as follows. Following the introduction, the second chapter reviews the relevance of this study within the current literatures. Chapter 3 investigates the response of the IRBP-assisted patients to exercise and head-up tilt (HUT), as well as the effect of alterations in the model parameter values on this response, using validated numerical models. Furthermore, we comparatively evaluated the performance of a number of previously proposed physiologically responsive controllers with regard to their ability to increase cardiac output during exercise while maintaining circulatory stability upon head up tilt (HUT). Chapter 4 outlines the functionality and performance of the preload-based Frank-Starling controller using a validated numerical model. All tests showed that the preload-based controller outperformed previously designed Starling-like controller based on pulsatility and constant speed operation. Chapter 5 discusses a sliding mode implementation of the preload-based control that could warrants a fast response and

robustness of the controller in the presence of noisy feedback signal. In chapter 6, the performance of the preload-based control and fixed speed mode undergoing various physiological changes was compared in vitro using a MCL. The preload flow sensitivity of these controllers was also investigated. Finally, Chapter 7 concludes the present dissertation with suggestions for future work.

CHAPTER 2: LITERATURE REVIEW

2.1 Introduction

The successful implementation of a physiological LVAD control system requires sufficient knowledge of the CV system (CVS), and therefore this chapter delivers the reader essential information to understanding the topic. It includes a brief but concrete description of the physiology and anatomy of the human heart and CVS, HF, its occurrence and coverage, and treatment of HF using LVADs.

2.2 The Human Circulatory System, Anatomy and Physiology

The CVS includes the heart, the blood, and the lymphatic vessels. A C Guyton and Hall (2005) explains that the heart is composed of the left and right sides (Figure 2.1). The left side undertakes the duty of delivering oxygenated blood to all tissues in the body through the systemic circulation. On the other hand, the right side carries deoxygenated blood to the lungs through the pulmonary circulation. Each side of the heart consists of an atrium and a ventricle that connects with a one-way valve. The ventricles produced most force required to push blood via the circulatory system. The atria, on the other hand, functions as a primer pump to help ventricular filling.

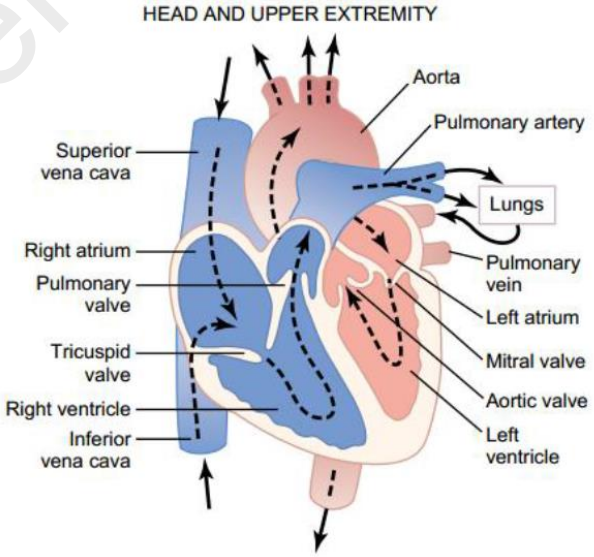

Figure 2.1: Anatomy of the human heart (A C Guyton & Hall, 2005).

Figure 2.2 shows the human circulatory system. Deoxygenated blood travels from the systemic venous circulation (SVC) into the right atrium (RA) through the superior and inferior vena cava. During diastole, which involves relaxation of the ventricular muscle, the deoxygenated blood flows into the right ventricle (RV) via the tricuspid valve. As the RV muscle contracts, it pumps the deoxygenized blood into the pulmonary artery via the pulmonary valve. While passing through the pulmonary circulation in the lung, the blood is oxygenated. The oxygenated blood travels into the left atrium (LA), where it then moves into the LV during the diastolic phase via the mitral valve. During systole, which involves contraction of the ventricular muscle, the oxygenated blood is pumped into the aorta through the aortic valve, and travels along the systemic circulation. The blood then returns to the RA through the vena cava and the cycle repeats again.

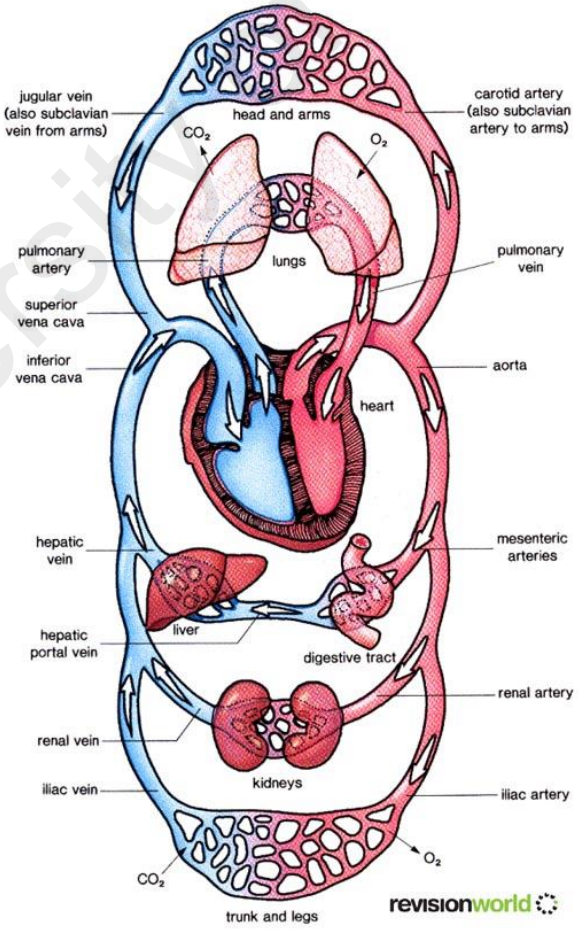

Figure 2.2: Human Circulatory System (RevisionWorld, 2015).

2.3 Cardiac Cycle

In each heartbeat, the cardiac muscles perform a period of contraction (systole) and relaxation (diastole). During diastole, the ventricles are filled with blood, whilst this blood is then ejected during systole. One cardiac cycle includes one contraction and one relaxation period. Typical healthy LV, LA, and aortic pressures during different cardiac phases in a cardiac cycle are shown in Figure 2.3.

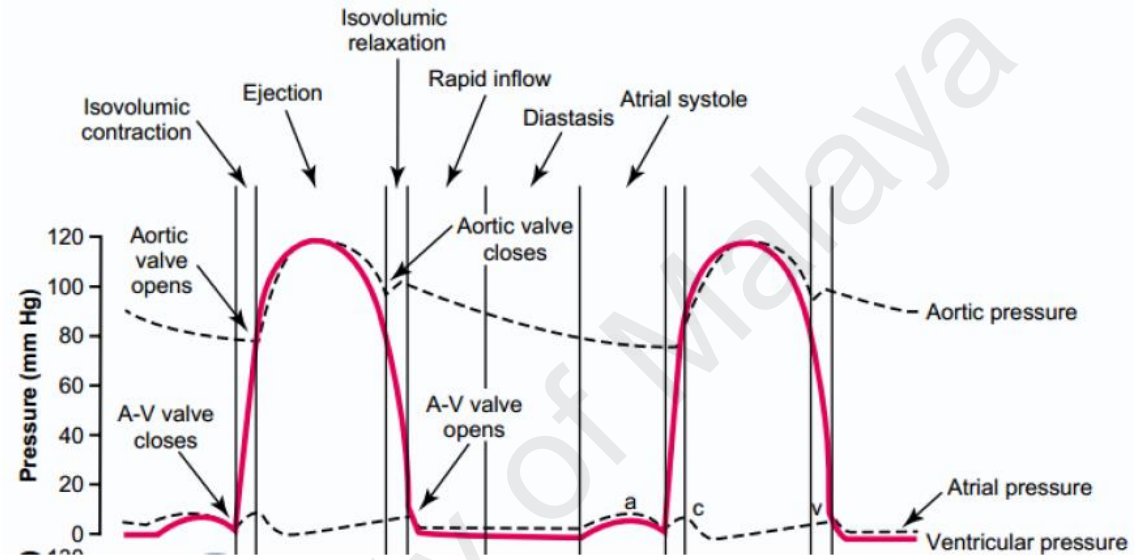

Figure 2.3: Aortic, left atrial and left ventricular pressure waveforms during a cardiac cycle (A C Guyton & Hall, 2005).

The cardiac cycle is divided into four distinctive phases (A C Guyton & Hall, 2005). Phase I begins with ventricular filling. During this phase, venous blood continuously flows from the atria into the ventricles through the atrioventricular valves, until the intraventricular pressure exceeds that of the atrial pressure. The ventricular filling phase is composed of three distinct stages. At the beginning (rapid filling), the pressure difference between the atrium and the ventricle causes the ventricles to be rapidly filled with blood. As this pressure difference gradually decreases, the heart enters into the next stage (diastasis), where the returning venous blood fills the ventricle at a much lower pace. Near the end of the ventricular diastolic phase, atrial systole occurs, where the atria contracts to pump more blood into the ventricle despite a near zero pressure difference

between the atria and the ventricles. The ventricular muscle relaxation in the first phase results in an increment in the ventricular volume and a small increase in the intraventricular pressure. The end-diastolic pressure-volume relationship (EDPVR) is commonly used to describe the relationship between the intraventricular volume and pressure during end diastole.

Isovolumetric contraction forms the beginning of the systolic phase. During this stage, the contraction of the ventricular muscle results in a drastic increment in the intravascular pressure. However, the ventricular volume remains unchanged as the one-way atrioventricular valves are closed, preventing backflow into the atria. Meanwhile, the aortic and pulmonary (semilunar) valves remain closed as the intraventricular pressure is less than the aortic pressure. Although this phase lasts only about 0.02 s to 0.03 s, it builds up enough pressure energy to open the semilunar valves.

The ejection stage commences when the intraventricular pressure exceeds that of the arterial pressure, allowing blood to be ejected from the LV into the aorta, and from the RV into the pulmonary artery. Upon opening of the semilunar valves, the intraventricular pressure continues to increase as the ventricles are still contracting. Eventually, the intraventricular pressures start to decrease as more blood is ejected from the ventricle. When the intraventricular pressure falls below that of the aortic pressure, the ejection phase ends. The end-systolic pressure-volume relationship (ESPVR) is typically used to describe the relationship between the intraventricular pressure and volume during end systole.

This is followed by the isovolumic relaxation phase, where the ventricular muscle relaxes, causing the intraventricular pressure to drop rapidly despite a constant volume. As the intraventricular pressure drops below that of the aortic pressure, the pulmonary and aortic

valves close. By the end of this phase, the intraventricular pressure falls below that of the atria, causing rapid filling of the blood into the ventricle, and the cardiac cycle repeats.

2.4 The Frank-Starling Law

According to the Frank-Starling mechanism (A C Guyton & Hall, 2005), the strength of the ventricular muscle contraction during systole is proportional to the volume of the blood (preload) returning to the ventricle during diastole. This mechanism indicates that an increment in the end diastolic volume resulting from an increase in the venous return causes the cardiac muscle fibers to pump stronger than normal. In the cellular level, this indicates that a higher stretching level of the myosin and actin filaments during end diastole results in an optimal force generation capability.

The Frank-Starling mechanism ascertains that the heart pumps all blood it receives from the veins (A C Guyton & Hall, 2005). Relying on this mechanism, the cardiac output (CO) is dependent on the interventricular end-diastolic pressure (preload), as shown in Figure2.4, referred to as preload sensitivity.

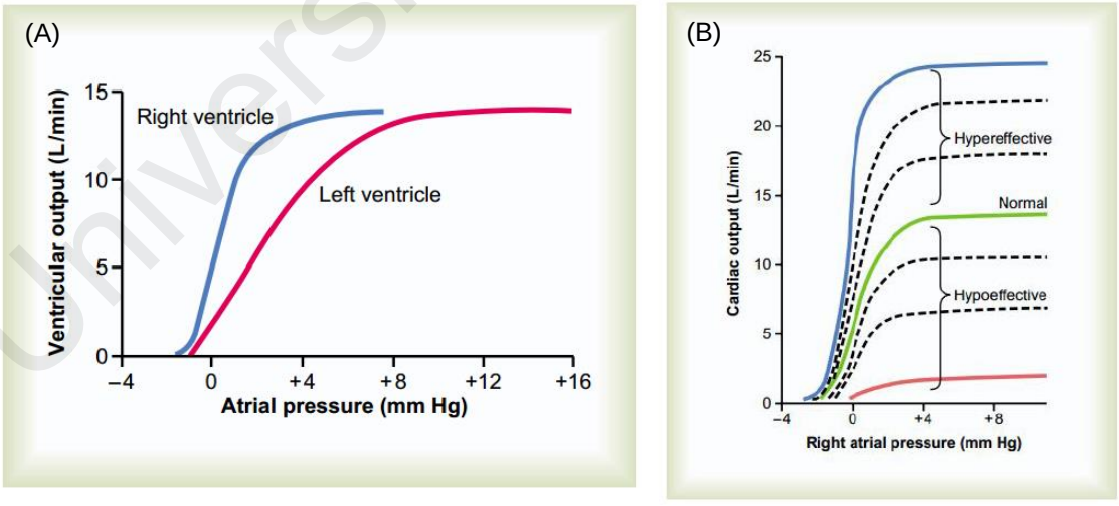

Figure 2.4: (A) Cardiac output curves, which show the relationship between left and right ventricular output and preload because of the Frank-Starling mechanism. (B) The sensitivity of cardiac output to preload and the maximum cardiac output increases with sympathetic nervous stimulation of the heart, and decrease with heart failure (A C Guyton & Hall, 2005).

It is worth noting that no single curve could demonstrate the relationship between CO and the preload across various physiological conditions. Instead, as shown in Figure 2.4, the sensitivity of CO to preload and the maximum cardiac output increases with sympathetic nervous stimulation of the heart, and decreases with heart failure.

2.5 Heart Failure

Heart failure (HF) is referred to as a condition that thwarts the heart from pumping sufficient amount of blood into the peripheral tissues and organs, preventing them from getting adequate oxygen (A C Guyton & Hall, 2005). Myocardial infarction, coronary artery disease, chronic hypertension, valve disease, and idiopathic cardiomyopathy are some common causes of HF (Klabunde, 2011). HF affects the pumping ability of the heart, resulting in a degraded preload sensitivity, pulmonary congestion, and a deteriorated maximum cardiac output.

Insufficient CO indicates that the oxygen supply to vital organs such as kidney, liver, and brain reduces. Consequently, the body activates the sympathetic nervous stimulation system in an attempt to maintain cardiac output above 5 L/min. This involves an increase in heart rate and contractility, as well as an increase in the venous tone to increase LV preload, which would subsequently increase CO via the Frank-Starling mechanism (A C Guyton & Hall, 2005).

This compensatory mechanism, though aimed to increase cardiac output, leads to a substantial increment in the preload. Although the patients may not exhibit symptoms of HF other than an increase in left atrial (LA) pressure (LAP) and right atrial (RA) pressure (RAP) at rest, they experience degradation in maximum cardiac output and thus exercise capacity, which affects their quality of life. Therefore, appropriate treatment is essential to increase the quality of life for these patients. HF can be treated by surgery, or using

pharmacological treatment. In addition, implantable rotary blood pumps are a practical, long-term option for supporting heart failure patients awaiting donor hearts.

2.6 Heart Failure Mechanical Therapy

Due to the limited availability of donor organs and limitations in drug therapies, various types of VADs have been developed, including the pulsatile VADs and the continuous flow VADs. With the advancement of the VAD technology, they can now be used as a bridge to recovery, bridge to transplant or permanent support (A.-H. H. AlOmari et al., 2013).

2.6.1 Generations of VADs

To date, three VAD generations have been developed and are classified according to their mode of operation (Yamane, 2002). Figure 2.5 shows examples of these three different generations.

Figure 2.5: Examples of first, second and third generation ventricular assist devices. (A) PVAD (Thoratec Corporation, Pleasanton, CA, USA). (B) HeartMate II (Thoratec Corporation, Pleasanton, CA, USA). (C) HVAD (HeartWare Inc., Massachusetts, USA) (M. C. Stevens, 2014).

The first generation, referred to as the pulsatile pumps, have unidirectional artificial valves and diaphragms surrounding the blood chambers. They eject flows at rates typically between 80 and 100 beats per minute, producing pulsatile flow like the natural heart (D. Timms, 2011). Although the pulsatile VADs have been the main emphasis for research in artificial heart pumps from 1960s to 1980s (Yamane, 2002), they provide limited support duration in spite of the improvement in survival rates. The mechanical

properties of their artificial valves and diaphragm limited their working life to 3~4 years. Furthermore, pulsatile VADs were large because the pulsation require driving elements in the pump (D. Timms, 2011).

The continuous flow pumps are the second generation VADs, improved to cover aforementioned shortage of the pulsatile pumps. These pumps are either centrifugal or axial pumps, which pump blood continuously. DeBakey pump (MicroMed Inc.) and HeartMate II (Thoratec Corp.) are the most commonly used continuous flow pumps. The impellers of these pumps are supported by mechanical bearings of several different designs. The drawback of these VADs are their vulnerability to bearing wearing and thrombosis around the bearing seal (Koh, Chan, Ng, & Li, 1999).

The magnetically levitated continuous flow pumps form the latest generation of the VADs. Incor VAD (Berlin Heart AG, Germany), VentrAssist (Ventracor Ltd., Sydney, Australia), and HeartQuest VAD (Medquest Inc.) are few magnetically suspended continuous flow pumps which have gone through clinical trials and animal tests (Lee et al., 2011). Compared to the second generation, the impeller is levitated by magnetic forces without any mechanical contact. Without the presence of the bearing, thrombosis around the bearing seal can be avoided. Moreover, their mechanical durability enables them to be used as long-term destination therapy.

2.6.2 Physiological Control of VADs

To date, most LVADs operate using constant speed control (Akimoto et al., 1999), which is insensitive to changes in the metabolic requirements of patients in their daily life course. Low preload sensitivity of rotary LVADs under constant speed operational mode increases the over-pumping (suction) or under-pumping risk, which can cause pulmonary congestion, renal insufficiency and other problems (Salamonsen et al., 2013). Therefore,

physiological control of LVAD is one of the most important concerns in providing a long-term support.

Over the years, many researches have been conducted to develop physiological control methods that could accommodate to the body demand. Any physiological LVAD control should fulfill three criteria (Boston, Antaki, & Simaan, 2003) as follows: (i) provide sufficient cardiac output to meet metabolic requirements, (ii) maintain systemic arterial pressure within a physiological range to maintain sufficient liver/kidney perfusion and to avoid over-perfusion or under-perfusion, and (iii) maintain left atrial pressure within a normal physiological range to avoid pulmonary congestion and suction (Boston et al., 2003). In addition, it is advisable to maintain positive left ventricular outflow for a portion of the cardiac cycle (during systole) and to avoid regurgitated blood from the aorta to the left ventricle in diastole (Wu, Allaire, Tao, & Olsen, 2007).

To date, more than 30 different pump control algorithms have been designed (A.-H. H. AlOmari et al., 2013), aiming to dynamically adapt to varying metabolic demand of the HF patients. These method include differential pressure control (G. Giridharan, Pantalos, Koenig, Gillars, & Skliar, 2005; Waters et al., 1999), flow control (Smith, Goodin, Fu, & Xu, 1999), pulsatility index (Choi, Antaki, Boston, & Thomas, 2001), and pulsatility ratio control (Salamonsen et al., 2012).

Waters et al. (1999) proposed a controller that used the pump head differential pressure as a feedback signal. Although the results of their numerical simulation demonstrated that the developed controller was able to maintain the head pressure, the pump flow and pump speed went beyond the normal operating levels whenever the systemic resistance changed. G. Giridharan et al. (2005) proposed another control that maintained a constant average pressure difference between the left ventricle and the aorta. Their hypothesis was that this provided sufficient physiological perfusion to the body over a wide range of

physical activities and clinical cardiac conditions. However, a prominent drawback of their controllers was that the estimation accuracy of the feedback signal (i.e. differential pressure) was only assessed under a steady state condition but not during transient changes. Furthermore, maintaining a constant pump differential pressure may increase the risk of suction under low systemic vascular resistance or blood volume conditions, while producing lower than optimal cardiac output under higher blood volume conditions (Einly Lim et al., 2012a).

Smith et al. (1999) suggested that pump flow is a more relevant physiological parameter for the control of an IRBP as compared to pump differential pressure. The main disadvantage of this control strategy is the difficulty in selecting an optimal pump flow level, as this varies with different hemodynamic conditions.

Fu and Xu (2000) developed a sensor-less fuzzy logic IRBP controller that regulated the LVAD flow to track a set value by applying the fuzzy to adjust the motor input. They estimated the motor flow using the electrical motor current and speed whilst the desired flow set point was set regarding the heart rate. The major limitation of their study was that the assumed pump flow is proportional to the heart rate besides they ignored the heart contractility and peripheral circulation on the desired flow rate effects (Arthur C Guyton & Hall, 1996).

Another commonly used control strategy is the constant pulsatility index control, developed based on the close relationship between the pump flow or differential pressure pulsatility (PI) and LV filling pressure (Choi et al., 2001). However, due to the dependency of PI on the heart contractility, afterload (the pressure in the wall of the left ventricle during ejection), and preload, controlling PI to a fixed set point may fail to avoid adverse pumping states such as suction during sudden perturbations of the circulatory system (Arndt, Nüsser, Graichen, Müller, & Lampe, 2008).

Salamonsen et al. (2012) proposed a linear Starling-like controller, which emulates the response of the natural LV to changes in preload. However, the use of pump flow pulsatility as the feedback variable to reflect changes in preload suffers from its dependency on pump characteristics, causing it to fail during various circumstances (Mansouri, Salamonsen, Lim, Akmeliawati, & Lovell, 2015).

In summary, most of the previously proposed controllers have shown various functional limitations. Therefore, the development of an adaptive and robust controller that could emulate the Frank-Starling mechanism of the heart is required.

CHAPTER 3: FIXED SET POINT BLOOD PUMP CONTROLLERS

3.1 Introduction

With the rapid advancement of IRBP technology, there is increasing evidence of successful experience for prolonged periods of implantation in patients (Park et al., 2005). In a long-term unsupervised environment, as patients go through different activity levels from sleep to exercise, under-pumping or over-pumping may occur, leading to inefficient operating conditions as well as unacceptable risks such as impairment of right heart function or collapse of the left ventricle (Vollkron et al., 2005). This is further complicated by the severely reduced sensitivity of IRBPs to preload as compared to the native heart (Mason, Hilton, & Salamonsen, 2008), as well as the residual ventricular function.

The native exercise response of an IRBP-assisted patient, as well as the inherent adaptability of an IRBP to exercise, has attracted considerable attention from researchers over the years (Akimoto et al., 1999; Brassard et al., 2011; Jacquet et al., 2011; Mancini et al., 1998; Salamonsen et al., 2013). Although it has been well established that there is a spontaneous increase in cardiac output in these patients during exercise under constant pump speed (Akimoto et al., 1999; Jacquet et al., 2011; Salamonsen et al., 2013), the underlying mechanisms remain unclear. Based on the separate analysis of experimentally obtained pump flow during systole and diastole, Akimoto et al. (1999) proposed that increases in heart rate and subsequently time spent in systole are the dominant mechanism leading to an increase in mean pump flow during exercise.

However, contradictory data by K Muthiah et al. (2012) indicated that pacemaker-induced increases in heart rate in resting patients did not significantly alter pump flow. Similarly, in a study conducted on ten IRBP-implanted patients undergoing bicycle exercise, Jacquet et al. (2011) could not correlate the change in pump flow with either heart rate or changes in heart rate. To the contrary, they demonstrated that the native heart plays a significant

role in flow adaptation, with total rise observed in the cardiac output during exercise mainly contributed by flow through the aortic valve. Using multiple linear regression of pump flow on factors considered to underlie the spontaneous increases in pump flow during exercise, Salamonsen et al. (2013) revealed that this was associated with increases in heart rate, pressure gradient across the left ventricle and right atrial pressure.

While exercise leads to an increase in venous return and consequently cardiac output, transition from lying to standing imposes an opposite effect, with anecdotal reports suggest some patients feeling faint during a change in posture. Despite the concern of suction risk, limited studies have looked into the effect of postural change on hemodynamics in patients assisted with an IRBP. To date, we are only aware of one clinical study by K. Muthiah et al. (2013), which demonstrated a 10% reduction in pump flow with 60^0 head up tilt, without any occurrence of suction events. Although both clinical and experimental studies have been very useful in providing insights into mechanisms underlying the observed responses in IRBP-assisted patients to exercise and postural changes, they are inconclusive at present due to various potentially confounding factors. Furthermore, limited measurements could be obtained from the patients due to the complexity of the experimental procedures. For instance, most studies have not measured native cardiac output (Akimoto et al., 1999; Mancini et al., 1998) and left ventricular end diastolic pressure (Akimoto et al., 1999; Mancini et al., 1998), which reflects venous return.

In order to maximize the quality of life of the implant recipients in a-long term unsupervised environment, various physiological control strategies which attempt to immediately adapt to varying cardiac demand and clinical states of the heart have been proposed (Arndt et al., 2008; M. A. Bakouri et al., 2014; Choi et al., 2001; Nicholas R. Gaddum et al., 2014; G. A. Giridharan, Pantalos, Gillars, Koenig, & Skliar, 2004; G. A. Giridharan & Skliar, 2006; Wu et al., 2003; Wu et al., 2004). These include the pulsatility

index (PI) (Choi et al., 2001; Schima et al., 2006), gradient of PI with respect to pump speed (GPI) (Arndt et al., 2008), differential pump pressure (G. A. Giridharan et al., 2004), aortic pressure (Wu et al., 2003; Wu et al., 2004), and the more recently proposed linear Starling-like controller (M. A. Bakouri et al., 2014; Nicholas R. Gaddum et al., 2014; Salamonsen et al., 2013). Despite the extensive efforts, none of these controllers have gained clinical acceptance in commercial devices due to their lack of confidence by clinicians (Salamonsen et al., 2012).

Moreover, with the possible exception of the automatic closed-loop controller proposed by Vollkron and Schima et al. (Schima et al., 2006; Vollkron et al., 2005), the performance of these controllers have not been evaluated in patients. Most controllers were evaluated using either a numerical model (Arndt et al., 2008; M. A. Bakouri et al., 2014; Choi et al., 2001; G. A. Giridharan & Skliar, 2006; Wu et al., 2003) or an in vitro mock circulatory loop (Choi et al., 2001; Nicholas R. Gaddum et al., 2014; G. A. Giridharan et al., 2004; Wu et al., 2004), with their performance compared against a constant speed controller. The major drawback of these studies is that the simulation environment was oversimplified and therefore could not accurately reflect physiological responses in the IRBP-assisted patients during various perturbations. For example, reflex mechanisms, which play a major role in determining the response of patients to exercise and postural changes, were not included in the simulation models (Arndt et al., 2008; M. A. Bakouri et al., 2014; Choi et al., 2001; Nicholas R. Gaddum et al., 2014; G. A. Giridharan et al., 2004; G. A. Giridharan & Skliar, 2006; Wu et al., 2003; Wu et al., 2004).

The major motivation for the present study was to investigate the response of the IRBP-assisted patients to exercise and HUT, using validated heart pump interaction models which takes into account various important features such as the arterial and cardiopulmonary reflexes, local metabolic vasodilation in the active muscles, the auto-regulation mechanism in the lower body, the muscle pump, as well as diastolic ventricular

interaction through the pericardium. Furthermore, the individual effect of parameters associated with heart failure, including LV and right ventricular contractility, baseline total blood volume, reflex sensitivity, heart rate, as well as pump speed on exercise capacity and HUT response in these patients were also assessed.

Using the numerical models, we comparatively evaluate the performance of a number of previously proposed physiologically responsive controllers, including constant speed, constant flow pulsatility index (PI) (Choi et al., 2001; Schima et al., 2006), constant average pressure difference between the aorta and the left atrium ($\overline{dP}$), constant average differential pump pressure ($\overline{dP_{pump}}$) (G. A. Giridharan et al., 2004), constant ratio between mean pump flow and pump flow pulsatility ($ratio_{PI}$) or linear Starling-like control (M. A. Bakouri et al., 2014; Nicholas R. Gaddum et al., 2014; Salamonsen et al., 2012), and constant mean left atrial pressure ($\overline{P_{la}}$) control.

3.2 Materials and Methods

3.2.1 Model Description

The basic structure of the heart-pump interaction model was adapted from our previous model (Einly Lim, 2009; Einly Lim et al., 2010; Einly Lim et al., 2012a, 2012b), which consists of the left and right sides of the heart, direct ventricular interaction via the inter-ventricular septum and pericardium, the pulmonary and systemic circulations as well as the left ventricular assist device (Figure 3.1). The LVAD component includes the description of the $IRBP^{blue}$ (VentrAssist^{TM}, which operates between 1600 and 3000 rpm), as well as the inlet and outlet cannula. The duration of the systolic periods were assumed to vary linearly with heart rate (Ursino, 1998). A detailed description of the model can be obtained from (Einly Lim et al., 2012a, 2012b).

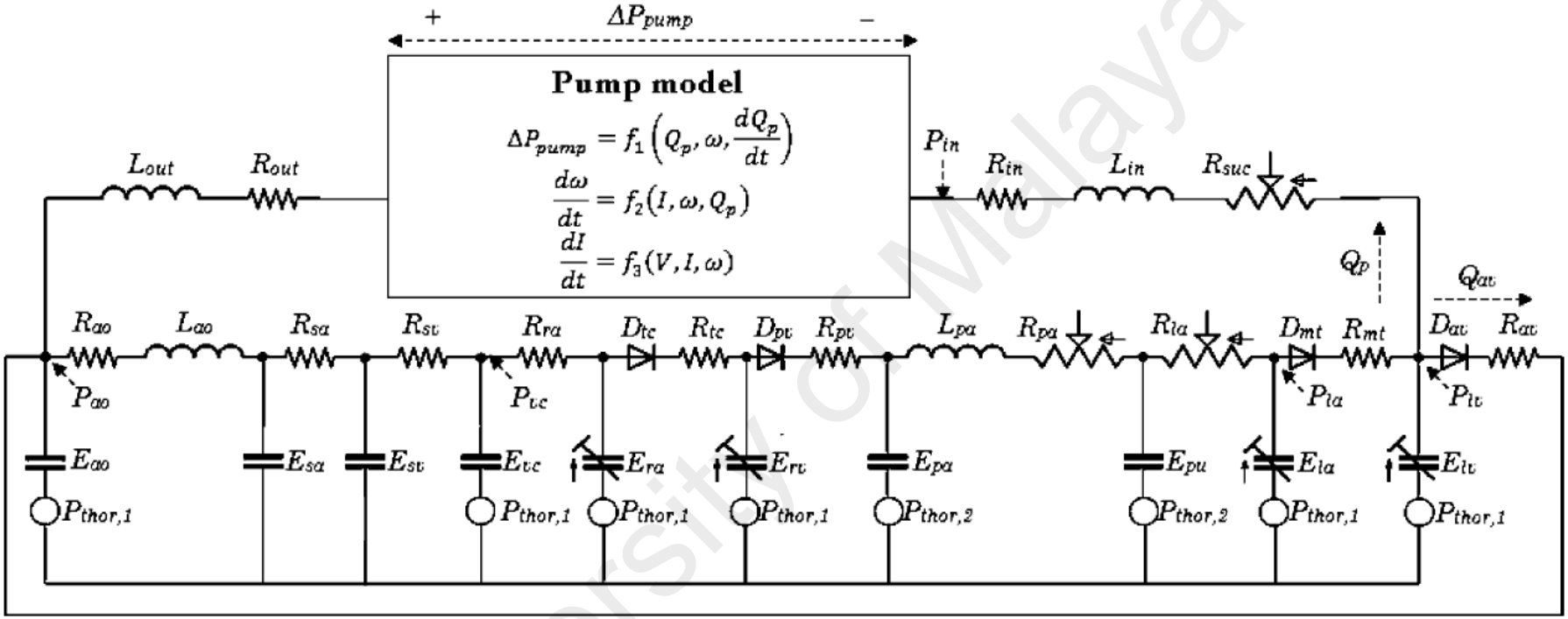

Figure 3.1: The lumped parameter model of Ventrassist™ LVAD and the cardiovascular system (Einly Lim et al., 2010).

P, pressures; R, resistances; E, elastances (=1/compliances); L, inertances; D, diodes. The model consists of two main components: (1) the CVS, which is further divided into ten compartments (la, left atrium; lv, left ventricle, ao, aorta; sa, systemic peripheral vessels, including the arteries and capillaries; sv, systemic veins, including small and large veins; vc, vena cava; ra, right atrium; rv, right ventricle; pa, pulmonary peripheral vessels, including pulmonary arteries and capillaries; pu, pulmonary veins and (2) the LVAD, which includes the rotary blood pump and the cannula (R_{in} and R_{out} , inlet and outlet cannula resistances; L_{in} and L_{out} , inlet and outlet cannula inertances; R_{suc} , suction resistance). The intrathoracic pressure, $P_{thor,1}$ and $P_{thor,2}$ were assigned the same values (–4 mmHg) during closed-chest simulated conditions.

3.2.2 Exercise Model

A model previously developed and validated by E Magosso and Ursino (2002), able to simulate both the steady state and transient cardiorespiratory response of healthy subjects at various levels of aerobic exercise intensities, was integrated into our heart-pump interaction model. Among features adopted included: (i) a division of the systemic circulation into 6 compartments, i.e. splanchnic, extrasplanchnic, resting muscles, active muscles, cerebral and coronary circulations; (ii) a functional description of the local metabolic vasodilation in active muscles; (iii) effect of the muscle pump on venous return; (iv) the arterial baroreflex and the lung inflation reflex, which consist of the afferent pathways, the efferent sympathetic and parasympathetic activities, and the responses of several distinct effectors, including the heart contractilities, peripheral resistances, unstressed volumes and heart rate; and (v) the action of the central command on the efferent sympathetic and parasympathetic activities.

The only input for the model is the relative intensity of the aerobic exercise, which has a direct effect on the vasodilatory mechanism as well as the sympathetic/parasympathetic systems through the direct action of the central command. In the present study, relative intensity of 0.6 was chosen to reproduce experimentally observed changes in the hemodynamic variables in IRBP-assisted patients during maximal exercise (Brassard et al., 2011; Jacquet et al., 2011; Mancini et al., 1998; Salamonsen et al., 2013).

3.2.3 HUT Model

To investigate the response of the IRBP-assisted patients to HUT, a cardiovascular system model previously developed by our research group (Einly Lim et al., 2013) was integrated into our heart-pump interaction model. The systemic circulation was divided into several parallel branches, i.e. cerebral, upper body, coronary, splanchnic, renal, and lower body, to account for the differences in heights of each compartment from the hydrostatic

indifference point (HIP) located at the heart level, as well as different impacts of regulatory mechanisms on these compartments. Furthermore, a number of important features were included: (i) separate effects of arterial and cardiopulmonary reflexes; and (ii) the autoregulation mechanism in the lower body. The fitted model has been shown to compare favorably with our experimental measurements and published literature at a range of tilt angles, in terms of both global and regional hemodynamic variables, under both healthy and congestive heart failure conditions.

3.2.4 Simulation Protocols

The models were implemented using the Simulink toolbox in MATLAB (The Mathworks, Inc., Natick, MA, USA). Initial software simulations were performed with the LVAD removed from the model in order to demonstrate the validity of the CVS model alone during exercise and HUT. As described in a previous study (Einly Lim et al., 2013), we simulated a heart failure scenario (NYHA Class II & III) by carefully modifying the parameters associated with heart failure to ensure that realistic simulation in terms of mean systemic arterial pressure, mean left atrial pressure, mean pulmonary arterial pressure, mean central venous pressure, heart rate, stroke volume and cardiac output was achieved. The baroreflex response was attenuated in both simulations by modifying the static characteristics of the effectors (Elisa Magosso, Cavalcanti, & Ursino, 2002), as congestive heart failure patients were known to have markedly depressed baroreflex function (Eckberg & Sleight, 1992). Subsequent simulations were performed with the LVAD model included, and these were used to investigate the response of the IRBP-assisted patients to exercise and HUT.

The resulting simulated key haemodynamic variables at rest and supine position, as well as their changes with respect to exercise and 70^0 HUT at a constant pump operating speed (i.e. 2100 rpm) are listed in Table 3.1 and Table 3.2, where the values are seen to agree

with the published data, except for a minor deviation in the mean pump flow. Considering the strong dependency of pump flow with pump operating speed, and the fact that most studies based their reported values on estimations rather than real measurements, we have allowed a 15% tolerance in the simulated pump flow value at baseline (both rest and supine) from that reported in the published literature during our model fitting process. Furthermore, in a study comparing the accuracy of the HeartMate II flow estimator with that measured by an ultrasonic flow probe, a difference of 15-20% has been reported (Markham et al., 2013).

Next, we varied parameters associated with heart failure, including LV and RV contractility (50% decrease), baseline total blood volume (600 mL increase), reflex sensitivity (by removing the reflex control mechanism), as well as pump speed (400 rpm increase), one at a time, and observed the resulting changes in the hemodynamic variables, to evaluate the individual effect of these parameters on the exercise capacity and HUT response in the IRBP-assisted patients. Furthermore, six separate control strategies were compared in the present study: constant speed, constant average PI (3.1), constant average pump head pressure (3.2), constant average pressure difference between the aorta and the left atrium (3.3), constant average ratio_{PI} controller (3.4), and constant average left atrial pressure controller.

$$\overline{PI} = \overline{(Q_{P_{MAX}} - Q_{P_{MIN}})} \tag{3.1}$$

$$\overline{dP_{pump}} = \overline{(P_{P_{IN}} - P_{P_{OUT}})} \tag{3.2}$$

$$\overline{dP} = (\overline{P_{SA} - P_{LA}}) \tag{3.3}$$

$$\overline{ratio_{PI}} = \theta = \frac{\overline{Q_P}}{\overline{PI}} \tag{3.4}$$

To compare these control strategies, the target values for all controllers were chosen to coincide with the corresponding values obtained at a fixed operating pump speed of 2100

rpm during the resting stage. This particular operating condition was selected as it most closely reproduced clinically reported values for key hemodynamic variables in IRBP-assisted patients under normal resting condition (Brassard et al., 2011; Jacquet et al., 2011; Mancini et al., 1998; Salamonsen et al., 2013). All the control modes were then implemented separately with a proportional-integral-derivative controller (Figure 3.2), which adjusted the pulse-width-modulation (PWM) signal to generate the desired set point. The proportional gains (K_P) and time constants (τ_i) for the proportional-integral type controllers were selected to yield minimal overshoot and rise time in the target variables for the respective controllers. Since the present study focuses on the steady state response of the various controllers to exercise and HUT rather than transient changes, the values chosen for K_P and τ_i has no effect on the simulation results at steady state.

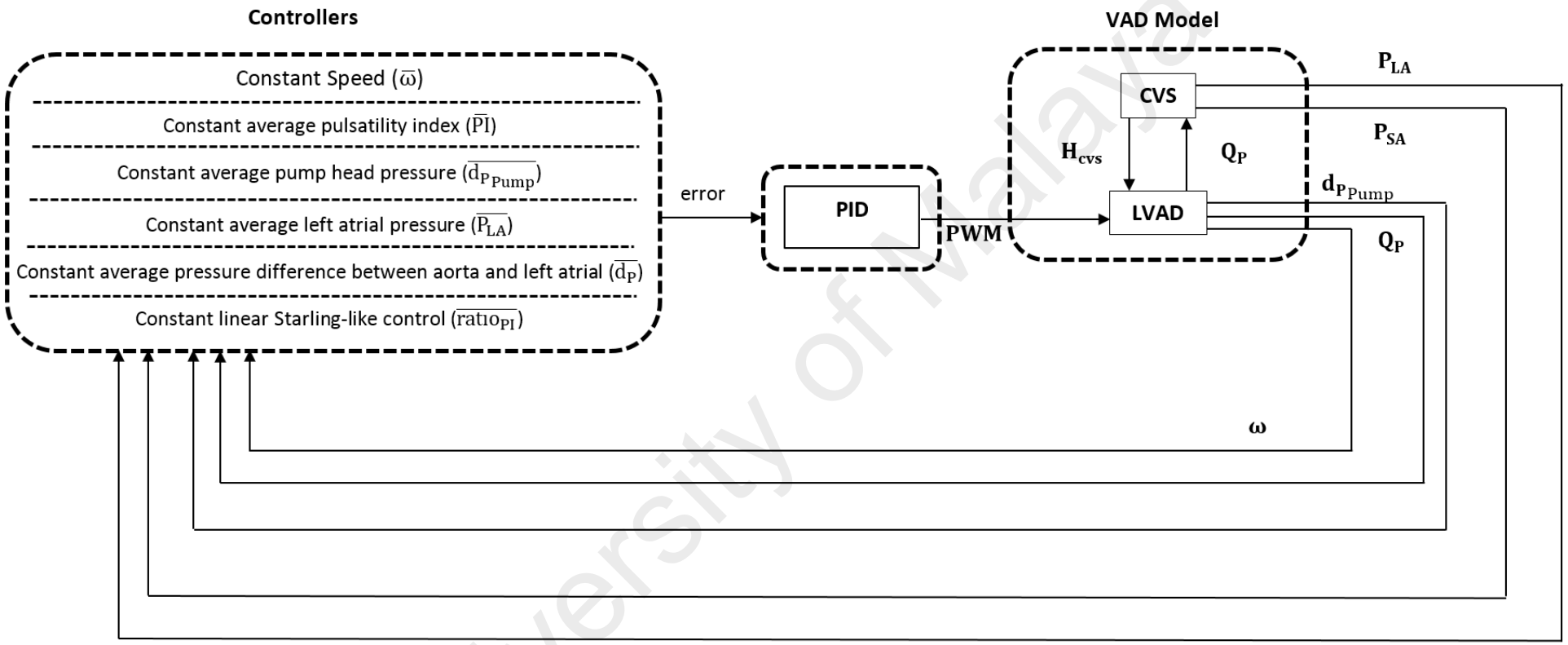

Figure 3.2: Block diagram of the PID controller for closed loop studies

Table 3.1: Model simulated and published hemodynamic data during rest and exercise

Variable	Simulation	Experiment
Absolute value at rest		
$\overline{P_{sa}}$ (mmHg)	92.0	89.9-94.0 (Jacquet et al., 2011)
$\overline{P_{la}}$ (mmHg)	14.92	5.0-16.7 (Jacquet et al., 2011)
$\overline{P_{Pa}}$ (mmHg)	28.1	18.0-32.0 (Jacquet et al., 2011)
$\overline{CVP}$ (mmHg)	6.0	3.0-6.3 (Jacquet et al., 2011)
HR (bpm)	85.8	75-102 (Jacquet et al., 2011)
$\overline{CO}$ (L/min)	4.74	4.6-7.0 (Jacquet et al., 2011)
SVR (mmHg.s/mL)	1.09	1.0-1.2 (Jacquet et al., 2011)
$\overline{Q_P}$ (L/min)	3.68	4.0-5.3 (Jacquet et al., 2011)
$\overline{Q_{av}}$ (L/min)	1.06	---
Changes from rest to exercise		
$\overline{P_{sa}}$ (mmHg)	5.8	2-9 (Jacquet et al., 2011)
$\overline{P_{la}}$ (mmHg)	8.2	5-9 (Jacquet et al., 2011)
HR (%)	55.1	48.1-55.8 (Jacquet et al., 2011)
$\overline{CO}$ (%)	81.1	67.9-128.6 (Jacquet et al., 2011)
$\overline{Q_P}$ (%)	20.9	17.0-30.0 (Jacquet et al., 2011)
$\overline{Q_{av}}$ (%)	290.0	---

Table 3.2: Model simulated and published hemodynamic data during supine and 70^0 HUT

Variable	Simulation	Experiment
Absolute value at supine positions		
$\overline{P_{sa}}$ (mmHg)	91.8	93.0-94.0 (Jacquet et al., 2011)
$\overline{P_{la}}$ (mmHg)	14.8	13.0-16.7 (Jacquet et al., 2011)
$\overline{P_{Pa}}$ (mmHg)	27.7	20.0-27.3 (Jacquet et al., 2011)
$\overline{CVP}$ (mmHg)	6.7	6.0-6.3 (Jacquet et al., 2011)
HR (bpm)	85.5	75-91 (Jacquet et al., 2011)
$\overline{CO}$ (L/min)	4.6	4.6-5.3 (Jacquet et al., 2011)
SVR (mmHg.s/mL)	1.11	1.0-1.2 (Jacquet et al., 2011)
$\overline{Q_P}$ (L/min)	3.94	4.5-5.3 (Jacquet et al., 2011)
$\overline{Q_{av}}$ (L/min)	0.66	---
Changes from rest to 70^0 HUT		
$\overline{P_{sa}}$ (mmHg)	1.6	0-9 (K Muthiah et al., 2012)
$\overline{P_{la}}$ (mmHg)	-4.5	---
HR (%)	9.0	5.8 (Markham et al., 2013)
$\overline{CO}$ (%)	-17.2	---
$\overline{Q_P}$ (%)	-11.2	-12.0(K Muthiah et al., 2012)
$\overline{Q_{av}}$ (%)	-60.0	---

3.3 Results

3.3.1 Comparison with Published Experimental Observations

Comparison between simulation results and published findings concerning exercise and HUT response at a constant operating speed of 2100 rpm were presented in Table 3.1 and Table 3.2. There was a high degree of correlation between the model and experimental

data about their absolute values at rest and supine position, as well as their respective changes during exercise and 70^0 HUT. As observed experimentally (Brassard et al., 2011; Jacquet et al., 2011; Mancini et al., 1998; Salamonsen et al., 2013), mean systemic arterial pressure, mean left atrial pressure, heart rate, mean cardiac output, mean pump flow and mean aortic valve flow increased spontaneously during exercise without variations in pump speed. The increase in mean cardiac output during exercise was mainly contributed by an increase in mean aortic valve flow through an increase in the LV end diastolic volume, i.e. LV preload. Consistent with published findings (Akimoto et al., 1999; Jacquet et al., 2011; Salamonsen et al., 2013), an increase in mean pump flow was also observed, however at a much lesser percentage change compared to that of the mean aortic valve flow. To the contrary, mean cardiac output, mean pump flow, and mean aortic valve flow showed a reduction during HUT, with their percentage changes comparable to that reported clinically (K Muthiah et al., 2012). Despite a decrease in mean left atrial pressure, mean systemic arterial pressure showed a minor increase during HUT.

3.3.2 Sensitivity Analysis: Effects of Individual Parameters on Exercise

Table 3.3 shows the effects of modifying individual factors associated with heart failure, including LV contractility (E_{lv}), RV contractility (E_{rv}), total blood volume (V_t) and desensitized reflex response (β), as well as pump speed (ω) on key variables during rest and exercise, using model settings described previously as baseline condition. In order to investigate the effect of increasing heart rate alone during exercise, an additional simulation was performed by removing the response of all effectors except that involving heart rate (β_{HR}).

Table 3.3: Effect of individual parameter on key hemodynamic variables during rest and exercise

Variable	**Baseline**	**E_{lv}**	**E_{rv}**	**V_t**	**ω**	**β**	**β_{HR}**
$\overline{P_{sa}}$ (mmHg)	92.0	83.1	89.2	95.6	100.1	92.0	92.0
$\overline{P_{la}}$ (mmHg)	14.9	19.3	10.5	20.5	10.8	14.9	14.9
$\overline{CO}$ (L/min)	4.7	4.1	4.4	4.9	5.3	4.7	4.7
$\overline{Q_P}$ (L/min)	1.1	0.0	0.9	1.1	0.0	1.1	1.1
$\overline{Q_{av}}$ (L/min)	3.7	4.1	3.6	3.8	5.3	3.7	3.7
$\overline{dP}$ (mmHg)	54.2	51.8	55.2	53.3	69.5	54.2	54.2
$\overline{dP_{pump}}$ (mmHg)	84.8	85.7	84.9	84.7	118.8	84.8	84.8
PI_{Qp} (L/min)	3.9	2.1	4.0	3.7	3.1	3.9	3.9
$ratio_{PI}$	0.95	1.9	0.9	1.0	1.7	1.0	1.0
Changes from rest to exercise							
$\overline{P_{sa}}$ (mmHg)	5.8	-0.8	5.4	5.1	0.4	-24.0	-12.5
$\overline{P_{la}}$ (mmHg)	8.2	13.0	6.5	7.7	10.4	-4.5	-0.3
$\overline{CO}$ (%)	81.1	71.7	81.0	79.2	66.2	38.5	63.5
$\overline{Q_{av}}$ (%)	289.87	N/A	334.4	290.9	N/A	68.7	176.8
$\overline{Q_P}$ (%)	20.9	29.2	21.3	19.1	19.6	29.84	30.7
$\overline{dP}$ (%)	-18.6	-38.4	-17.6	-18.6	-29.6	-26.6	-28.2
$\overline{dP_{pump}}$ (%)	-2.47	-6.4	-2.2	-2.5	-5.8	-3.0	-3.5
PI_{Qp} (%)	-10.88	-0.1	-9.7	9.7	-2.6	-20.7	-25.0
$ratio_{PI}$ (%)	35.64	29.3	34.2	31.9	22.7	87.4	74.1

Columns 3 to 8 refer to the simulation repeated (using baseline parameters) by individually modifying the following quantities to that used for the baseline scenario.

Decreasing LV and RV contractility caused a fall in resting mean systemic arterial pressure, mean cardiac output and mean aortic valve flow, but produced directionally opposite changes in mean left atrial pressure and mean pump flow. On the other hand, resting mean systemic arterial pressure, mean cardiac output and mean pump flow increased substantially with increasing total blood volume and mean pump speed. Due to a significant rise in mean pump flow with increasing mean pump speed, mean aortic valve flow fell to 0 L/min and as a result, IRBP contributed completely to the total cardiac output. Out of all six simulated conditions, mean pump speed has the most significant effect on resting $\overline{dP}$ and $\overline{dP_{pump}}$ followed by LV contractility, while RV contractility and total blood volume contributed to a lesser degree of changes in these variables. Directionally opposite changes were observed between resting flow pulsatility index (PI_{Qp}) and $ratio_{PI}$, with decreasing LV contractility, increasing total blood volume and increasing mean pump speed reduced PI_{Qp} but increased $ratio_{PI}$.

3.3.3 Sensitivity Analysis: Effects of Individual Parameters on HUT Response

Table 3.4 shows the effects of modifying LV contractility, RV contractility, total blood volume, desensitized reflex response, as well as pump speed on key variables during supine and 70^0 HUT, using model settings described previously as baseline condition. As observed from the simulation results, effects of these parameters on all hemodynamic variables at the supine position were similar to that obtained during the resting condition.

Concerning the changes from supine to 70^0 HUT, mean systemic arterial pressure and mean left atrial pressure showed directionally opposite changes in all simulated conditions except that in the case of desensitized reflex response. Decreasing LV contractility and increasing mean pump speed augmented the rise in mean systemic arterial pressure and the reduction in mean left atrial pressure at 70^0 HUT, leading to an increase in $\overline{dP}$ and $\overline{dP_{pump}}$, while opposite observations were obtained with decreasing

RV contractility and increasing total blood volume. To the contrary, desensitized reflex response led to a substantial decrease in mean systemic arterial pressure and mean left atrial pressure at 70^0 HUT. In terms of blood flow, increasing total blood volume imposed the most significant effect among all simulated conditions, where it substantially lessened the decrease in mean cardiac output, mean aortic valve flow and mean pump flow. Similarly, decreasing LV contractility, increasing mean pump speed and desensitized reflex response also reduced the percentage reduction in mean cardiac output at 70^0 HUT. With respect to PI_{Qp}, increasing LV contractility augmented the percentage increase in PI_{Qp} at 70^0 HUT, while opposite and lesser degree of changes were observed with decreasing RV contractility and increasing total blood volume. As opposed to other simulated conditions, increasing mean pump speed and desensitized reflex response produced a drop in PI_{Qp} at 70^0 HUT.

Table 3.4: Effect of individual parameter on key hemodynamic variables during supine and 70° HUT

Variable	**Baseline**	**E_{lv}**	**E_{rv}**	**V_t**	**ω**	**β**
$\overline{P_{sa}}$ (mmHg)	91.8	85.1	89.5	96.3	100.3	91.8
$\overline{P_{la}}$ (mmHg)	14.8	17.5	13.0	20.3	11.0	14.8
$\overline{CO}$ (L/min)	4.6	4.1	4.4	4.9	5.4	4.6
$\overline{Q_P}$ (L/min)	0.7	0.0	0.5	0.9	0.0	0.7
$\overline{Q_{av}}$ (L/min)	3.9	4.1	4.0	4.0	5.4	3.9
$\overline{dP}$ (mmHg)	50.8	51.9	50.8	50.0	69.2	50.8
$\overline{dP_{pump}}$ (mmHg)	84.0	85.6	84.1	83.8	118.8	84.0
PI_{Qp} (L/min)	3.9	2.2	3.8	3.8	2.9	3.9
$ratio_{PI}$	1.0	1.8	1.1	1.1	1.8	1.0
Changes from rest to exercise						
$\overline{P_{sa}}$ (mmHg)	2.1	3.9	2.5	1.3	4.0	-8.6
$\overline{P_{la}}$ (mmHg)	-4.7	-5.7	-3.9	-4.6	-4.9	-6.0
$\overline{CO}$ (%)	-17.2	-14.6	-15.1	-8.6	-12.7	-10.0
$\overline{Q_{av}}$ (%)	-60.0	N/A	-68.4	-16.1	N/A	-75.5
$\overline{Q_P}$ (%)	-10.1	-14.6	-9.0	-6.9	-12.7	1.0
$\overline{dP}$ (%)	8.5	14.2	7.6	5.7	16.5	0.6
$\overline{dP_{pump}}$ (%)	0.9	1.4	0.9	0.5	2.5	0.4
PI_{Qp} (%)	15.1	19.8	13.3	13.3	-6.9	-6.5
$ratio_{PI}$ (%)	-21.9	-28.7	-19.6	-17.9	-6.2	8.0

Columns 3 to 7 refer to the simulation repeated (using baseline parameters) by individually modifying the following quantities to that used for the baseline scenario.

3.3.4 Comparison of Various Control Strategies

To evaluate the performance of various control strategies in response to exercise and HUT, changes in mean systemic arterial pressure, mean left atrial pressure, mean cardiac output, mean pump flow and mean aortic valve flow from rest to exercise, as well as from supine to 70^0 HUT were plotted in Figure 3.3 and Figure 3.4. For the constant $\overline{P_{la}}$ mode, the target mean left atrial pressure could not be reached during both exercise and supine conditions, and so the maximum pump speed threshold of 3000 rpm was imposed during exercise while the minimum pump speed threshold of 1600 rpm was imposed during 70^0 HUT.

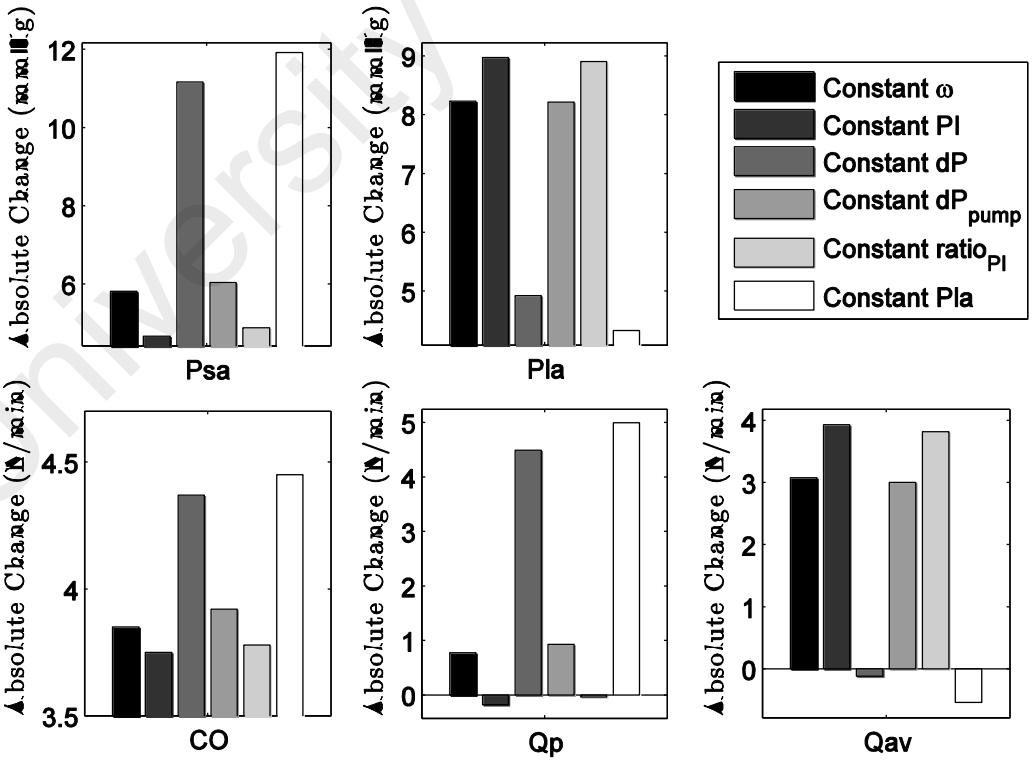

Figure 3.3: Comparison among the controllers rest to exercise

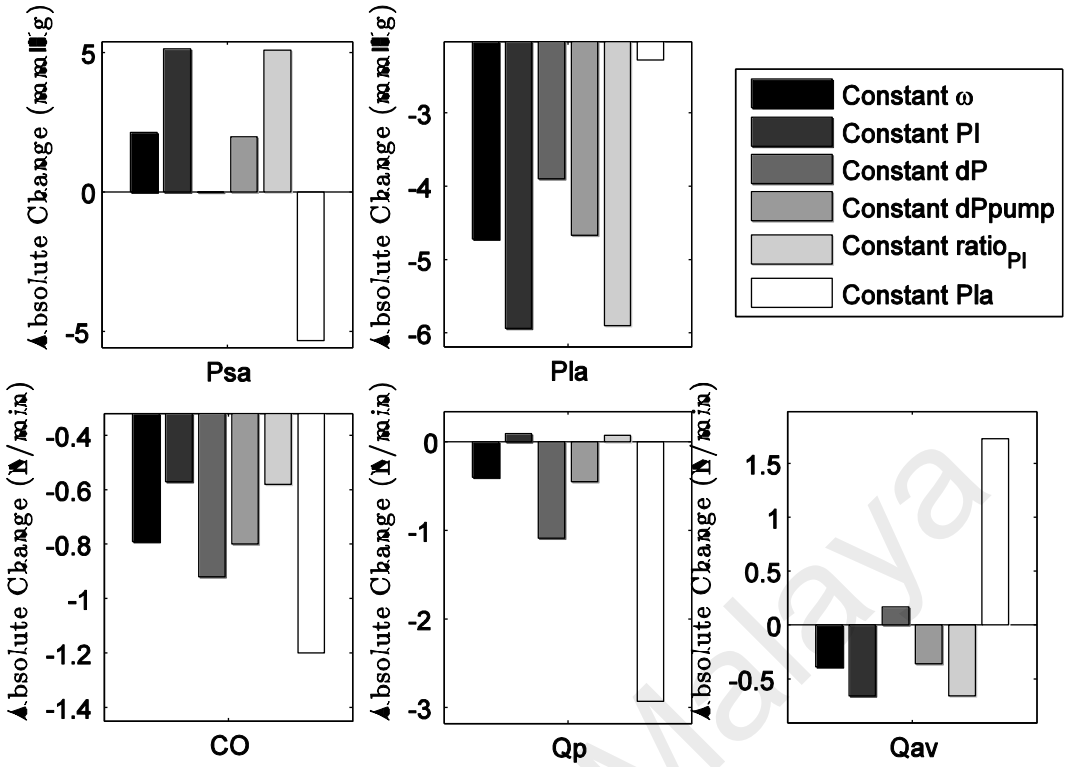

Figure 3.4: Comparison among the controllers from supine to 70^0 HUT.

With regards to the ability of the controllers to increase mean cardiac output during exercise, constant $\overline{P_{la}}$ mode yielded the best performance, with an increase of 4.45 L/min (ω = 3000 rpm), followed by constant $\overline{dP}$ (4.37 L/min, ω = 2891 rpm), constant $\overline{dP_{pump}}$ (3.92 L/min, ω = 2130 rpm), constant ω (3.85 L/min, ω = 2100 rpm), constant $ratio_{PI}$ (3.78 L/min, ω = 1953 rpm) and constant PI_{Qp} (3.75 L/min, ω = 1932 rpm), respectively. While same trend was observed for mean systemic arterial pressure (constant $\overline{P_{la}}$: 11.91 mmHg, constant $\overline{dP}$: 11.16 mmHg, constant $\overline{dP_{pump}}$: 6.04 mmHg, constant ω: 5.81 mmHg, constant $ratio_{PI}$: 4.88 mmHg, constant PI: 4.67 mmHg), opposite order was obtained for mean left atrial pressure (constant PI: 8.97 mmHg, constant $ratio_{PI}$: 8.90 mmHg, constant ω: 8.23 mmHg, constant $\overline{dP_{pump}}$: 8.21 mmHg, constant $\overline{dP}$: 4.92 mmHg, constant $\overline{P_{la}}$: 4.33 mmHg). Since the model produced a fall in PI_{Qp} and a rise in $ratio_{PI}$ from rest to exercise at a constant target speed, it follows that average pump speed must be reduced in these two controllers to maintain the target set point value. Consequently, a reduction

in mean pump flow was observed during exercise despite an overall increase in mean cardiac output (contributed by the native heart).

The avoidance of ventricular suction during a change in posture is mainly determined by the change in LV preload, which is reflected by the level of mean left atrial pressure. In this regard, constant $\overline{P_{la}}$ mode showed the least decrease in mean left atrial pressure at 70^0 HUT (-2.28 mmHg, ω = 1600 rpm), followed by constant $\overline{dP}$ (-3.90 mmHg, ω = 1963 rpm), constant $\overline{dP_{pump}}$ (-4.67 mmHg, ω = 2090 rpm), constant ω (-4.72 mmHg, ω = 2100 rpm), constant $ratio_{PI}$ (-5.90 mmHg, ω = 2231 rpm), and constant PI (-5.94 mmHg, ω = 2233 rpm), respectively. Nevertheless, compared to other controllers, constant $\overline{P_{la}}$ control produced the largest drop in mean cardiac output (-1.20 L/min) and mean systemic arterial pressure (-5.33 mmHg) at 70^0 HUT, which may cause circulatory instability. To the contrary, constant PI attained the greatest increase in mean systemic arterial pressure (5.14 mmHg) and the least fall in mean cardiac output (-0.54 L/min) at 70^0 HUT.

3.4 Discussion

Clinical observations under pump assistance showed an increase in cardiac output during exercise without variations in the pump control parameters (Akimoto et al., 1999; Jacquet et al., 2011; Salamonsen et al., 2013; Slaughter et al., 2009). Akimoto et al. (1999) observed an increase in pump flow during exercise under partial LVAD assist and hypothesized that this was caused by an increase in heart rate, which increased the ratio between systolic and diastolic period. However, we have demonstrated in our simulation results (Table 3.3) that since varying heart rate has not significantly altered differential pump pressure, mean pump flow remained relatively constant regardless of heart rate. Furthermore, we observed from our model simulations that exercise leads to an increase in mean cardiac output through greater contribution from the native heart compared to the assist device. Our observations are consistent with findings inpatients and in vivo animal experiments (Jacquet et al., 2011; Slaughter et al., 2009), which revealed that the

increase in total cardiac output during exercise was dominated by an increase in the aortic valve flow (contribution from the native heart) rather than the pump output. Factors contributing to an enhanced venous return and thus aortic valve flow during exercise include vasodilation mediated by production of local metabolites as well as the autonomic reflex response causing venoconstriction, increases in heart rate and left/right ventricular contractilities (Elisa Magosso et al., 2002).

The efficiency of the LVAD in improving exercise capacity in a heart failure patient has gained considerable interest in the field of rotary blood pumps. Since LV output contributes to a large percentage of increase in cardiac output during exercise, reduced cardiac reserve (i.e. reduced ability to augment LV end diastolic volume) caused by deterioration in the LV contractility severely affects the ability of the patient to increase cardiac output in response to exercise. Moreover, as observed clinically (Schima et al., 2006), the inherent flow adaptation to exercise was achieved at a cost of an elevated LV filling pressure, thereby imposing a considerable load on the lung. Apart from LV contractility, our simulation results (Table 3.3) also revealed that the autonomic reflex mechanism has a significant influence on the response of the IRBP-assisted patients to exercise. Desensitized effector response not only reduced the percentage increase in total cardiac output significantly, but also led to a marked reduction in the mean arterial pressure. Although total cardiac output increases automatically during exercise, we found that increasing mean pump speed has the ability to improve total cardiac output. This concurs with previous studies (Brassard et al., 2011; Salamonsen et al., 2013; Schima et al., 2006), which led to the development of automatic speed adaptation modes (Schima et al., 2006) aimed to further increase cardiac output and alleviate elevated filling pressures during strenuous exercise.

Sudden upright posture is associated with a redistribution of blood volume to the lower portion of the body, leading to a rapid fall in the central venous pressure, marked

reduction in the ventricular filling pressure and subsequently a decrease in the stroke volume (Einly Lim et al., 2013). Despite the concern regarding the possibility of ventricular suction occurring with reduced venous return, (K. Muthiah et al., 2013) has not observed suction events in their passive HUT studies performed on 9 IRBP-assisted patients. Similarly, even though our simulation results demonstrated a decrease in the left atrial pressure at 70^0 HUT (Table 3.4), the pressure was within an acceptable range and did not induce any suction event, partly due to the slightly elevated LV filling pressure in the supine position. As proposed by Pepi, Guazzi, Maltagliati, Berna, and Tamborini (2000), gradual preload reduction in congestive heart failure patients with elevated filling pressure enhances ventricular relaxation and diminishes the constraining effect of the pericardium, therefore yielding a much smaller decrease in the LV end diastolic volume, stroke volume, and cardiac output as compared to a normal subject. Our simulation results also revealed that desensitized reflex function imposed deleterious effects on the IRBP-assisted patients through a marked reduction in the mean arterial pressure upon HUT.

Comparing various control strategies, left atrial pressure control, having an infinite preload sensitivity, outperformed other control modes in its ability to increase cardiac output during exercise and minimize the fall in LV filling pressure during a reduction in preload (i.e. HUT). However, it is worth noting that while left atrial pressure control mode minimizes the risk of suction with upright posture, patients may experience a sharp reduction in arterial pressure, thus unable to maintain circulatory stability and prevent the clinical syndrome of orthostatic hypotension. This is further aggravated in patients with severe baroreflex impairment, considering the important role reflex mechanism plays in regulating arterial pressure during HUT. Furthermore, as proposed by (Nicholas Richard Gaddum et al., 2012), signal drift in currently available implantable pressure transducers hampers the applicability of left atrial pressure in long-term control systems.

In view of this, researchers have looked into ways to indirectly estimate preload (Arndt et al., 2008; Choi et al., 2001; Nicholas Richard Gaddum et al., 2012; Schima et al., 2006). One of the most popular noninvasive preload-based control strategies is PI control, based on the close relationship between pump flow or differential pressure pulsatility and LV filling pressure (Choi et al., 2001; Schima et al., 2006). In a study performed on five patients who underwent bicycle ergometry, Schima et al. (2006) demonstrated that exercise increased pulmonary venous return and thus pump flow pulsatility, with a simultaneous increase in pump flow (28%) at a constant target operating speed with an axial flow pump. An automatic, closed loop speed controller, which maintains the flow pulsatility, further increased pump flow but produced negligible change in the total cardiac output. Nevertheless, contradictory findings were observed in a multicenter study involving nine patients implanted with a centrifugal blood pump (Salamonsen et al., 2013), where pump speed pulsatility fell significantly during each maximal exercise study despite an increase in LV preload. Similarly, our simulation results revealed that pump flow pulsatility decreased during exercise despite an increase in the left atrial pressure, and increased at 70^0 HUT in spite of a reduction in the left atrial pressure. (Salamonsen et al., 2013) suggested that the reduction in pump speed pulsatility during exercise at a fixed speed setting might be due to a substantial increase in the pump flow. The difference in findings between these studies may be attributed to the difference in the pump characteristics (i.e. axial vs. centrifugal), where pump flow pulsatility has been shown to not only depend on venous return, but also on the slope of the pump differential pressure versus pump flow (H-Q) curve at which it is operating (Choi et al., 2007). Furthermore, pump flow pulsatility has demonstrated more correspondence with changes in LV filling during the aortic valve non-opening phase, and lack sensitivities during aortic valve opening (Salamonsen et al., 2012). Coincidentally, our model simulations revealed that directionally opposite changes in pump flow pulsatility occurred at a high pump speed

when the aortic valve is mostly closed, with an increase during exercise and a decrease with HUT, which follows that of the LV filling pressure (reflected by left atrial pressure). On the other hand, $ratio_{PI}$ controller, previously proposed by Salamonsen et al. (2012), showed very similar performance with PI control. This is as expected since ratioPI controller operates by relating pump flow output to pump flow pulsatility values. Furthermore, our simulation results revealed a close correlation between PI_{Qp} and $ratio_{PI}$ in all simulated conditions. As suggested by Salamonsen et al. (2013), both PI and $ratio_{PI}$ controller would respond to the increase in pump flow and associated fall in pump flow pulsatility during exercise by reducing pump speed, thus leading to an undesirable reduction in the increase of total cardiac output.

Maintaining a constant average pressure difference between the left ventricle and the aorta demonstrated superior performance over PI, $ratio_{PI}$ and constant speed controller, where it substantially increases total cardiac output while reducing LV filling pressure during exercise, and minimizes the reduction in LV filling pressure during upright posture. Compared to the left atrial pressure control mode which requires excessive variation in pump speed to achieve a target set point, constant $\overline{dP}$ controller, which takes into account the level of the mean arterial pressure, is more stable as it does not produce a substantial fall in the mean arterial pressure as that occurring in the left atrial pressure control mode upon upright posture. Meanwhile, maintaining a constant average differential pump pressure performs similarly to constant speed control, mainly due to the relatively flat H-Q curve for a centrifugal blood pump. The observed significant differences in performance between the $\overline{dP}$ and the $\overline{dP_{pump}}$ controllers can be explained by the substantial pressure drop across the cannula, especially under the higher pump flow conditions.

To date, most commercially available IRBPs operate at a constant speed level determined by the physician. As demonstrated in the present study and reported in the published literature (Jacquet et al., 2011; Salamonsen et al., 2013; Schima et al., 2006), although there is an inherent adaptation of pump flow and native cardiac output to physiologic demand at constant pump speed, this occurs at an expense of increased loading on the lung and the left ventricle. Among the six controllers we evaluated, our simulation results revealed that maintaining a constant average pressure difference between the aorta and the left atrium appears to be the most robust. However, it is worth noting that except for the constant speed controller, successful clinical implementation of the other controllers relies heavily on the estimation accuracies of pressures and flow, due to the issues of signal drift and thrombus occlusion associated with currently available implantable flow and pressure transducers. Blood viscosity as well as native heart interaction has been reported as potential factors, which affect the accuracy of the flow and head estimation models (Tagusari et al., 1998). Apart from that, previous study has also revealed a large difference between dP and pump differential pressure at end systole, especially under high pump flow conditions, due to the dependency of the pressure drop across the cannula with pump flow. Therefore, in constant dP control, a reliable model describing cannula pressure drop has to be developed to derive dP from the estimated pump differential pressure.

3.5 Limitations

Comparison results of the various controllers concerning their response to exercise and HUT were based on a moderate heart failure condition (NYHA Class II & III) rather than a more severe heart failure scenario, where the aortic valve is closed most of the time at rest. Since pump flow pulsatility demonstrated more correspondences with changes in LV filling during the aortic valve non-opening phase (Salamonsen et al., 2012), slight improvement is to be expected for the constant PI controller under this condition. This is

confirmed by our additional simulations (not shown) assessing the performance of the controllers at lower LV contractility and higher pump speed, which demonstrated that the rankings of the individual controller were not substantially affected by this new set of model parameters, except for a minor improvement in the constant PI controller. In terms of exercise response, the constant PI controller climbed to the forth position in its ability to increase pump flow and cardiac output, surpassing the constant speed controller. However, it is worth noting that even in patients with severe heart failure condition, opening of the aortic valve can frequently be observed, thus affecting the sensitivities of the flow pulsatility to LV filling (Brassard et al., 2011; Mancini et al., 1998; Salamonsen et al., 2013). Since the present study focused on the steady state response of the IRBP-assisted patients to exercise and HUT, evaluation results comparing the performance of the previously proposed controllers were based on steady state results. The responsiveness of the various controllers in the face of sudden physiological perturbations has not been taken into consideration. Future studies should also look into the transient changes of the important hemodynamic variables from rest to exercise, as well as from supine to HUT.

3.6 Conclusion

We have investigated the response of the IRBP-assisted patients to exercise and HUT, as well as the effect of alterations in the model parameter values on this response, using validated heart pump interaction models. Furthermore, the performance of a number of previously proposed controllers were evaluated with regards to their ability to increase cardiac output during exercise and maintaining circulatory stability upon HUT. It was observed that the increase in cardiac output during exercise was dominated by an increase in the aortic valve flow rather than pump flow. Increasing pump speed further improves total cardiac output and reduces elevated filling pressures, thus improving exercise capacity in the IRBP-assisted patients. On the other hand, due to elevated supine filling

pressure, reduced venous return associated with upright posture has not shown to induce LV suction. Among various control strategies, LAP control outperformed other control modes in its ability to increase cardiac output during exercise. However, it causes a fall in the mean arterial pressure upon HUT, which may lead to cases of orthostatic hypotension and affect circulatory stability. To the contrary, constant $\overline{dP}$control, which takes into account both, left atrial and arterial pressure, demonstrated superior performance under both exercise and HUT scenarios, potentially due to the preload and afterload sensitivity of IRBPs. PI and $ratio_{PI}$ control, on the other hand, performed poorly during exercise and HUT, due to their strong dependency on the pump operating point.

In particular, pump flow pulsatility lacks sensitivity to venous return (reflected by mean left atrial pressure) during the aortic valve-opening phase. The importance of the reflex mechanism in determining the response of the IRBP-assisted patients to exercise and postural changes is highlighted by our simulation results where the desensitized reflex response attenuates the percentage increase in cardiac output during exercise and substantially reduces arterial pressure upon HUT.

CHAPTER 4: PRELOAD-BASED STARLING-LIKE CONTROL FOR ROTARY BLOOD PUMPS

4.1 Introduction

Preload sensitivity of the ventricular myocardium is an essential requirement for the Frank-Starling mechanism by which the left ventricular end-diastolic pressure controls the force of contraction of the left ventricle in proportion to the blood flow received from the right heart and pulmonary circulation. Unfortunately, implantable rotary blood pumps which are currently the preferred technology for assisting the failing LV do not have sufficient preload sensitivity to perform this task automatically (Salamonsen et al., 2011). It would seem logical therefore, that LV preload be selected as the feedback variable of choice in physiological control systems designed for IRBPs. However, this has not happened seemingly because LV preload is not easily estimated nor measured. In a comprehensive review conducted recently, A.-H. H. AlOmari et al. (2013) reported few instances of physiological control based on invasive pressure measurements (Bullister, Reich, & Sluetz, 2002; G. A. Giridharan & Skliar, 2002; Saito et al., 2010; Wu et al., 2003).

On the other hand, there is a widespread view that currently available implantable pressure transducers are rendered virtually unusable due to a range of problems. These include limited reliability, drifts in transducers' response over time, and the anatomical distortion they present to pump inlet cannula, resulting in unwanted flow turbulence and associated clotting disorders. As an alternative, there has been much interest in non-invasive estimation of pump pulsatility measures derived from various pump parameters, either as a display to aid manual adjustment of pump speed (Esmore et al., 2008; Farrar, Bourque, Dague, Cotter, & Poirier, 2007; Letsou, Reverdin, & Frazier, 2013; Slaughter et al., 2009), or as a feedback variable for physiological controllers (Arndt, Nüsser, & Lampe, 2010; M. A. Bakouri et al., 2014; Choi et al., 2007; Endo et al., 2002; Salamonsen

et al., 2012). The theoretical link between pulsatility (the difference between maximum and minimum points on a waveform measured over a cardiac cycle) and PLVED is via the effect of PLVED on the left ventricular stroke work, which in turn affects pulsatility. Pulsatility measures reported include pump flow pulsatility, pressure head pulsatility, speed pulsatility, and motor current pulsatility.

New technology in blood pressure measurement however brings with it the promise of greater biocompatibility and stability over time. In a multicenter study, Troughton et al. (2011) reported that in the Heart Pod pressure transducer, after an initial 'bedding in' process in the left atrium, the pressure response was essentially stable over the study period of four years. In addition, they reported an overall 95% freedom from failure over two years, 88% over four years and 100% freedom from failure in the last 41 consecutive patients. More recently, pressure transducers based on optical fibers have been described (Konieczny et al., 2010; Zhou, Yang, Liu, Cysyk, & Zheng, 2012), which may achieve the required stability in the constant temperature environment of the heart and are small enough to be embedded in the walls of the pump inlet and outlet cannulae without anatomical distortion.

It is therefore of interest to examine the performance of preload control in comparison with PI_{Qp} control and constant speed operation (prevalent in the majority of IRBPs currently implanted clinically). If preload control was shown to be functionally superior to both PI_{Qp} and constant speed modes, this might provide the impetus for further development of preload-based Starling-like control. We report such a study using a sophisticated and experimentally validated computer model of the human circulation and the VentrAssist^{TM} left ventricular assist device.

4.2 Methods

4.2.1 Description of the Heart-Pump Interaction Model

The heart-pump interaction model used in the present study has recently been developed and validated to investigate the response of IRBP-assisted patients to exercise and head up tilt (Einly Lim et al., 2015). The basic structure of the model consists of the left and right sides of the heart, the pulmonary and systemic circulations, as well as the LVAD. The LVAD component includes the description of the VentrAssist^{TM} LVAD operating between 1600 and 3000 rpm, as well as the inlet and outlet cannula. Furthermore, the model takes into account various important items such as the arterial and cardiopulmonary reflexes, local metabolic vasodilatation in the active muscles, the auto-regulation mechanism in the lower body, as well as the muscle pump. The model was implemented using the SIMULINK toolbox in MATLAB (The Math Works, Inc., Natick, MA, USA). A detailed description of the model validation procedures together with the optimized model parameter values can be obtained from (Einly Lim et al., 2013; Einly Lim et al., 2010; Einly Lim et al., 2012a, 2012b; Einly Lim et al., 2015).

4.2.2 Description of the Control Systems

4.2.2.1 Preload-Based Starling-Like Controller

The immediate response of the preload controller emulates the Frank-Starling control mechanism of the natural heart, which was first identified by Starling and Visscher Starling and Visscher (1927) as a sigmoid relationship between LV stroke work and PLVED. This was subsequently modified by A.C. Guyton (1963) to give a similar sigmoid relationship between LV flow and PLVED.

The Frank-Starling curve forms the basis of the control line (C_{Ln}), as illustrated in Figure **4.1** (A). In the proposed preload controller, C_{Ln} is generated by a third order polynomial function (4.1) fitted directly to Guyton's data (A.C. Guyton, 1963), which

relates desired mean pump flow to PLVED. A scaling factor (K) is also added to provide a means of altering sensitivity of the pump to changes in PLVED, which makes (4.1) adaptive with different patients' preload sensitivity (Nicholas R. Gaddum et al., 2014; A C Guyton & Hall, 2005).

$$\overline{Q_{P_{ref}}} = (0.0003 * PLVED^3 - 0.0276 * PLVED^2 + 0.9315 * PLVED - 0.0928) * K \qquad (4.1)$$

where PLVED represents the LV end diastolic pressure provided by the numerical CVS model. In our study, PLVED is automatically sampled at end diastole of each heart cycle by the model and then fed to the controller. Although the full controller is able to adapt to longer term changes in the circulation by adjustment of the scaling factor, this communication deals only with the immediate response of the controller in which changes in PLVED cause migration of the operating point to different positions on C_{Ln}.

Figure **4.1** (A) gives an overall view of how the preload controller functions in a diagrammatic form. As changes in state of the subject evolve (transition from state S_1 to states S_2 or S_3), these changes are tracked by the controller which then returns the operating point back to the control line. For example, the white circle in Figure **4.1** (A) gives the position of the original operating point, while the grey circles give its position after a deviation from the control line, induced by changes in the system state from S_1 to S_2 or S_3. Figure **4.1** (B) presents details on how the controller returns the operating point back to C_{Ln} along a linear path in a series of steps (indicated by the small arrows), until it settles to a new position located at the intersections between C_{Ln} and the altered system states (indicated by black circles). Thus, deviations of the operating point from C_{Ln} either to the right or to left side of the control line move the operating point upwards or downwards along C_{Ln}.

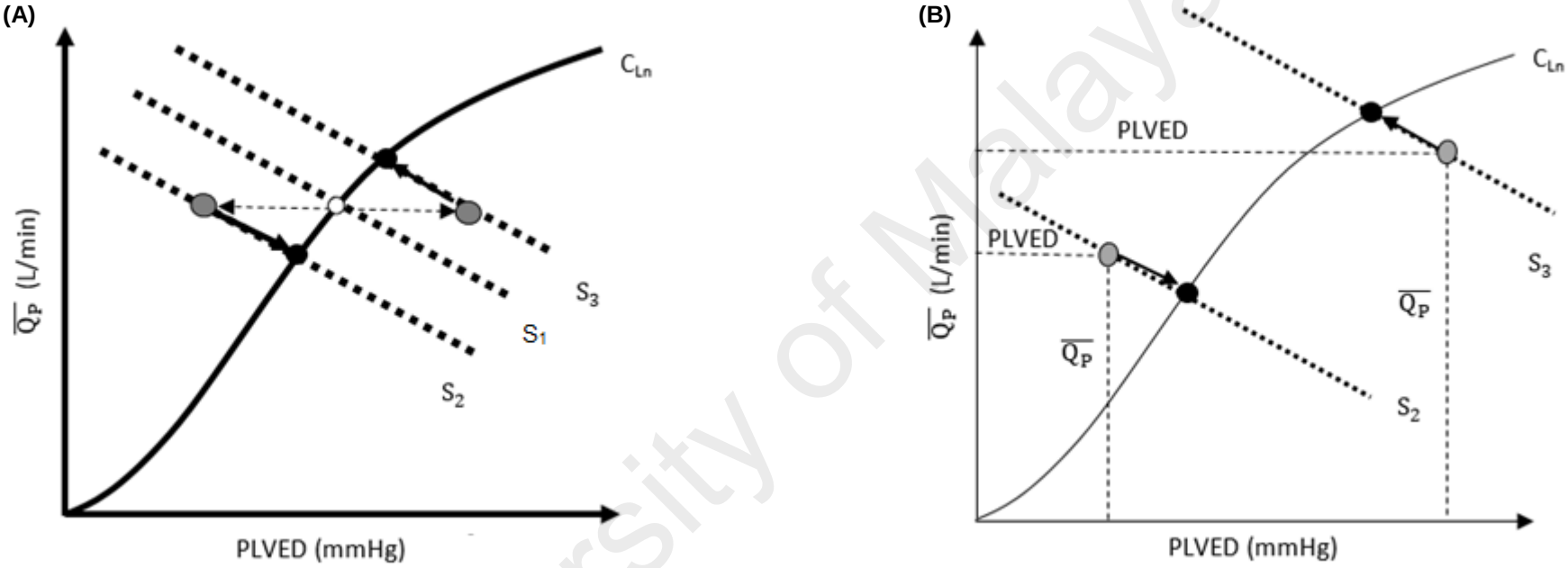

Figure 4.1: (A) and (B): Schematic describing the preload-based Starling-like control. White circle, position of operating point (current combination of PLVED and $\overline{Q_P}$) before a change of state; Grey circles, position of operating points after changes in states; Black circles, position of operating points upon arriving at the new steady state located at the intersection between the control line and the new system line. The controller drives the changes in the operating points along the path indicated by the arrows along the new system line.

4.2.2.2 Pulsatility Controller

The pulsatility controller, on the other hand, relates the desired mean pump flow with pump flow pulsatility (PI_{QP}), defined as the absolute difference between the maximum and the minimum pump flow (Nicholas R. Gaddum et al., 2014) over a heartbeat. Instead of being curvilinear, the control line for the pulsatility controller is linear (4.2) as derived by Salamonsen et al., with the gradient defined by the tangent of the angle (θ) it makes with the pulsatility axis in radians. Similar to preload control, reference changes are applied by movements of the operating point up or down C_{Ln}. However, since C_{Ln} is linear, the controller is able to force the deviated operating point back to the appropriate position on C_{Ln} along a circular path, as defined by (4.2) (Salamonsen et al., 2012).

$$\overline{Q_{P_{ref}}} = \left(\sqrt{(\overline{Q_P})^2 + \left(PI_{QP}\right)^2}\right) * \sin(\theta) \tag{4.2}$$

where $\overline{Q_P}$ represents the desired average pump flow, $\overline{Q_P}$ is the mean pump flow provided by the model, and PI_{QP} is the pump flow pulsatility. More detailed descriptions of the pulsatility controller can be obtained from (Salamonsen et al., 2012) and (M. A. Bakouri et al., 2014).

4.2.3 Simulation Protocols

In order to determine the gradient for the return path to the control line, model simulations were performed for the baseline, exercise, blood loss and reduced LV contractility conditions, in which mean pump speed ($\bar{\omega}$) was increased from 1600 rpm to 3000 rpm in 100 rpm increments. Mean flow through the aortic valve and pump as well as PLVED were obtained from the model, with the relationship between $\overline{Q_P}$ and PLVED plotted in Figure 4.2. System gradients with aortic valve (AV) open and AV closed were calculated separately for each test scenario, and the mean value for each AV state was then selected as the gradients of the return path.

It can be shown from Table **4.1** that although system lines for the different test scenarios showed wide displacements among each other, their gradients grouped according to whether the aortic valve was opening or closing were similar.

In normal clinical practice, RBP speed is set to stop the aortic valve from opening in order to provide full assist to the patients (Arndt et al., 2008). The aortic valve opening condition is only used while attempting to wean a patient from the pump or used intermittently to prevent inappropriate sealing of the aortic valve cups. In order to determine the optimal scaling factor (K) for C_{Ln}, another set of simulations was conducted in the baseline state, where K was increased from a basal value of 0.2 to the maximal value of 2.3 in 0.1 increments. Blood flow through the aortic valve was obtained from the model to indicate whether the aortic valve was opening or closing. The optimal scaling factor was identified as the minimum value of K that allowed the aortic valve to be closed in the baseline condition. In the present study, K value was set to 1.0, while the corresponding control line of the pulsatility controller had a gradient (angle),θ of 62^0.

Both pulsatility and preload-based Starling-like control modes were then implemented separately with a proportional-integral-derivative controller (Figure 4.3), which adjusted the pulse-width-modulation (PWM) signal to generate the desired $\overline{Q_P}$. The transfer function of the PID controller is defined in (4.3), and was discretized automatically by MATLAB/SIMULINK using a sampling period of 0.002 s.

$$G(S_l) = K_P + \frac{K_I}{S_l} + K_D S_l \qquad (4.3)$$

S_l stands for complex number frequency, K_P, K_I and K_D represent the proportional, integral and derivative gains of the controller, respectively (Table 4.2). The values of these constant gains were tuned manually to achieve a 5% settling time of 10 s with minimal overshoot (i.e. a maximum overshoot within 10 % of the final value)

(Salamonsen et al., 2012). In each iteration, the PID controller compared the mean pump flow obtained from the model with the desired mean pump flow, and moved the operating point back to the control line following the selected return path.

Table 4.1: Gradients for return lines (ratio of mean pump flow to PLVED) for baseline and three test scenarios, i.e. exercise, blood loss, and reduced LV contractility scenario.

System States	Gradient with AV Open (L/min/mmHg)	Gradient with AV Closed (L/min/mmHg)
Baseline	-0.64	-0.13
Exercise	-0.92	---
Blood Loss	-0.94	-0.19
Low LVC	---	-0.14
Mean	-0.83	-0.15

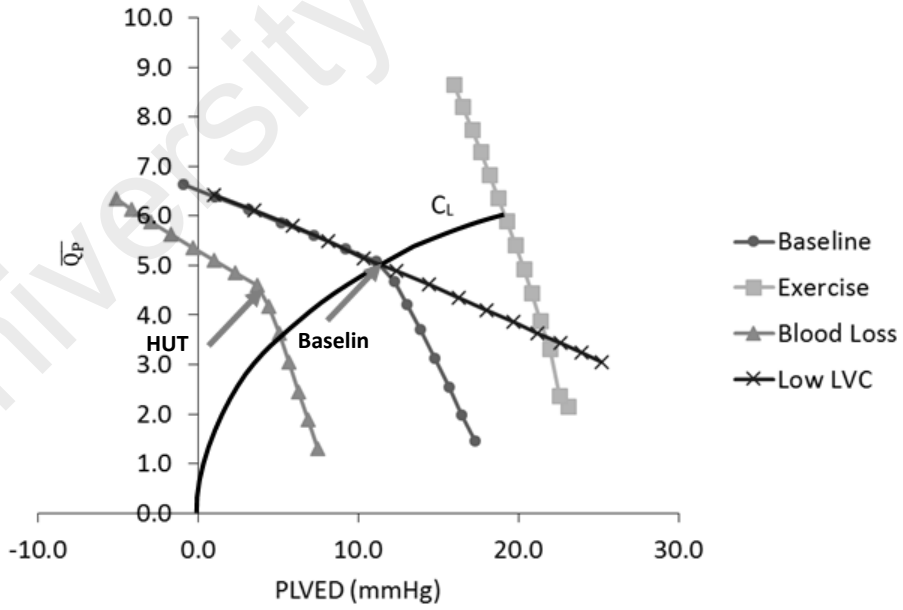

Figure 4.2: System response to variations in mean pump flow for baseline and three test conditions. Figure also shows the superimposed control line (C_{Ln}), where the minimum scaling factor (K) that allows the aortic valve to be closed in the baseline condition was chosen. Arrows indicate points where the aortic valve starts to open for Baseline and HUT scenarios.

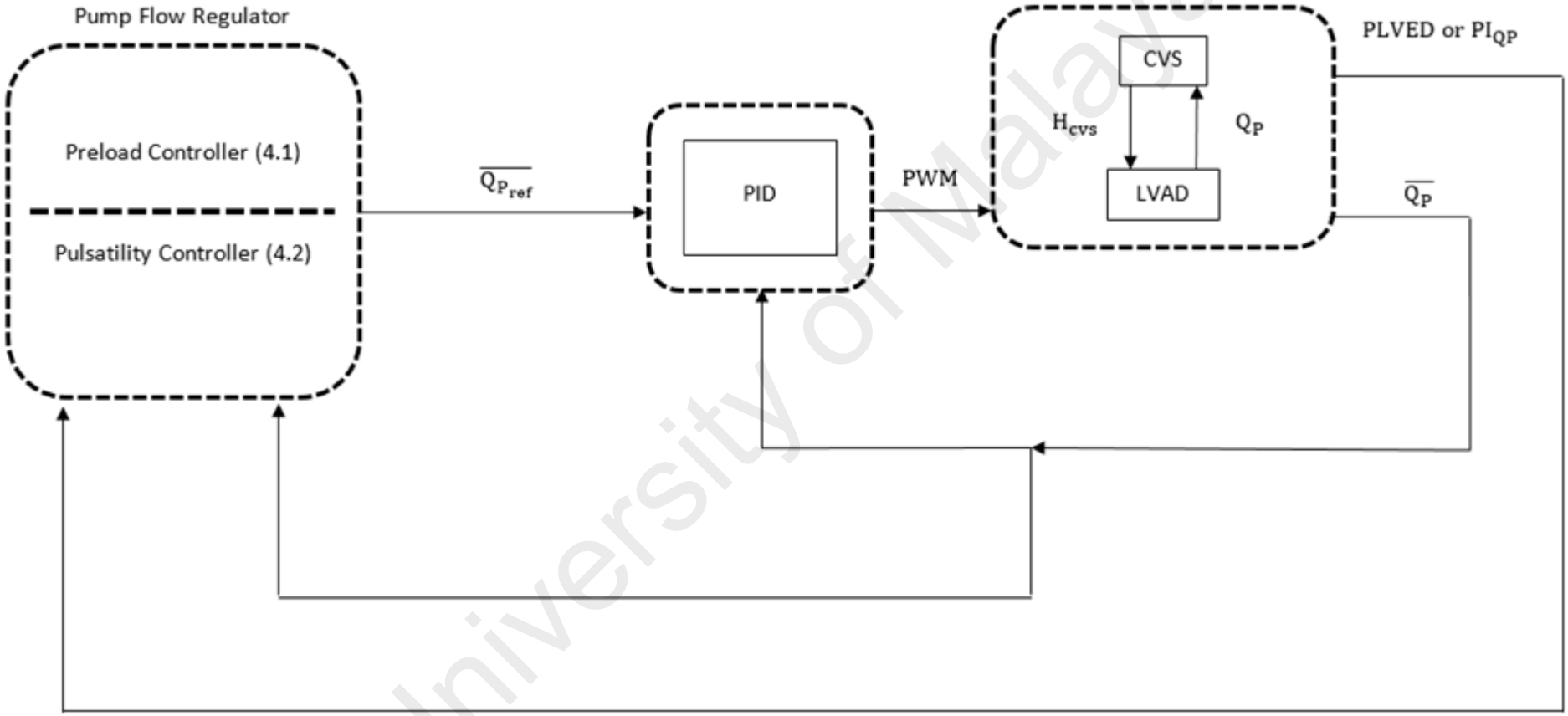

Figure 4.3: Block diagram of the PID controller for closed loop studies.

Table 4.2: PID gains used for both preload and pulsatility controlling methods.

Control constants	Gains
K_P	0.28
K_I	0.22
K_D	0.05

K_P, Proportional gain; K_I, Integral Gain; K_D, Derivative Gain.

In addition to the baseline state at rest, three other scenarios, including exercise, blood loss and reduced LV contractility were simulated. For the exercise simulation, a relative intensity of 0.55 was chosen to represent the maximal exercise condition as defined by Lim et al. (Einly Lim et al., 2015). To simulate blood loss and reduced LV contractility conditions, total blood volume (V_t) and maximum LV end systolic elastance ($E_{max,lv}$) were reduced by 1000 mL and 78%, respectively. The steady-state performance of both preload and pulsatility control were compared to each other as well as with the constant speed mode. For all simulations, we waited for the hemodynamic variables to settle to a steady state condition before transitioning from the baseline into one of the three test conditions. The simulation was then continued for a sufficient period to allow the control modes to achieve a post transition steady state.

4.3 Results

The performance of the three control methods was compared by observing the changes in mean pump flow, mean cardiac output, mean aortic valve flow, mean systemic arterial pressure (MAP), and mean left atrial pressure from baseline to exercise (Figure 4.4), hemorrhage (Figure 4.5) and reduced left cardiac contractility (Figure 4.6) scenario.

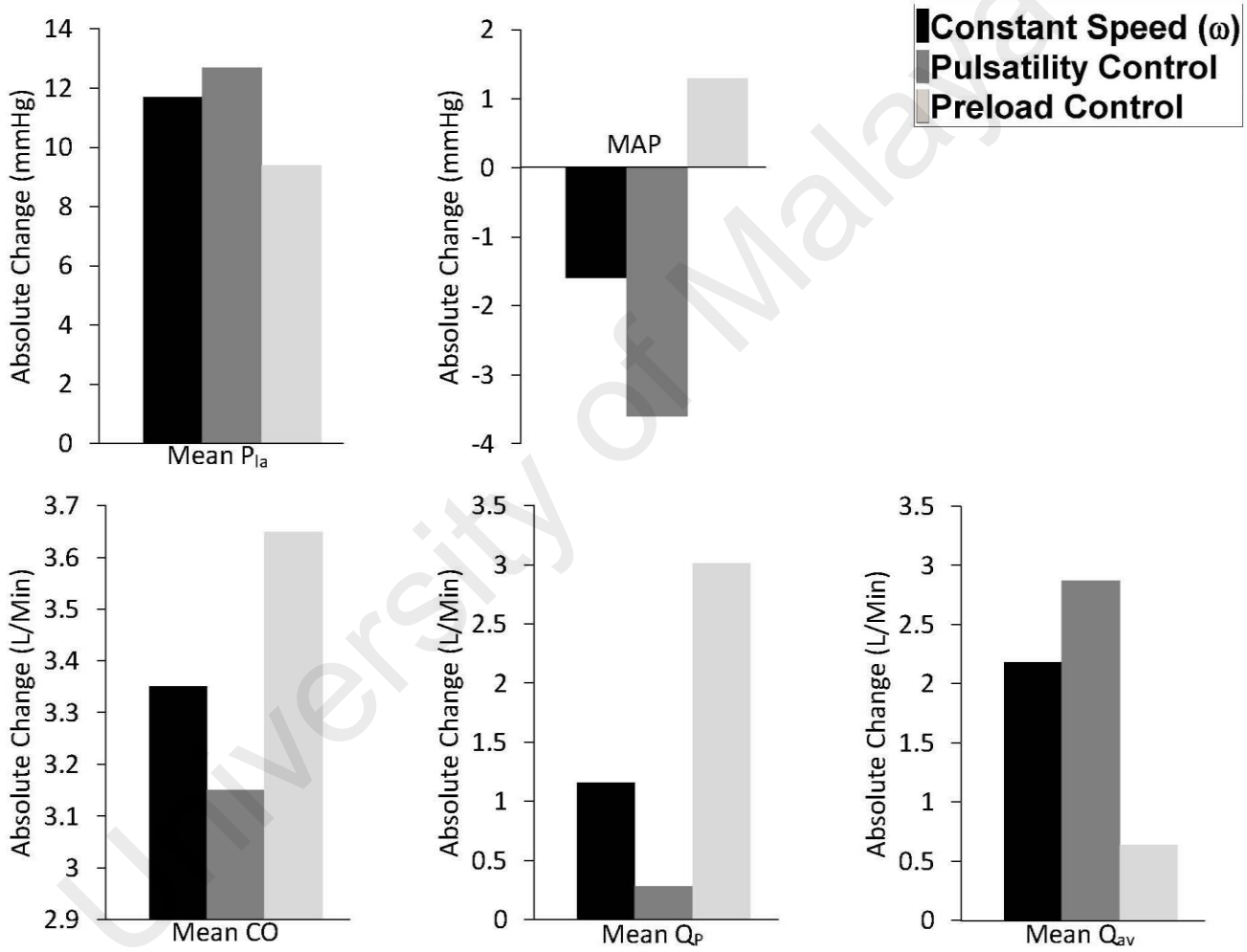

Figure 4.4: Comparison of preload controller vs. pulsatility and constant speed modes from baseline to exercise (absolute value changes).

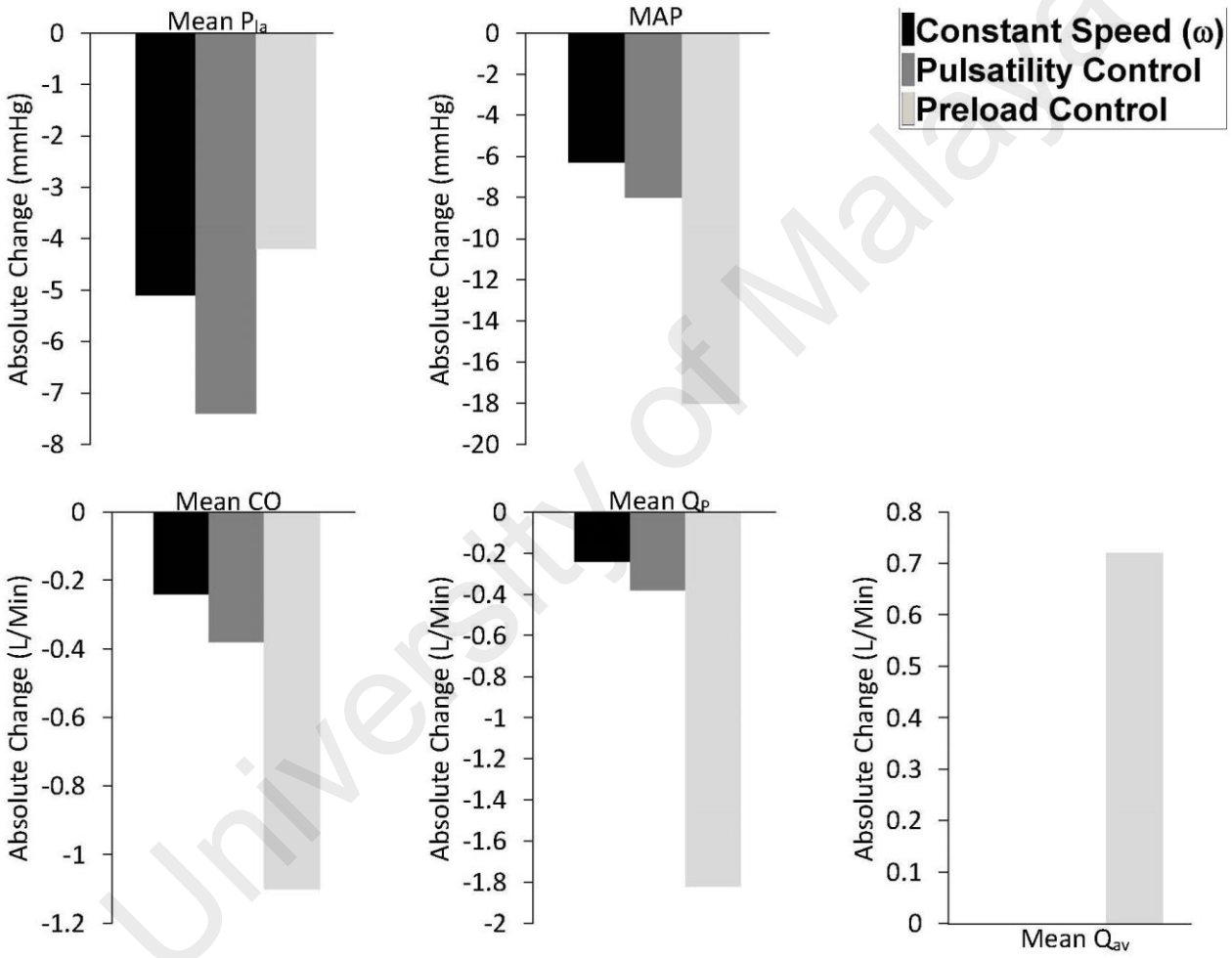

Figure 4.5: Comparison of preload controller vs. pulsatility and constant speed modes from baseline to hemorrhage (absolute value changes).

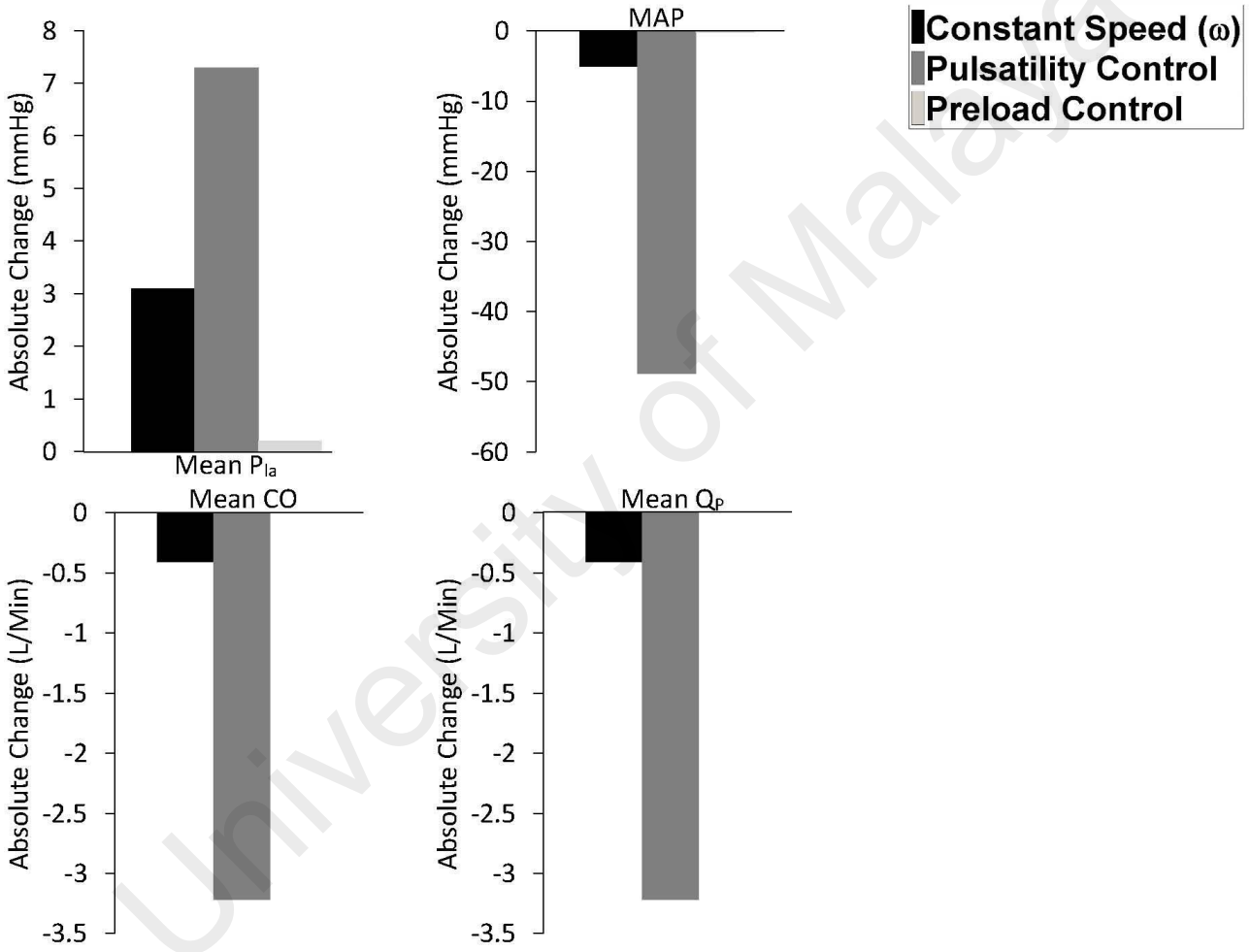

Figure 4.6: Comparison of preload controller vs. pulsatility and constant speed modes from baseline to reduced left ventricular contractility scenario (absolute value changes).

Results indicate that during exercise, preload control was the best controlling modality, causing a 55% increase in $\overline{Q_P}$ and a 66% increase in $\overline{CO}$. This was associated with the lowest values for both PLVED (16.1 mmHg) and $\overline{Q_{av}}$ (0.64 L/min) among the three controllers, indicating minimum load on the LV, as depicted in Table 4.3 and Figure 4.4. Pulsatility control gave the poorest performance among the three control modes, with a mere increase of 5% in $\overline{Q_P}$, associated with a fall in $\bar{\omega}$. This was due to an increase of 21% in $\overline{Q_P}$ at constant speed ($\bar{\omega}$=2570 rpm), to which pulsatility was very sensitive, and the resultant failure of PI_{QP} to rise in proportion to the degree of exercise. This results in an increase in the LV stroke work index. Consequently, pulsatility control was associated with the highest $\overline{Q_{av}}$ (2.87 L/min) during exercise and the maximum increase in PLVED (168% rise).

Table 4.3: Model simulated hemodynamic data at baseline (rest) and exercise with different controllers.

Variable	**Unit**	**Constant $\bar{\omega}$**		**Constant ratio$_{PI}$**		**Preload-Based**	
		Rest	**Exercise**	**Rest**	**Exercise**	**Rest**	**Exercise**
$\bar{\omega}$	RPM	2570	2570	2585	2410	2570	2980
MAP	mmHg	102.4	100.8	103.4	99.8	102.4	103.7
$\overline{P_{la}}$	mmHg	9.5	21.2	8.9	21.6	9.6	19.6
PLVED	mmHg	7.8	18.7	7.2	19.3	8.0	16.1
$\overline{CO}$	L/min	5.54	8.89	5.62	8.77	5.52	9.17
$\overline{Q_P}$	L/min	5.54	6.70	5.62	5.90	5.52	8.53
PI_{Qp}	L/min	2.90	2.90	3.07	3.28	3.05	2.68
$\overline{Q_{av}}$	L/min	0.00	2.18	0.00	2.87	0.00	0.64

The challenge for an LVAD during a blood loss scenario is to avoid LV suction by reducing its flow output sufficiently to match a substantial reduction in the right ventricular preload and subsequent reduction in the delivery from the RV. In our model simulation, LV suction was indicated by a negative PLVED (i.e. $PLVED \leq 0$). As observed in our previous animal experimental studies (E Lim, Alomari, Savkin, & Lovell, 2009), LV suction involves obstruction of the pump inlet cannula due to suction of the LV walls at relatively high pump speeds. In this state, LV volume is low, resulting in steady near zero LV pressure and negative pump inlet pressure throughout the cardiac cycle. Our observations were consistent with Karantonis, Lovell, Ayre, Mason, and Cloherty (2006) and Boston et al. (2003), who suggested that LV suction caused a negative pressure in the LV, and thus it is imperative to maintain left atrial pressure (substitute of PLVED) above 0 mmHg to avoid LV suction. Based on this suction indicator and results in Table 4.4 and Figure 4.5, preload control was the only modality that was able to reduce flow sufficiently to maintain an adequate safety margin against LV suction. PLVED was 4.9 mmHg for preload control after a reduction in the total blood volume, in contrast to near zero PLVEDs for constant speed mode (0.2 mmHg) and pulsatility control mode (0.4 mmHg). Baroreceptor reflexes, which the model was equipped with, were sufficient to avoid abrupt falls in the mean arterial pressure, even though this particular parameter was not specifically addressed in the controlling policy. MAP was reduced from 102 mmHg to 84 mmHg upon blood loss, which is more than sufficient to maintain auto-regulation of flow by the body tissues (minimum threshold = 60 mmHg) (Berne, 1981).

Table 4.4: Model simulated hemodynamic data at baseline (rest) and with blood-loss for different controllers.

Variable	Unit	Constant $\bar{\omega}$		Constant ratio$_{PI}$		Preload-Based	
		Rest	**Exercise**	**Rest**	**Exercise**	**Rest**	**Exercise**
$\bar{\omega}$	RPM	2570	2570	2585	2550	2570	2115
MAP	mmHg	102.4	96.1	103.4	95.4	102.4	84.4
$\overline{P_{la}}$	mmHg	9.5	4.4	8.9	1.5	9.6	5.4
PLVED	mmHg	7.8	0.2	7.2	0.4	8.0	4.9
$\overline{CO}$	L/min	5.54	5.30	5.62	5.24	5.52	4.42
$\overline{Q_P}$	L/min	5.54	5.30	5.62	5.24	5.52	3.7
PI_{Qp}	L/min	2.90	2.54	3.07	2.87	3.05	4.06
$\overline{Q_{av}}$	L/min	0.00	0.00	0.00	0.00	0.00	0.72

Preload control was able to maintain an adequate $\overline{CO}$ despite a reduction in LV contractility, where $\overline{Q_P}$ and MAP remained constant at 5.52 L/min and at 102 mmHg respectively, without a major rise in PLVED (Table 4.5 and Figure 4.6). To the contrary, with pulsatility control, $\overline{Q_P}$ (equivalent to $\overline{CO}$ as aortic valve was closed) fell to the non-viable level of 2.4 L/min and MAP to 51 mmHg. In doing so, it was less supportive to the circulation than the constant speed mode, which maintained an average pump flow of 5.13 L/min and MAP of 97 mmHg.

Table 4.5: Model simulated hemodynamic data at baseline (rest) and fall in left ventricular contractility.

Variable	Unit	Constant $\bar{\omega}$		Constant ratio$_{PI}$		Preload-Based	
		Rest	**Exercise**	**Rest**	**Exercise**	**Rest**	**Exercise**
$\bar{\omega}$	RPM	2570	2570	2585	1575	2570	2700
MAP	mmHg	102.4	97.4	103.4	54.5	102.4	102.2
$\overline{P_{la}}$	mmHg	9.5	12.6	8.9	16.2	9.6	9.8
PLVED	mmHg	7.8	11.0	7.2	15.7	8.0	8.0
$\overline{CO}$	L/min	5.54	5.13	5.62	2.40	5.52	5.52
$\overline{Q_P}$	L/min	5.54	5.13	5.62	2.40	5.52	5.52
PI_{Qp}	L/min	2.90	0.52	3.07	0.80	3.05	0.57
$\overline{Q_{av}}$	L/min	0.00	0.00	0.00	0.00	0.00	0.00

4.4 Discussion

This numerical simulation study clearly establishes the utility of a single preload-based Starling-like control line to control $\overline{Q_P}$ appropriately in the transition from rest to three simulated scenarios: vigorous exercise, severe blood loss and a major fall in LV contractility. It consistently outperformed the pulsatility controller, whose performance was inferior even to the fixed speed mode. These results agree with a recent study reported by Lim et al. (Einly Lim et al., 2015), which highlighted the deficiencies of the pulsatility control in exercise and 70^0 head-up-tilt.

4.4.1 Physiological Mechanisms

On a theoretical basis, there are sound physiological mechanisms underlying these results. Pump pulsatility (flow, current, pressure gradient, or speed) is a consequence of LV

contraction whereas LV preload is one of the determinants of LV contraction. With severe LV failure, as is the case for all LVAD recipients, the LV does not have the ability to induce major changes in pulsatility. Therefore, the dynamic range of the pulsatility index is small, and consequently its ability as a control input is limited. In the extreme case where LV contractility is zero, pulsatility control is not feasible. By contrast, LV preload increases as LV failure progresses and its dynamic range is wide in the presence of LVAD.

These fundamental characteristics account for the superiority of the preload control in all three test simulations. In addition, other mechanisms come into play with each of the three test states. With exercise, the natural increase in $\overline{Q_P}$ during exercise at constant speed severely reduces PI_{Qp}. Consequently, when the operating point is returned to the control line in pulsatility control, there is an actual decrease in mean pump speed as reported by Salamonsen et al. (2013). Preload is much less sensitive to this effect and progressively rises with increasing exercise intensity, thus accounting for the observed superiority of preload control.

In blood loss, because of the low dynamic range of the pulsatility index, the ability of the pulsatility control to reduce $\overline{Q_P}$ effectively is limited and thus the risk of LV suction is greater. Another major problem with pulsatility control is that PI_{Qp}, being a consequence of the LV stroke work, is unable to distinguish between blood volume loss and a fall in LV contractility since PI_{Qp} falls in both occasions. This is a major disadvantage as the role of the LVAD in the two conditions should be very different. By contrast, preload control responds to both conditions effectively, with a loss of blood volume causing a reduction in $\overline{Q_P}$ to avoid LV suction while a reduction in LV contractility causing an opposite effect to provide sufficient flow to the systemic circulation.

By emulating the Frank-Starling control mechanism of the natural heart, preload-based Starling-like control is able to synchronize LV and right ventricular outputs irrespective of variations in venous return (Salamonsen et al., 2012). Compared to constant pulsatility and constant speed modes (Table 4.3 and Table 4.5), preload control produced the least increase in PLVED during exercise and reduced LV contractility scenarios, thus reducing the chances of pulmonary congestion, which may lead to right-sided circulatory failure in the long term (Haddad, Doyle, Murphy, & Hunt, 2008). In addition, preload control was able to maintain an adequate safety margin against LV suction with a reduction in the total blood volume. LV suction may cause a significant reduction in the right ventricular performance through endocardia damage and septal shift (Salamonsen et al., 2012). Depending on the status of the pulmonary vascular resistance, right ventricular contractility and volume status, sustained suction-induced hemodynamic collapse lasting for more than 15 min may occur in serious circumstances, causing unfavorable conditions for effective LVAD unloading (Reesink et al., 2007).

4.4.2 Nature of Preload-Based Starling-Like Control

To date, most control methods are based on a fixed set point, such as constant speed (Akimoto et al., 1999), preload (Bullister et al., 2002), differential pressure (G. Giridharan et al., 2005) or pulsatility (Choi, Boston, & Antaki, 2005; Schima et al., 2006). Although Bullister et al. Bullister et al. (2002) also made use of PLVED as their main input variable, they adopted a completely different approach from the preload-based Starling-like controller proposed in the present study. In Bullister's method, a set point for PLVED which lies within a physician-programmable range was chosen based on the desired range for mean arterial pressure. Apart from this, a Level 2 control algorithm was activated when the heart rate increased above a resting threshold value, which continuously modified PLVED to achieve the new target value for MAP determined based on the measured heart rate. There are several limitations associated with Bullister's method. As

demonstrated in previous clinical (Jacquet et al., 2011; Mancini et al., 1998; Salamonsen et al., 2013) and simulation studies (Einly Lim et al., 2015), the level of resting PLVED varies significantly among individuals (5 – 16.7 mmHg (Jacquet et al., 2011; Mancini et al., 1998; Salamonsen et al., 2013)), and in the face of various physiological perturbations in the circulatory system (5 – 9 mmHg during exercise (Jacquet et al., 2011; Mancini et al., 1998; Salamonsen et al., 2013) and -4.5 mmHg during 70^0HUT (Einly Lim et al., 2015)). Maintaining PLVED at a fixed set point in the presence of various physiological perturbations, therefore, would require excessive variation in the pump speed. We have shown from our previous simulation studies that constant left atrial pressure control (equivalent to constant PLVED) caused a drastic fall in MAP upon 70^0HUT (Einly Lim et al., 2015), which may lead to cases of orthostatic hypertension and subsequently affect circulatory stability. Although Bullister et al. attempted to maintain the MAP within a physician-programmable range, this control loop is reacting much slower, and thus may not be able to cater for sudden circulatory stability caused by abrupt changes in the mean pump speed. Furthermore, heart rate dependency was built into Bullister et al.'s algorithm to increase MAP during exercise, in an attempt to further increase cardiac output. As shown from our simulation results which integrated the reflex mechanism and previous clinical findings (Jacquet et al., 2011; Mancini et al., 1998; Salamonsen et al., 2013), the level of MAP is mostly determined by the circulatory system (e.g. through a change in the venous unstressed volume and systemic vascular resistance) as well as the sensitivity of the reflex mechanism. In addition, especially in heart failure patients, increasing venous return produced a substantial increase in PLVED during exercise, and in most cases more than the amount of increase in MAP. In view of this, building a MAP-heart rate dependency into the model is redundant in most circumstances, as this may actually slow down the response of the controller to a change in PLVED due to the slower reacting MAP control loop.

To the contrary, our preload-based Starling like controller emulates the Frank-Starling control mechanism of the natural heart, which regulates stroke volume in proportion to the level of venous return (reflected by PLVED) only. Instead of fixing a set point for PLVED which is expected to vary significantly with different physiological perturbations, we regulated mean pump flow in accordance to the measured PLVED using a predefined control line (4.1), which indicates the state of the circulation and the degree to which it is meeting the physiological requirements of the body at each instant. Apart from that, as described in Section 4.2.2, preload sensitivity for individual patients could be modified by changing the scaling factor (K in (4.1)) which provides a means of altering sensitivity of the pump to changes in PLVED. In addition, we did not induce an explicit MAP control, but instead relies on the regulation of MAP by the baroreceptors and other circulatory reflexes (Berne, 1981). Consequently preload controller is more robust in providing the appropriate level of blood flow to the systemic circulation under various clinical circumstances (Einly Lim et al., 2015).

This study also indicates that due to its unique shape, a single preload control line (Frank-Starling curve) is able to provide a major decrease in flow at low LV preloads to avoid LV suction and to limit increases at high preloads to avoid over-pumping. Although this study evaluates a single control line, the full controller is able to adapt to longer term changes in the LV function and circulation by adjustment of the scaling factor for the control line to yield different Frank-Starling curves. Having different curves with varying gradients not only provides inherent protection against LV suction, but also determines the degree of LV unloading. Consequently, apart from controlling the level of cardiac output, the preload controller would be able to determine the amount of work performed by the ventricle. Particularly, in the early postoperative phase, it is important that the scaling factor of the control line be selected and modified accordingly by the attending medical staff based on additional clinical requirements, besides the provision of adequate

blood flow to the tissues. Later after implantation, the use of upper and lower limits for PLVED and $\overline{Q_P}$ would enable the controller to adapt the degree of pump assistance automatically by modifying the scaling factor of the control line (Salamonsen et al., 2012). It is noteworthy that the upper and lower limits for PLVED and $\overline{Q_P}$ can be adjusted by the clinicians to accommodate for changes in the patients' condition over time.

4.4.3 Deficiencies of the Preload-Based Starling-Like Control

The Frank-Starling mechanism in the native heart, being a property of the myocardium, effectively eliminates complications like LV suction, as the ventricle does not pump when it is empty. In addition, the adjustment of the contractile force following an increase in the myocyte length is virtually immediate, being mediated by an adjustment of the number of myofilament cross bridges that interact, as well as by an alteration in the calcium sensitivity of the myofilaments (Berne, 1981). In order to avoid suction in the presence of an IRBP with low preload sensitivity, the controller must be able to implement reference changes in $\overline{Q_P}$ as soon as a change in PLVED is sensed. This is a challenge to most control methods particularly if they require an estimation of $\overline{Q_P}$ or pressure head across the pump. While most published methods took two to three heartbeats to estimate the average values of the flow (A.-H. H. AlOmari et al., 2013), only one report estimated instantaneous flow in a pulsatile environment (A. AlOmari, A. Savkin, D. Karantonis, E. Lim, & N. Lovell, 2009). Similarly, estimation of PLVED presents difficulties, with only one report existing for non-invasive estimation of the mean diastolic pressure, which is closely related to PLVED (A.-H. AlOmari et al., 2011). Therefore, PLVED measurement by pressure transducers is clearly superior because the response is instantaneous.

The approach described herein involves direct LV preload adjustment, but does not induce an explicit MAP control. In contrast to a previous study, which implemented MAP

control (Bullister et al., 2002), the preload controller relies on the regulation of MAP by the baroreceptors and other circulatory reflexes (Berne, 1981). Attending medical staffs usually provide additional pharmacological control of systemic blood pressure if required. This usually takes the form of vasodilators rather than vasoconstrictors due to the over action of the sympathetic nervous system in response to the low cardiac output seen in most heart failure patients.

4.4.4 Inadequacies of the Study and Future Work

The model used in this study has been well validated against animal studies conducted by our group and reported in the scientific literature (Einly Lim et al., 2012b; Einly Lim et al., 2015). In our study, the PLVED was obtained from the model at end diastole of each heartbeat. However, in reality, it may need to be averaged over two or three heartbeats due to the presence of measurement noise (Maeda, Tsutamoto, Wada, Hisanaga, & Kinoshita, 1998), especially if there are abnormalities in the cardiac rhythm. Similarly, new values for $\overline{Q_P}$ will also take at least one or two heartbeats to be measured. It thus remains to be tested if the controller is able to adjust $\overline{Q_P}$ quickly enough to avoid suction during changes in posture, protracted abdominal straining, or coughing in the implanted subject, where the fall in PLVED may be rapid. These points will be addressed in future work.

4.5 Conclusion

This study establishes the clear superiority of the preload control over both constant speed and pulsatility control modes. It provides safe and effective adjustments of $\overline{Q_P}$ despite the widely varying states of exercise, blood loss and a fall in LV contractility. This provides impetus for continued efforts to develop miniaturized pressure transducers that are stable over time and small enough to be embedded into the inlet and outlet pump cannula without distortion to their normal shape, thus avoiding flow disturbance and consequent formation of blood clots.

CHAPTER 5: THE ROBUST PRELOAD-BASED CONTROL

5.1 Introduction

Left ventricular assist devices are mechanical pumps that now enjoy a clinically accepted role in supporting the failing heart in a number of scenarios, including destination therapy, bridge to recovery and bridge to transplantation. Implantable rotary blood pumps are continuous flow ventricular assist devices that have become increasingly popular due to the negligible blood trauma along with their light weight and small size, which facilitate their usage for in-home patient care (D. Timms, 2011). Currently, most commercially available IRBPs still function at a fixed speed predetermined by physicians, which is insensitive to changes in the metabolic requirements of the patients (Salamonsen et al., 2011). Such insensitivity increases the risk of over-pumping, causing left ventricular suction, or under-pumping, which can cause pulmonary congestion, renal insufficiency and other problems (Salamonsen et al., 2013).

Moreover, many of so-called physiological control methods were developed based on the pulsatility index (M. A. Bakouri et al., 2013; Nicholas R. Gaddum et al., 2014; Salamonsen et al., 2012; Schima et al., 2006). Pump pulsatility (flow, current, pressure gradient, or speed) is a consequence of LV contraction whereas LV preload is one of the determinants of LV contraction. With severe LV failure, as is the case for all LVAD recipients, the LV does not have the ability to induce major changes in pulsatility. Therefore, the dynamic range of the pulsatility index is small, and therefore its ability as a control input is limited. In the extreme case where LV contractility is zero, pulsatility control is not feasible. By contrast, LV preload increases as LV failure progresses, and its dynamic range is wide in the presence of LVAD (Mansouri et al., 2015).

These deficiencies have driven the development of physiological control methods to match pump output to physiological requirements. Recently, researchers have proposed a number of studies using a novel technique called Frank-Starling-like control (FSLC)

(Bullister et al., 2002; Mansouri et al., 2015). A preload-based controller (Mansouri et al., 2015) was developed based on a modification of the Frank-Starling response first proposed by Guyton (Arthur C Guyton, 1965). The controller adjusts IRBP speed to relate total cardiac output to LV preload as represented by left ventricular end-diastolic pressure using a Frank-Starling curve representative of a healthy human.

Developing a controller with fast response that can reach the pump flow set point within ten seconds (Salamonsen et al., 2012) is a real challenge in any physiological control system, because a slow response may result in suction after hemorrhage or changes in posture. Additionally, one of the main concerns relating to preload control implementation regards measuring LV pressure. Currently available implantable pressure transducers are rendered virtually unusable due to a range of problems; particularly, the noise (disturbance) that generally affects the signal measured in ventricular pulsatility waveform (Lin et al., 2014).

PID is a standard controlling method widely used in biomedical field. Two main approaches to tune the PID controller that is either a) tight control that makes the fastest possible response , or b) smooth control that tunes the PID how to achieve acceptable disturbance rejection (Skogestad, 2006). The cited matters signified the importance of providing a controller that not only could react to the changes swiftly, but also could function robustly under noisy operational conditions, the tasks PID could not perform properly. On the contrary, there are publications have demonstrated sliding mode control (SMC) is robust in various applications (M. Bakouri, Savkin, & Alomari, 2015; M. A. Bakouri et al., 2013; Elsayed, Hassan, & Mekhilef, 2013; Shahnazi, Shanechi, & Pariz, 2008) and in delivering swift system response, minimal overshoot and high tolerance to noisy sensor signals (Shahnazi et al., 2008). Herein, an experimentally validated mathematical model of the cardiovascular system (CVS) and VentrAssist LVAD (Einly Lim et al., 2015) enriched with a baroreflex module was employed to compare preload-

based and fixed speed operational mode. We advanced the hypothesis that the preload-based SMC is superior to the preload-based proportional-integral-derivative (PID) (Bubnicki, 2005) control in terms of speed of response and handling noisy feedback signals.

This chapter is organized as follows. Section 5.2 presents the study methodology, which provides a detailed description of the heart chamber and circulatory model with emphasis on the ventricles' pressure-volume relationship. The regulatory reflex mechanism is also explained in detail. Moreover, the methodology section includes the LVAD component, preload-based control, sliding mode design and implementation, and simulation protocols. The methodology section concludes by describing the performance evaluation criteria, and controller performance assessment from a clinical and engineering perspective. Section 5.3 presents the effect of adding a baroreflex module on the temporal behavior of the CVS key parameters during hemodynamic transition, a comparison of fixed speed and preload-based methods under ideal conditions, and a robustness assessment of the different preload-based methods with noisy feedback signals. Section 5.4 comprises an extensive discussion of the results attained, presents the clinical and control implications, and a comparison of the results with the literature. Finally, inadequacies of this study and future works as well as concluding remarks are given in Sections 5.5 and 6.6 respectively.

5.2 Methodology

5.2.1 Model Description

The numerical model consists of two main components: the CVS and the LVAD. The model has been extensively validated using both in vivo and in-vitro experiments, and has proven to be able to replicate the response of the LVAD-assisted patients to exercise and head up tilt (Einly Lim et al., 2010; Einly Lim et al., 2015). A heart failure scenario (NYHA Class II & III) was simulated by carefully modifying the parameters associated

with heart failure to ensure that realistic hemodynamics was achieved (Table 5.1). A detailed description of the CVS model integrated with an IRBP for different heart failure scenarios is given in (Einly Lim et al., 2015; Mansouri et al., 2015).

Table 5.1: Hemodynamic data for the normal and heart failure conditions.

Variable (unit)	Normal	Heart Failure
Mean arterial pressure (mmHg)	88.4	87.9
Mean left atrial pressure (mmHg)	6.7	24.4
Mean pulmonary arterial pressure (mmHg)	15.3	34.1
Heart rate (bmp)	68.8	82.3
Mean cardiac output (L/min)	4.84	3.51
Systemic vascular resistance (mmHg.s.mL-1)	1.04	1.34
Left ventricular end diastolic volume (mL)	122.7	185.8

5.2.1.1 CVS Component

The lumped CVS model consists of ten compartments including the left and right sides of the heart as well as pulmonary and systemic circulations.

i. *Heart Chambers:* The chambers' states vary from exponential during diastole to linear during systole, depending on the time-varying elastance function ($e_I(t)$) (Sagawa, Maughan, Suga, & Sunagawa, 1988). A linear end systolic pressure–volume relationship (Sagawa et al., 1988) is adopted for both the left and right atria and also to describe the left and right ventricles. Moreover, the systolic period duration is assumed to change linearly with heart rate (Ursino, 1998). A detailed description of the heart chambers is provided in (Einly Lim et al., 2010; Einly Lim et al., 2012b). The heart valves are modeled in this study using resistance (R) in

series with a diode, permitting flow to pass only when the pressure gradient across them is positive. The flow through a valve is formulated as follows:

$$Q_v = \begin{cases} \frac{P_{v_1} - P_{v_2}}{R}, P_{v_1} > P_{v_2} \\ 0, P_{v_1} \leq P_{v_2} \end{cases} \quad (5.1)$$

where P_{v1} and P_{v2} are the upstream and downstream valve pressure respectively, and Q_v represents the blood flow through the valve.

ii. *Circulatory Model*: The circulatory model consists of both systemic and pulmonary circulations. The systemic circulation is partitioned into six parallel vascular compartments (Einly Lim et al., 2015). In accordance with Einly Lim et al. (2013), the net volume change for each compartment is:

$$\dot{V}_i = Q_i - Q_{i+1} \quad (5.2)$$

where Q_i and Q_{i+1} are the inflow and outflow respectively. Based on the linear PV relationship, the pressure in the i^{th} compartment, P_i, is given by:

$$P_i = E_i(V_i - V_{0,i}) + P_{e,i} \quad (5.3)$$

where $P_{e,i}$ stands for the extravascular pressure, V_i and $V_{0,i}$ represent the volume and unstressed volume of the compartment, and E_i is the compartment elastance.

iii. *The Regulatory Reflex Mechanism*: The regulatory model comprising both arterial and cardiopulmonary (CP) baroreceptors was adopted from Ursino (1998) and E Magosso and Ursino (2002). The model incorporates the afferent pathways from the baroreceptors together with the associated efferent sympathetic and parasympathetic activities. The afferent arterial baroreflex pathway is formulated as a function of the arterial pressure, while the afferent CP baroreflex pathway is modeled as a function of the central venous pressure. The model describes the response of several distinct effectors including heart contractility, peripheral resistance, unstressed volumes, and heart rate (Einly Lim et al., 2013; Einly Lim et al., 2015). A detailed description of the regulatory model is given in (Einly Lim et

al., 2013; E Magosso & Ursino, 2002; Ursino, 1998).

5.2.1.2 LVAD Component

VentrAssist LVAD is a centrifugal blood pump with hydrodynamic bearings. Three differential equations are applied to model each pump component: the motor winding electrical equation, electromagnetic torque transfer equation, and pump hydraulic equation. A detailed description and validation procedure of the LVAD model are available in (Einly Lim et al., 2012b).

5.2.2 Preload-Based Control

The immediate response of the preload-based control emulates the Frank-Starling control mechanism of the natural heart. The Frank-Starling curve forms the basis of the control line, which defines the target pump flow for any specific PLVED. The control line is generated by a third-order polynomial function (4.1) fitted directly to Guyton's data (Arthur C Guyton, 1965).

In our study, the model automatically samples PLVED at end diastole of each heart cycle and supplies it to the controller. Although the full controller is able to adapt to longer term changes in the circulation by adjustment of the scaling factor (K), this communication deals only with the immediate response of the controller in which changes in PLVED cause migration of the operating point to different positions on C_L.

Any changes in state (Figure 5.1) cause deviations of the system operating point from the original position on the control line to system-line S_2 or S_3. The controller then forces the operating point back to the control line along a linear path, which conforms closely to the trajectories of the linearized system lines, as described previously by Mansouri et al. (2015). Changes in state are thus countered by moving the target operating point up or down the control line. The pump flow defined by each new location of the operating point on the control line is the set-point value to be attained for the next iteration.

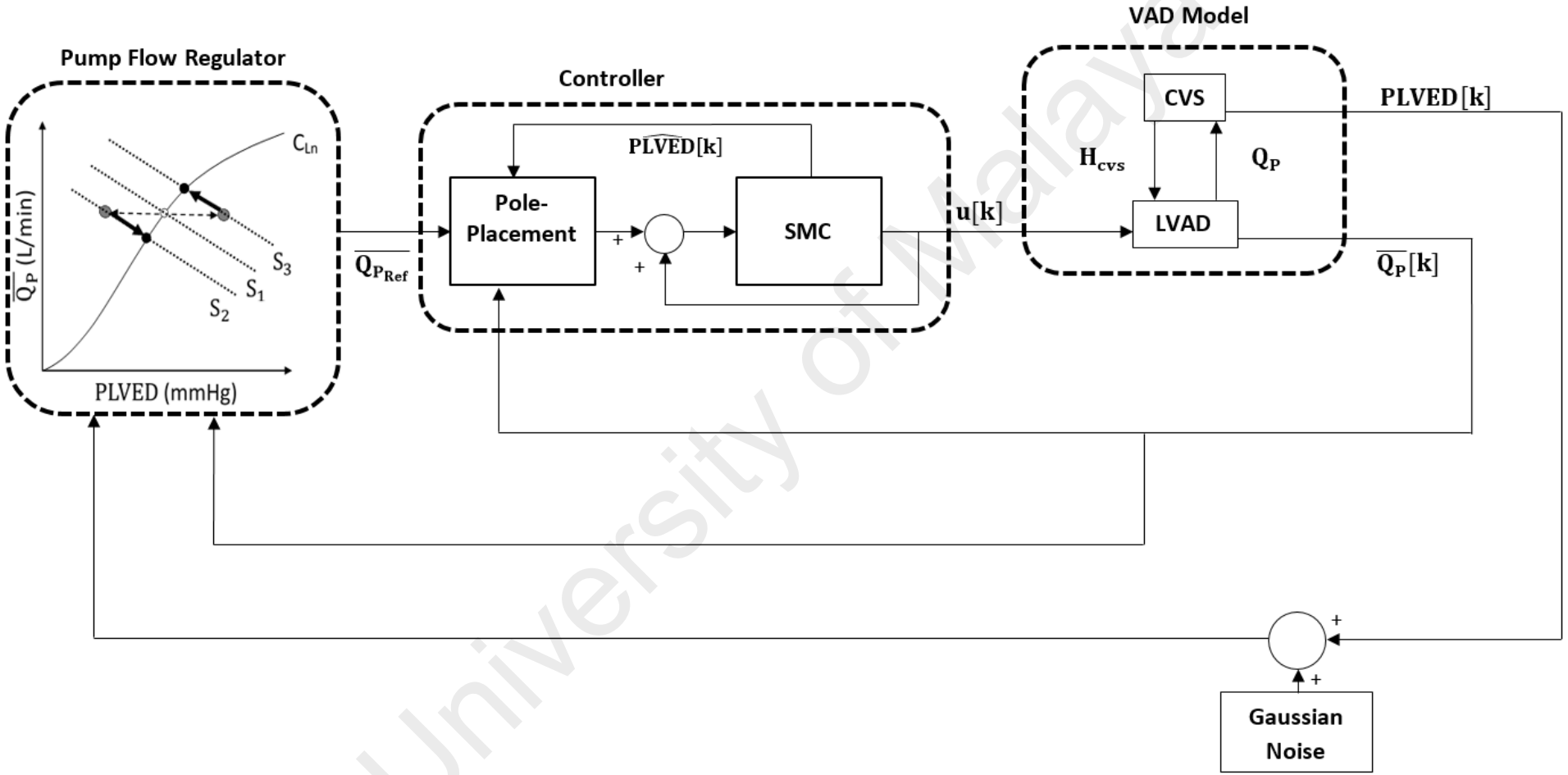

Figure 5.1: Block diagram of control system

5.2.3 Sliding Mode Controller

5.2.3.1 Estimator

In this study, two autoregressive exogenous (ARX) dynamic linear time-variant models were employed to estimate the mean pump flow. The first ARX model was established to model the relation between PLVED and mean pulse-width modulation signal ($\overline{PWM}$), and the second ARX model was developed to model the relation between estimated averaged pump flow ($\widehat{\overline{Q_P}}$) and estimated PLVED ($\widehat{PLVED}$) as follows:

$$\hat{x}_1[k+1] + a[k]\hat{x}_1[k] = b[k]u[k] + e_1[k], \tag{5.4}$$

$$\hat{x}_2[k+1] + c[k]\hat{x}_2[k] = d[k]\hat{x}_1[k] + e_2[k], \tag{5.5}$$

where $\hat{x}_1[k]$ is the estimated PLVED, $\hat{x}_2[k]$ is the estimated $\overline{Q_P}$, u[k] is the mean PWM, a[k], b[k], c[k] and d[k] are time-varying model parameters, and $e_1[k]$ and $e_2[k]$ are the noise components. For the SMC controller design, the system defined in (5.4) and (5.5) was reformatted as a linear time-varying (LTV) state space system in the following form:

$$\begin{cases} \widehat{\mathbf{X}}[k+1] = \mathbf{A}[k]\widehat{\mathbf{X}}[k] + \mathbf{B}[k]u[k] + e[k], \\ y[k] = \mathbf{C}\,\hat{x}[k], \end{cases} \tag{5.6}$$

where $\mathbf{A}[k] = \begin{bmatrix} -a[k] & 0 \\ d[k] & -c[k] \end{bmatrix}$, $\mathbf{B}[k] = \begin{bmatrix} b[k] \\ 0 \end{bmatrix}$, $\mathbf{C} = [0 \quad 1]$, $\widehat{\mathbf{X}}[k] = [\hat{x}_1[k] \quad \hat{x}_2[k]]^T$, $e[k] = [e_1[k] \quad e_2[k]]^T$ and y[k] are the system output. Model parameters a[k], b[k], c[k] and d[k] were estimated using the ARX recursive least square algorithm. With this model, the experimental results showed that a[k], c[k] and d[k] are bounded and parameter b[k] is close to a constant value. Therefore, the state space model in (5.7) can be reformulated as:

$$\begin{cases} \widehat{\mathbf{X}}[k+1] = (\mathbf{A} + \delta\mathbf{A})\widehat{\mathbf{X}}[k] + \mathbf{B}u[k] + e[k], \\ y[k] = \mathbf{C}\,\hat{x}[k], \end{cases} \tag{5.7}$$

where $\delta\mathbf{A}$ is the system parameter variation and e[k] is the system disturbance. Figure 5.2 shows that all system poles and zeros resides within the unit circle, thus guaranteeing the system's stability criteria (Levine, 1996).

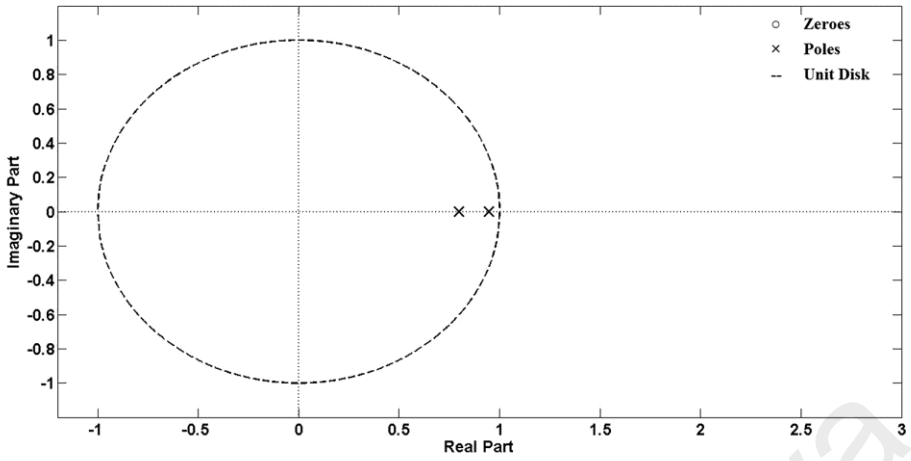

Figure 5.2: Poles-zeros of the model estimator.

5.2.3.2 Sliding Mode Control Design

Discrete sliding mode control (DSMC) is normally defined based on the state-space model (Monsees, 2002). In this case, the design is divided into two steps, a) choosing an appropriate switching function, and b) establishing a control law. The switching function for the system (5.7) is defined as:

$$s[k] = S\widehat{\mathbf{X}}[k] \tag{5.8}$$

where S is a constant vector designed based on the pole placement technique to assure that $\widehat{\mathbf{X}}[k]$ is asymptotically stable on s[k] = 0 (Gao, Wang, & Homaifa, 1995).

So far, multiple control techniques with different reaching laws have been proposed for SMC (Bartolini, Ferrara, & Utkin, 1995; Gao et al., 1995). Gao's reaching law explains the ideal conditions to guarantee robust reachability and perfect sliding motion as follows (Gao et al., 1995):

$$s[k+1] = (1-\tau T)s[k] - \epsilon T\,\mathrm{sgn}(s[k]), \begin{cases} \mathrm{sgn}(r) = 1, r > 0 \\ \mathrm{sgn}(r) = 0, r = 0 \\ \mathrm{sgn}(r) = -1, r < 0 \end{cases} \tag{5.9}$$

The following conditions must be satisfied in the equation above:

$$0 < 1 - \tau T < 1 \tag{5.10}$$

$$0 < \epsilon T < 1 \tag{5.11}$$

$$T > 0, \epsilon > 0, \tau > 0 \tag{5.12}$$

where T stands for the sampling period, ϵ is the reaching velocity and τ represents the converging exponential.

To satisfy the reaching law in (5.8), we have:

$$s[k+1] = S\hat{\mathbf{X}}[k+1] \tag{5.13}$$

Then from (5.9) and (5.13), the following is obtained:

$$s[k+1] = S\hat{\mathbf{X}}[k+1] = S(\mathbf{A}\hat{x}[k] + \delta\mathbf{A}\hat{x}[k] + \mathbf{B}u[k] + e[k]) \tag{5.14}$$

Equating (5.9) and (5.14) results in:

$$S\mathbf{A}\hat{\mathbf{X}}[k] + S\delta\mathbf{A}\hat{\mathbf{X}}[k] + S\mathbf{B}u[k] + Se[k] = (1-\tau T)s[k] - \epsilon sgn(s[k]) \tag{5.15}$$

Solving the equation above for u[k] results in:

$$u[k] = -(S\mathbf{B})^{-1}\left(S\mathbf{A}\hat{\mathbf{X}}[k] - (1-\tau T)S\hat{\mathbf{X}}[k] + \epsilon T sgn(s[k])\right) -$$

$$(SB)^{-1}(S\delta\mathbf{A}\hat{\mathbf{X}}[k] + Se[k]) \tag{5.16}$$

The equation above can be used if $(S\delta\mathbf{A}\hat{\mathbf{X}}[k] + Se[k])$ is bounded (M. Bakouri et al., 2015):

$$-\beta_s < \left(S\delta\mathbf{A}\hat{\mathbf{X}}[k] + Se[k]\right) < \beta_s \tag{5.17}$$

Thus, the final control algorithm could be reformulated as:

$$u[k] = -(SB)^{-1}(S\mathbf{A}\hat{\mathbf{X}}[k] - (1-\tau T)S\hat{\mathbf{X}}[k] + (\epsilon T + \beta_s)sgn(s[k])) \tag{5.18}$$

where β_s stands for the maximum system variation (M. Bakouri et al., 2015), as determined as follows:

$$(\beta_s < \left(S\delta\mathbf{A}\hat{\mathbf{X}}[k] + Se[k]\right)) < \beta_s \equiv (\beta_s sgn(s[k])) \tag{5.19}$$

It should be noted that high frequency chattering does not exist in discrete variable structure controller in general, especially when the system sampling period is low (Gao et al., 1995). However, chattering-like phenomena that may arise in system with high sapling frequency could be alleviated using chattering placement techniques (Hung, 1993).

5.2.3.3 Tracking Design

We simplified our dynamic ARX system identifier for the sliding mode control design and implementation; however, it reduced the controller's sensitivity and estimation accuracy; thus, a pole-placement tracking module added to counter the deficiencies of such simplification. In our controller design, the tracking performance is achieved by the modified state feedback control as follows:

$$u_{sf}[k] = -K_{cl}\,[\overline{Q_P}[k] \quad \widehat{PLVED}[k]]^T + \overline{Q_{P_{Ref}}}[k] \tag{5.20}$$

where u_{sf} is the pole-placement output fed to sliding and K_{cl} stands for the state-feedback gain matrix. As a result, the final sliding mode control input signal, $u_{fi}[k]$, can be written as:

$$u_{fi}[k] = u_{sf}[k] + u[k] = -K_{cl}\,[\overline{Q_P}[k] \quad \widehat{PLVED}[k]]^T + \overline{Q_{P_{Ref}}}[k] + u[k] \tag{5.21}$$

5.2.3.4 System Design Results

The design parameters of the sliding controller were given as $\mathbf{A} = \begin{bmatrix} 0.78 & 0 \\ 0.06 & 0.94 \end{bmatrix}$, $\mathbf{B} = \begin{bmatrix} 0.5 \\ 0 \end{bmatrix}$, ϵ=2.5, τ= 5.0, and $S = [-2.0 \quad 1.0]$ for (5.18), while the state-feedback gain matrix, K_{cl} was given as [1.5 1.0]. A block diagram of the control system is illustrated in Figure 5.1.

5.2.4 Simulation Protocol

The models were implemented using the Simulink toolbox in MATLAB (The Mathworks, Inc., Natick, MA, USA) with a sampling period of 0.005 s. Simulations of the baseline state at rest, exercise, and after blood loss were conducted in the ideal condition (no noise) and in the presence of disturbance. A relative intensity of 0.55 was selected for the exercise simulation to represent the maximal exercise condition as defined by Einly Lim et al. (2015), whilst the total blood volume was reduced by 1000 mL to mimic the hemorrhage condition (Mansouri et al., 2015). For all simulations, an

immediate transition from the baseline to the respective test scenario was performed after the hemodynamic variables reached steady state conditions. The simulation was then sustained for a sufficient length of time to allow the system to achieve post-transition steady state.

In order to determine the optimal scaling factor (K) for C_L, another set of simulations was conducted in the baseline state, where K was increased from a basal value of 0.2 to the maximal value of 2.3 in 0.1 increments. Blood flow through the aortic valve ($\overline{Q_{av}}$) was obtained from the model to indicate whether the aortic valve was opening or closing. The optimal scaling factor was identified as the minimum value of K that allowed the aortic valve to be closed in the baseline condition. In the present study, K value was set to 1.0. Both PID and SMC methods were initially tuned to (i) provide a 5% settling time within 10 s, and (ii) generate a maximum of 10% overshoot of the final value under no noise condition (Mansouri et al., 2015). In this study, the PID gains were chosen using the standard Ziegler-Nichols(Ziegler & Nichols, 1942) method how K_P, K_I and K_D, to be 0.28, 0.22 and 0.05 respectively, while the SMC parameters were given in section 5.2.3. The current study progressed with assessing the robustness of the preload-based control implementations against external disturbances. The two levels of normal Gaussian noise employed in this study were signal-to-noise ratios of 15 dB (corresponding to unified white noise with ±3.0 mmHg amplitude -- the upper bound of a non-invasive estimator error reported by A.-H. AlOmari et al. (2011)) and 7 dB (corresponding to unified white noise with ±6.0 mmHg amplitude).

5.2.5 Performance Evaluation

Four performance metrics, with each assessing a different aspect of performance, were used to provide a quantitative comparison among the different control methods. First, the set-point tracking performance of each strategy was evaluated by calculating the mean

absolute error (MAE) between the set point and the actual value of the average pump flow. MAE is the average absolute set-point deviation per second, expressed as a percentage of the target value (5.22) (M. C. Stevens, 2014).

$$\mathrm{MAE} = \frac{1}{T_d}\int_0^{T_d} \left| \frac{A(t)-Y(t)}{A(t)} \right| \tag{5.22}$$

where T_d stands for the whole simulation length, A is for the target value and Y is the actual value.

Secondly, the root mean squared hemodynamic deviation (RMSHD) (Michael C Stevens et al., 2014), which measures the average deviation per second of the mean arterial pressure, PLVED, and mean cardiac output from their respective predefined physiological limits, was evaluated. These variables were selected because physicians are typically concerned with more than just cardiac output when setting the pump speed (Boston et al., 2003). During LVAD support, mean arterial pressure should be kept within physiological limits and PLVED must not be reduced (otherwise it may lead to increased suction risk) or elevated (as it may lead to pulmonary edema) beyond the thresholds. Moreover, cardiac output must remain within a safe range to guarantee end-organ perfusion. The upper and lower limits for the three hemodynamic parameters shown in Table 5.2 were selected based on discussions with the clinicians. RMSHD is important because it delivers a clinical context for identifying controller performance (Michael C Stevens et al., 2014). For example, there might be a controller with a good set-point tracking performance (i.e. low MAE), but which results in high cardiac output and reduced PLVED. While low MAE means the control system exhibits acceptable tracking performance, low RMSHD promises good physiological performance.

For calculating RMSHD, let y_x stands for any of the three previously mentioned hemodynamic variables, and let LL_x and UL_x define the lower and upper limits of a safe operating bound for that variable, respectively. The normalized square deviation ($NSD_x(t)$) of $y_x(t)$ outside of LL_x and UL_x is calculated as follows:

$$\mathrm{NSD_x(t)} = \left(\frac{\mathrm{v_x(t)}}{\frac{\mathrm{LL_x + UL_x}}{2}} \right)^2 \tag{5.23}$$

where

$$\mathrm{v_x(t)} = \begin{cases} \mathrm{y_x(t) - UL_x};\ \mathrm{y_x(t)} > UL_x \\ 0; \mathrm{LL_x} < \mathrm{y_x(t)} < UL_x \\ \mathrm{LL_x - y_x(t)};\ \mathrm{y_x(t)} < LL_x \end{cases} \tag{5.24}$$

Table 5.2: Upper and lower limits for three key hemodynamics variables.

Variable (unit)	Lower Limit	Upper Limit
Mean arterial pressure (mmHg)	65	105
Left ventricular end diastolic pressure (mmHg)	2	15
Cardiac output: Rest and hemorrhage (L/min)	4	7
Cardiac output: Exercise (L/min)	7	11

Equation (5.25) formulates the squared hemodynamic deviation (SHD) of variable y_x:

$$\mathrm{SHD_x} = \int_0^{\mathrm{T_d}} \mathrm{NSD_x(t)} \tag{5.25}$$

Finally, RMSHD is calculated as (5.26):

$$\mathrm{RMSHD} = \left(\frac{1}{\mathrm{T_d}}\right) \sqrt{\left(\mathrm{SHD_{P_{ao}}^2} + \mathrm{SHD_{PLVED}^2} + \mathrm{SHD_{CO}^2}\right)} \tag{5.26}$$

It should be noted that comparable weightings were chosen for the SHD variables in (5.26) because physicians consider all these variables equally when setting pump speed (Boston et al., 2003). When comparing physiological control systems, a system with the lowest RMSHD is considered best at maintaining key hemodynamic variables. Additionally, the length of time that LV spends in suction for each control strategy was measured and calculated. In the proposed model, LV suction is represented by a negative PLVED (i.e. PLVED<0 mmHg) (Mansouri et al., 2015). Index ρ is expressed as a percentage of total simulation time during which suction occurs (5.27):

$$\rho = \frac{\sum_{i=1}^{i=I_s} \Delta t_i}{T} \times 100 \tag{5.27}$$

where Δt_i is the i^{th} interval over which the actual pump speed exceeds the suction speed and I_s is the number of such intervals. Finally, η serves as a measure of how deep, on

average, the pump speed progresses into the suction region.

$$\eta = \frac{\overline{\omega_s} - \omega_s}{\omega_s} \times 100 \tag{5.28}$$

where ω_s is the speed at which suction occurs (3200 rpm and 2600 rpm for exercise and blood loss scenarios, respectively) and $\overline{\omega_s}$ is defined by:

$$\overline{\omega_s} = \frac{\sum_{i=1}^{I} \int_{\Delta t_i} \omega(t) dt}{\sum_{i=1}^{I} \Delta t_i} \tag{5.29}$$

5.3 Results

5.3.1 Dynamic Cardiovascular Response to Exercise and Blood Loss under Constant Speed Mode

The temporal patterns of the arterial pressure and pump flow while transitioning from rest to exercise and blood loss are shown in Figure 5.3. In line with E Magosso and Ursino (2002), the simulated transient patterns for exercise displayed three distinct phases: i) initial phase lasting approximately 5 s, ii) middle phase lasting around 25 s, and iii) steady state phase. In the early phase of transition to exercise, heart rate and cardiac output delivery increased immediately with relatively unchanged peripheral resistance, leading to an immediate rise in P_{SA}. Entering the second phase, the total peripheral resistance smoothly reduced with a slower dynamic, resulting in a significant drop in P_{SA}. Consequently, the baroreceptor acted to restore the P_{SA} by increasing systemic venous tone, heart rate, and cardiac contractility. In contrary to P_{SA}, pump flow was observed to increment gradually from rest to exercise. Immediately after blood loss, reduction in cardiac output led to a substantial drop in P_{SA} (Figure 5.3 (B)). On the contrary, Q_P demonstrated a transient rise initially due to a reduction in the pump differential pressure (caused by a drop in P_{SA}). The reflex mechanism then reacted to increase P_{SA} by constricting the vessels, increasing heart rate, cardiac contractility and venous tone. Consequently, P_{SA} increased gradually while Q_P fell, leading to a lower value as compared to the original levels.

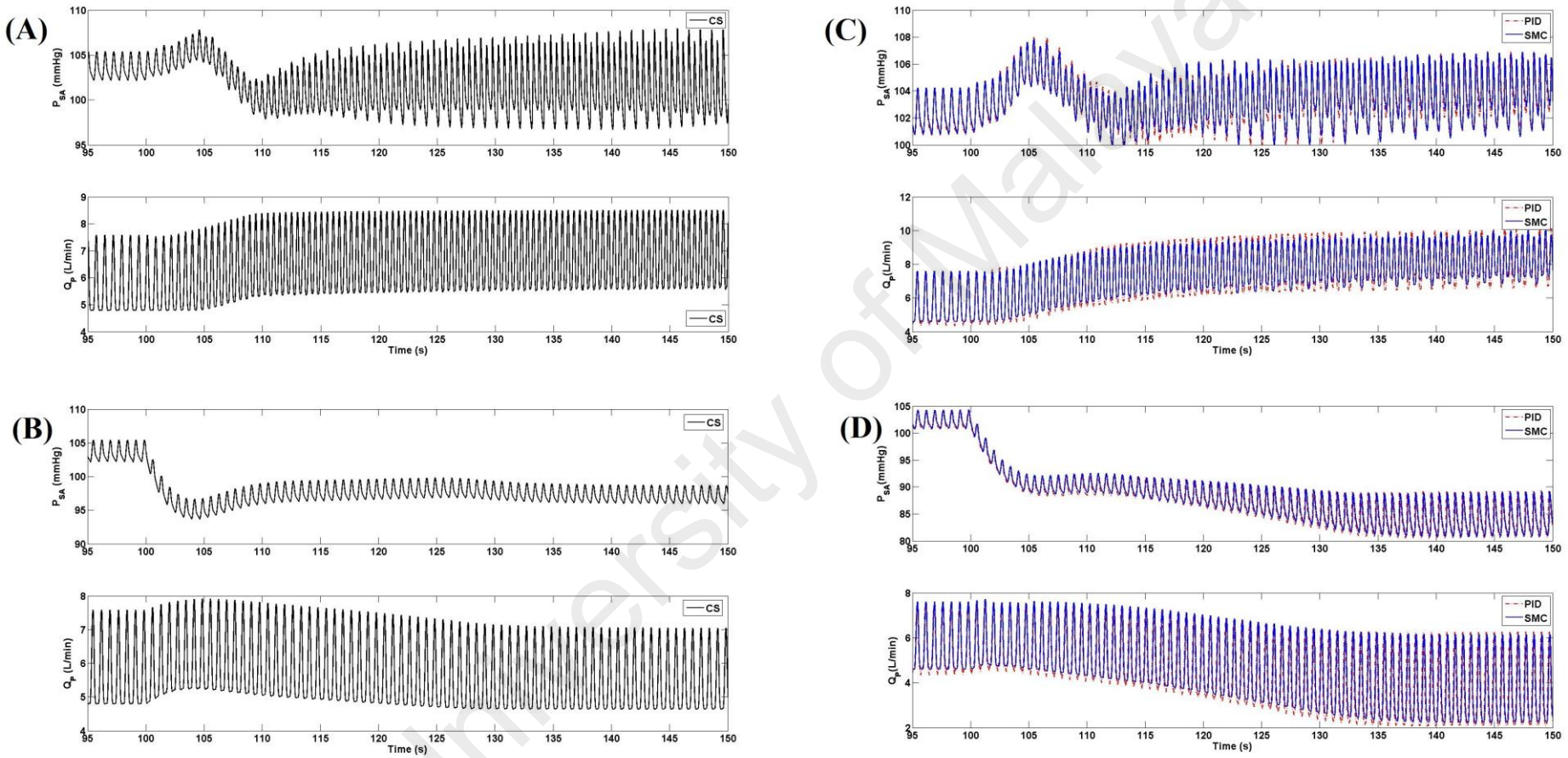

Figure 5.3: Arterial pressure and pump flow from baseline to (A) exercise and (B) blood loss, at the constant speed mode. Mean arterial pressure and mean pump flow from baseline to (C) exercise and (D) blood loos at no noise condition, preload-based control methods.

5.3.2 Controllers Comparison

5.3.2.1 Noise Free Condition

The performance of the fixed speed mode and the two preload-based implementations (i.e. PID and SMC) was compared by observing the changes in $\overline{Q_P}$, $\overline{CO}$, and MAP from baseline to exercise and from baseline to a blood loss state. There was no significant difference between the two preload implementation methods (Figure 5.3 (C) and Figure 5.3 (D)). A comparison with the constant speed operational mode indicated that the preload-based control was the better modality, as it provided a 51% increase in $\overline{Q_P}$ and 64% increase in $\overline{CO}$ during transition to exercise. The flow increments were associated with a lower PLVED value of 15.6 mmHg, indicating less load on the LV (Table 5.3). On the contrary, the constant speed mode increased mean pump flow by 20% only, corresponding to a higher load on LV (PLVED of 18.9 mmHg).

Table 5.3: Model simulated hemodynamic data at baseline (rest), exercise, and blood loss with constant speed and preload-based controllers.

Variable (unit)	**Rest**	**Exercise**		**Blood Loss**	
	Constant Speed/ Preload	**Constant Speed**	**Preload**	**Constant Speed**	**Preload**
$\overline{\omega}$ (rpm)	2600	2600	2980	2600	2115
MAP(mmHg)	103	101	104	96	84
$\overline{P_{la}}$(mmHg)	9	21	19	4	5.4
PLVED (mmHg)	7.4	18.9	15.6	-0.4	4.9
$\overline{CO}$ (L/min)	5.6	8.9	9.2	5.3	4.4
$\overline{Q_P}$ (L/min)	5.6	6.7	8.5	5.3	3.7
$\overline{Q_{av}}$	0.0	2.2	0.6	0.0	0.7
LVEDV	147	170	161	120	146

Suction is the challenge faced in automated LVAD control during a blood loss scenario. During hemorrhage, a preload-based LVAD control system can avoid this crucial state by reducing its flow output sufficiently to match an ample volume reduction in the right ventricle. During the transition from baseline to blood loss, the preload-based controller was able to maintain PLVED at 4.9 mmHg compared with -0.4 mmHg for the constant speed control system. A negative value for PLVED indicates a suction event when using the constant speed system (Mansouri et al., 2015).

Analytical data (in Table 5.4) shows that the incidence of suction under constant speed mode lasted for 8.8% of the entire blood loss simulation, although the suction depth was only 0.1%. The results also illustrate the fixed speed mode's deficiency in maintaining hemodynamic variables within clinically acceptable limits. While RMSHD was nearly zero for both preload-based methods, a major hemodynamic deviation of 13.0% was recorded for the fixed speed mode.

Table 5.4: Mean absolute error (MAE), root mean squared hemodynamic deviation (RMSHD), suction duration and suction depth for mean Q_P (pump flow) in each control strategy subject for Constant speed, PID preload-based and SMC preload-based testing protocol at noise free and noisy conditions.

SNR (dB)	Control strategy	Rest			Exercise			Blood Loss			Summation			
		M	ρ	R	M	ρ	R	M	ρ	R	M	ρ	η	R
no noise	Constant Speed	---	0.0	0.0	---	0.0	11.2	---	8.8	1.8	---	8.8	0.1	13.0
	Preload-PID	1.9	0.0	0.0	2.3	0.0	0.6	4.7	0.0	0.0	8.9	0.0	0.0	0.6
	Preload-SMC	1.8	0.0	0.0	2.2	0.0	0.3	4.3	0.0	0.0	8.3	0.0	0.0	0.3
15	Preload-PID	9.8	0.0	0.0	5.2	0.0	0.7	16.5	0.0	0.0	31.5	0.0	0.0	0.7
	Preload-SMC	7.1	0.0	0.0	4.4	0.0	0.4	13.5	0.0	0.0	25.0	0.0	0.0	0.4
7	Preload-PID	19.9	0.0	0.0	10.4	0.0	1.0	134.2	26.1	18.7	164.5	26.1	19.2	19.7
	Preload-SMC	10.6	0.0	0.0	7.7	0.0	0.8	20.4	0.0	0.4	38.7	0.0	0.0	1.2

5.3.2.2 Noisy Condition

The results in Table 5.4 indicate that SMC delivered better control and physiological performance than PID under noisy conditions. With an SNR of 15 dB, PID tracking performance dropped to 31.5% whilst the SMC controller improved the system performance by 6.5% and maintained MAE of 25%. The results also portrayed no significant degradation in hemodynamic performance in either method, as reflected by the low RMSHD values. At a higher noise level (SNR = 7 dB), the SMC controller led to a final MAE of 38.7%, demonstrating a superiority over the PID system with a MAE of 164.5%. During blood loss, the PID could not tolerate the noisy preload feedback signal and failed. The failure resulted in a dramatic pump flow increment, and a persistent negative PLVED was observed for the remaining simulation (26.1% of the entire simulation). The suction penetration was reportedly very deep (19.2%), which led to a vast hemodynamic deviation (RMSHD) of 19.7% compared with the RMSHD value of 1.2% when using the SMC system.

5.4 Discussion

Herein we initially developed a baroreflex model and integrating with the original cardiovascular system (CVS) that could properly replicate the dynamic CVS response to exercise and hemorrhage variations. Such completion realize to study the dynamic behavior of CVS whist transferring from the baseline condition to exercise and blood loss under both constant speed and Preload-based controller. Moreover, this article is within the first studies utilizing sliding mode controller for IRBP control. We could claim that it is the first publication demonstrating a robust physiological LVAD control that could tolerate different levels of noisy feedback signals in the transition from baseline to different hemodynamic alternations. The SMC consistently outperformed the PID control, whose hemodynamic maintenance performance was inferior even to the constant speed mode in the presence of a noisy feedback signal. These results are in agreement

with recent studies (M. Bakouri et al., 2015; Gwak, Kim, Lee, Park, & Kim, 2015), which highlighted the superiority of the SMC.

5.4.1 Preload-Based Frank-Starling-Like Control

Deficiencies in the fixed speed operational mode have motivated researchers to develop various physiological responsive controllers. Bullister et al. (2002) established a controller that uses PLVED as its main input variable, where its set point was chosen to lie within a physician-programmable range based on the desired range for MAP. One limitation of this method was that maintaining PLVED at a fixed set point in the presence of various physiological perturbations would require excessive variation in the pump speed, as the level of resting PLVED varies significantly among individuals and in the face of different perturbations in the circulatory system.

On the other hand, the current preload-based control method emulates the Frank-Starling mechanism of the natural heart, where the stroke volume is regulated in proportion to the level of the venous return (reflected by PLVED) using a predefined control line (4.1). In addition, modifying the scaling factor (K) provides a means of altering pump sensitivity to the change in PLVED. As shown in our simulation results (Figure 5.3, Table 5.3, and Table 5.4), the preload-based controller outperforms the conventional fixed speed operational modes during exercise and blood loss. With exercise, although mean pump flow naturally increases at a constant speed mode (Salamonsen et al., 2013), preload-based control, upon sensing a simultaneous increase in the preload (PLVED), further enhances the increment of the average pump flow. On the other hand, the preload-based control responds to a preload reduction in blood loss by reducing $\overline{Q_P}$ to avoid LV suction (Mansouri et al., 2015). Consequently, the preload-based control generates a lower MAP than constant speed during the steady state for blood loss scenario (Figure 5.3 (B) and Figure 5.3 (D)). However, during the occurrence of severe blood loss event, the PLVED will keep reducing and eventually compromising the cardiac output, in which case an

alarm should be raised to alert the clinician or caregiver that the patient needs volume treatment.

5.4.2 Comparison between SMC and PID controllers

This is the first study which demonstrates the proper functionality of SMC with the recently proposed preload-based method (Mansouri et al., 2015) for physiological control of an LVAD. The present data analysis signified that employing SMC consistently results in superior tracking performance and less hemodynamic deviation as compared to the PID controller, which is in agreement with previous research works (M. Bakouri et al., 2015; M. A. Bakouri et al., 2014; Gwak et al., 2015).

Under an ideal (noise free) condition, the SMC delivered a marginally better set-point tracking performance and respectively less hemodynamic deviation as compared to the PID controller. This issue originates from the SMC adaptive rule (5.21). The cardiovascular system is uncertain and time-varying, thus a physiologic control system must maintain stability and deliver fast responses in such a dynamic system. Most conservative control systems, which are vulnerable to oscillations, fail to provide a fast enough response to preload changes, thus increasing the suction risk. While utilizing the SMC provides a flexible controlling law, a rapid response provided by setting a high K_P gain for the PID results in an underdamped transient response, overshooting and pump oscillations (Goodwin, Graebe, & Salgado, 2001).

The derivative component in the PID system (K_D) was added to compensate for the unwanted effect of having a high K_P gain. However, this comes at a cost of amplifying the process noise, resulting in huge output alternation. Consequently, although the noise added to the preload feedback signal affected both methods by degrading the tracking performance, the influence was more deleterious to the PID system (Figure 5.4 and Table 5.4). The results showed that both PID and SMC could tolerate a lower noise level (SNR = 15 dB) at the cost of increasing MAE; however, their hemodynamic indices

(RMSHD) were relatively unaffected. At higher noise level (SNR = 7 dB), the PID system collapsed and the system penetrated deeply into the suction zone during blood loss. This was associated with a large MAE (165%) and a dramatic RMSHD increment (19.7%). On the contrary, the SMC tracking performance dropped 39% only with a minor (1.2%) deviation of the hemodynamic indices, indicated by RMSHD. In particular, the derivative component of the PID controller responded to the substantial drop in PLVED with larger amounts of change in the output. At a high noise level with a SNR of 7 dB, such large output oscillations rendered the system unstable and finally caused an abrupt speed increment, exceeding the suction threshold of 2600 rpm. On the other hand, the SMC inherently provided robustness in facing large perturbations or model uncertainties (Utkin, 2013) besides delivering a fast, zero steady state error as reflected in the smaller MAE. The system stability prevented the sliding mode from hemodynamic instability as marked by a negligible RMSHD value. It is noteworthy that the Gaussian noise generator module was set automatically off as the system entered the suction zone.

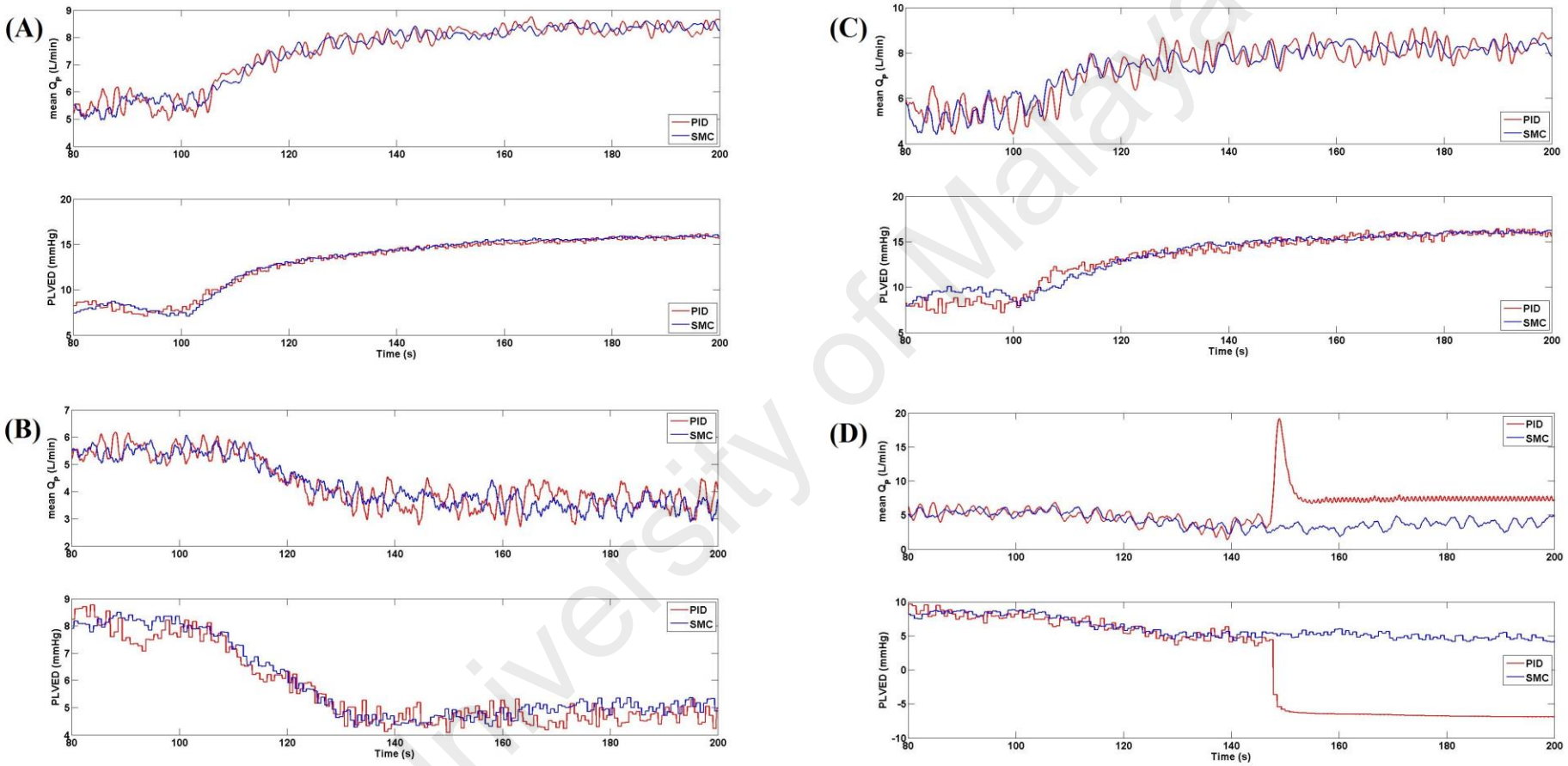

Figure 5.4: Average pump flow and PLVED from baseline to (A) exercise and (B) of preload-based control methods, SNR of 15dB. Average pump flow and PLVED from baseline to (C) exercise and (D) blood loss of preload-based control methods, SNR of 7dB.

5.5 Limitations and Future Works

Although we used a numerical model in this study, it should be considered that we the model used is a well-validated model against in-vivo data (Einly Lim et al., 2012b; Einly Lim et al., 2015). Moreover, the numerical model developed herein could properly replicate the dynamic CVS response to exercise and hemorrhage variations. Additionally, a preload-based control system with a single control line was evaluated in this study, but the full controller should be able to adapt to longer-term changes in the LV function and circulation by adjusting the scaling factor for the control line.

Furthermore, the cardiovascular LVAD system was initially modeled using a dynamic ARX system identifier, after which a linear time invariant system was simplified. This simplification eased control design and implementation, although it degraded the controller's high activity and estimation accuracy, which was compensated by the addition of a pole-placement tracking module. All disturbances were also assumed to be normally distributed, where the PLVED noise was introduced using a MATLAB/SIMULINK unified (Gaussian) white noise block. In addition, in our study, the model automatically samples PLVED at end diastole of each heart cycle and supplies it to the controller. Whereas in reality, PLVED has to be extracted out of the measurement of the sensors. It is noteworthy that the detection algorithm of PLVED from sensor measurement is beyond this study context.

5.6 Conclusion

The robustness of the physiological controller against noise is an important subject, particularly when utilizing an implanted LVAD. A quick response to hemodynamic change was also required because poor tracking performance may result in suction. In this study, we compared two preload-based implementation methods (i.e. PID and SMC) from an engineering and clinical perspective under both noise-free and noisy preload feedback signal conditions, using a dynamic CVS-LVAD model. Four performance metrics were used to provide a quantitative comparison between the controllers, which

include the set-point tracking performance, hemodynamic stability, and suction avoidance indices. The results showed no prominent difference in performance between the PID and SMC methods in the noise-free condition. While both controllers could tolerate a relatively lower noise level, the PID system faced system instability, substantial hemodynamic deviation, and LV suction during blood loss. In contrast, the response of the SMC was sufficiently rapid and robust against the noisy feedback signals.

CHAPTER 6: THE IN-VITRO EVALUATION OF THE PRELOAD-BASED CONTROL

6.1 Introduction

Left ventricular assist devices are the first choice in medical management for supporting end-stage heart failure patients awaiting heart implantation. In spite of the development of more than 30 different control methods, most LVADs are operated at fixed speeds, adjusted manually by the physicians. The constant speed operational mode is insensitive to changes in the metabolic requirements of the body (Salamonsen et al., 2011).

The left ventricular end-diastolic pressure naturally controls the force of LV contraction in proportion to the blood flow it receives from the right heart and pulmonary circulation, a mechanism commonly referred to as the Frank-Starling mechanism (Mansouri et al., 2015). As reported by previous publications, the natural heart output control can be emulated by providing accurate measurements of both flow and preload during VAD support (Nicholas Richard Gaddum et al., 2012). In real instances, LVAD flow is measured either using a flow sensor integrated in the LVAD cannula (Noon & Loebe, 2010) or estimated by non-invasive methods that use LVAD power and speed signals (A.-H. H. AlOmari, A. V. Savkin, D. M. Karantonis, E. Lim, & N. H. Lovell, 2009). In contrast, LV preload is not easily estimated or measured. In a recent comprehensive review, A.-H. H. AlOmari et al. (2013) reported few instances of physiological control based on non-invasive pressure measurements (A.-H. AlOmari et al., 2011). Although there is a prevalent view that currently available implantable pressure transducers are rendered virtually unusable due to a range of problems, new technology in blood pressure measurement promises greater biocompatibility and stability over time. Troughton et al. (2011) reported a pressure sensor with stable responses over a study period of four years. Moreover, another publication described optical fibers that could achieve the required stability in a constant-temperature environment of the heart and that is sufficiently small

to be embedded in the walls of the pump inlet and outlet cannulas (Konieczny et al., 2010; Zhou et al., 2012).

Mansouri et al. (2015) proposed a preload-based LVAD control that imitates the native flow sensitivity to preload, but this control mode has not been validated experimentally in an in vitro mock circulatory setting. It is therefore of interest to evaluate the performance of the preload-based control in comparison with a constant speed operation mode using a validated, mock circulation loop. In this work, the response of the preload-based controller to three different test scenarios, including moderate exercise, 70^0 head-up-tilt (HUT) and a major reduction in LV contractility (LVC) was assessed and compared with the constant speed operational mode. Both steady state and transient responses to these testing scenarios were investigated.

This chapter is organized as follows. The study methodology is presented in Section 6.2 along with a detailed description of the MCL and the preload-based control mechanism. In addition, the methodology section includes a broad description of the simulation protocols, which provide an accurate and repeatable hemodynamic transition from the baseline state to exercise, HUT and LVC reduction. The methodology section concludes with the criteria for performance evaluation. In Section 6.3, the temporal and steady state behavior of the key parameters for the cardiovascular system (CVS) during these hemodynamic transitions are reported. The preload sensitivity of each controller is also assessed. Section 6.4 comprises an extensive discussion on the results attained, clinical implications, and a comparison of the results with the literature. Finally, inadequacies of this study and future works, as well as concluding remarks, are included in Sections 6.5 and 6.6, respectively.

6.2 Methodology

6.2.1 Description of the Mock Circulation Loop

A physical mock circulation loop (Figure 6.1) including the systemic and pulmonary circulations was used for this study (D. L. Timms et al., 2011). Four independent Windkessel chambers were employed to represent the lumped systemic and pulmonary arterial and venous compliance. The systemic and pulmonary vascular resistances were easily manipulated by socket valves (VMP025.03X.71, AKO Alb. Klein Ohio LLC, USA). A series of electro-pneumatic regulators (ITV2030-012BS5, SMC Pneumatics, Tokyo, Japan) and 3/2 way solenoid valves (VT325-035DLS, SMC Pneumatics, Tokyo, Japan) were instrumented to control ventricular systole (i.e. contractility, heart rate and systolic interval) and passively fill the heart chambers. A Frank-Starling mechanism was implemented for both the left and right ventricles to actively control the ventricular pressure through the electro-pneumatic regulatory supply current based on ventricular preload. The mitral, aortic, tricuspid, and pulmonary valves were simulated using the mechanical check valves. The Bainbridge reflex mechanism was implemented to regulate the heart rate in response to hemodynamic changes (Gregory, Stevens, Timms, & Pearcy, 2011). In this study, a mixture of water and glycerol (60% water/40% glycerol by mass) was used as the working fluid to deliver asymptotic viscosity (3.5 mPa.s) and density (1100 kg/m3) similar to that of blood at 37°C.

A VentrAssist LVAD (VentraCor, Sydney, Australia) was used to support the simulated failing heart in the loop. The LVAD was cannulated with inflow connected to the LV and outflow to the aorta. The left and right atrial, left and right ventricular, systemic arterial, pulmonary arterial and LVAD inlet/outlet pressures were measured using the silicon-based transducers (PX181B-015C5V, OMEGA Engineering, Connecticut, USA). The systemic, pulmonary and LVAD flow rates were monitored by ultrasonic flowmeters

(TS410-10PXL, Transonic Systems, NY, USA). All data were sampled at 2 KHz and recorded using the dSpace 1103 hardware (Ceanet Pty Ltd, Sydney, Australia). The MCL operational and control software were developed in MATLAB/SIMULINK (The MathWorks, Natick, MA).

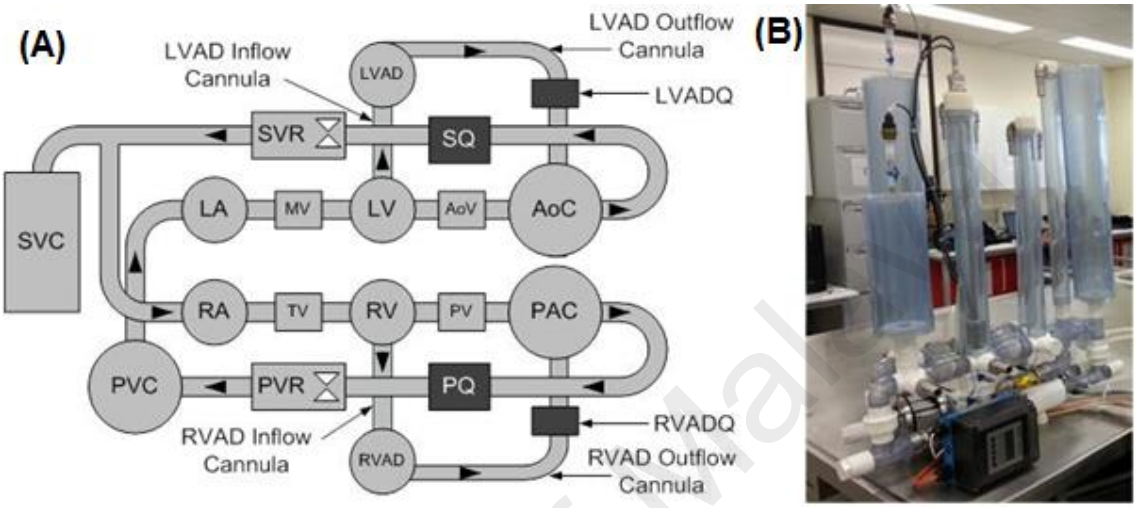

Figure 6.1: (A) Schematic of the dual circuit Mock Circulation Loop, and (B) Photograph of the MCL. LA, left atrium; MV, mitral valve; LV, left ventricle; AoV, aortic valve; AoC, systemic arterial compliance; SQ, systemic flow meter; SVR, systemic venous resistance; SVC, systemic venous compliance; RA, right atrium; TV, tricuspid valve; RV, right ventricle; PV, pulmonary valve; PAC, pulmonary arterial compliance; PQ, pulmonary flow meter; PVR, pulmonary venous resistance; PVC pulmonary venous compliance; LVAD left ventricular assist device.

6.2.2 Preload-Based Control

The immediate response of the preload-based controller emulated the Frank-Starling mechanism of the natural heart and was formulated as a sigmoid relationship between LV stroke work and PLVED (A.C. Guyton, 1963). A control line was generated by a third-order polynomial function (4.1) fitted to Guyton's data (A.C. Guyton, 1963). It should be noted that in this chapter I used mean PLVED (PLVEDm) on behalf of PLVED in the original equation.

Any change in state (Figure 6.2) causes a deviation in the operating point from its original position on the control line to other system lines (detailed descriptions provided in section 6.2.3). The controller then forces the operating point back to the control line (C_{Ln}) along a linear path, which conforms closely to the trajectories of the linearized system lines. Changes in state are thus countered by moving the operating point up or down the control line. The pump speed was controlled to maintain the operating point at its intersection between the control line and the system line.

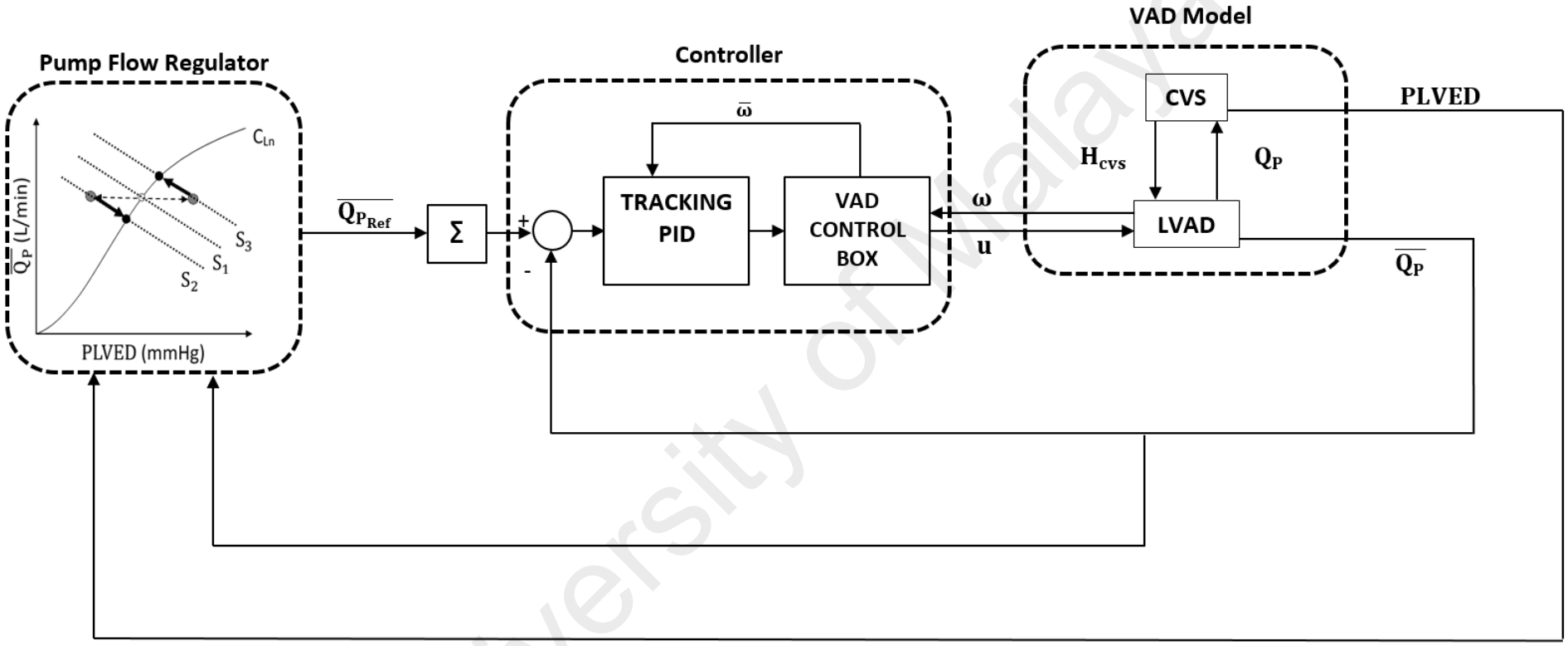

Figure 6.2: Block diagram of the control system. Grey circles, position of operating points after changes in states; White circle, position of operating point (current combination of PLVED and $\overline{Q_P}$) before a change of state; Black circles, position of operating points upon arriving at the new steady state located at the intersection between the control line and the new system line. The controller drives the changes in the operating points along the path indicated by the arrows along the new system line; $PLVED_m$ serves as the input to the preload controller; ∑, 1-second moving average.

6.2.3 System Lines

In order to understand how the CVS responds to various system perturbations, the first test was designed to define the characteristic system lines, which represent the paths undergone by the cardiovascular system over a range of LVAD speeds. The system lines for the baseline, exercise, HUT, and reduced LV contractility conditions during LVAD support were obtained by increasing the mean pump speed ($\bar{\omega}$) from 1800 rpm to 2800 rpm in increments of 100 rpm. The average flow through the pump ($\overline{Q_P}$) and the aortic valve ($\overline{Q_{av}}$) as well as $PLVED_m$ were recorded. The orientation of the system lines, which describe the relationship between $\overline{Q_P}$ and $PLVED_m$ during various hemodynamic conditions are depicted in Figure 6.3. As shown in Figure 6.3, in spite of the wide displacement among the system lines with varying test scenarios, the gradient of the system lines were similar regardless of the testing scenarios, and only changed while transitioning from AV open to AV close. For each scenario, the system gradients with respect to the closed and open aortic valve (AV) were calculated, and the average values were selected and tabulated in Table 6.1.

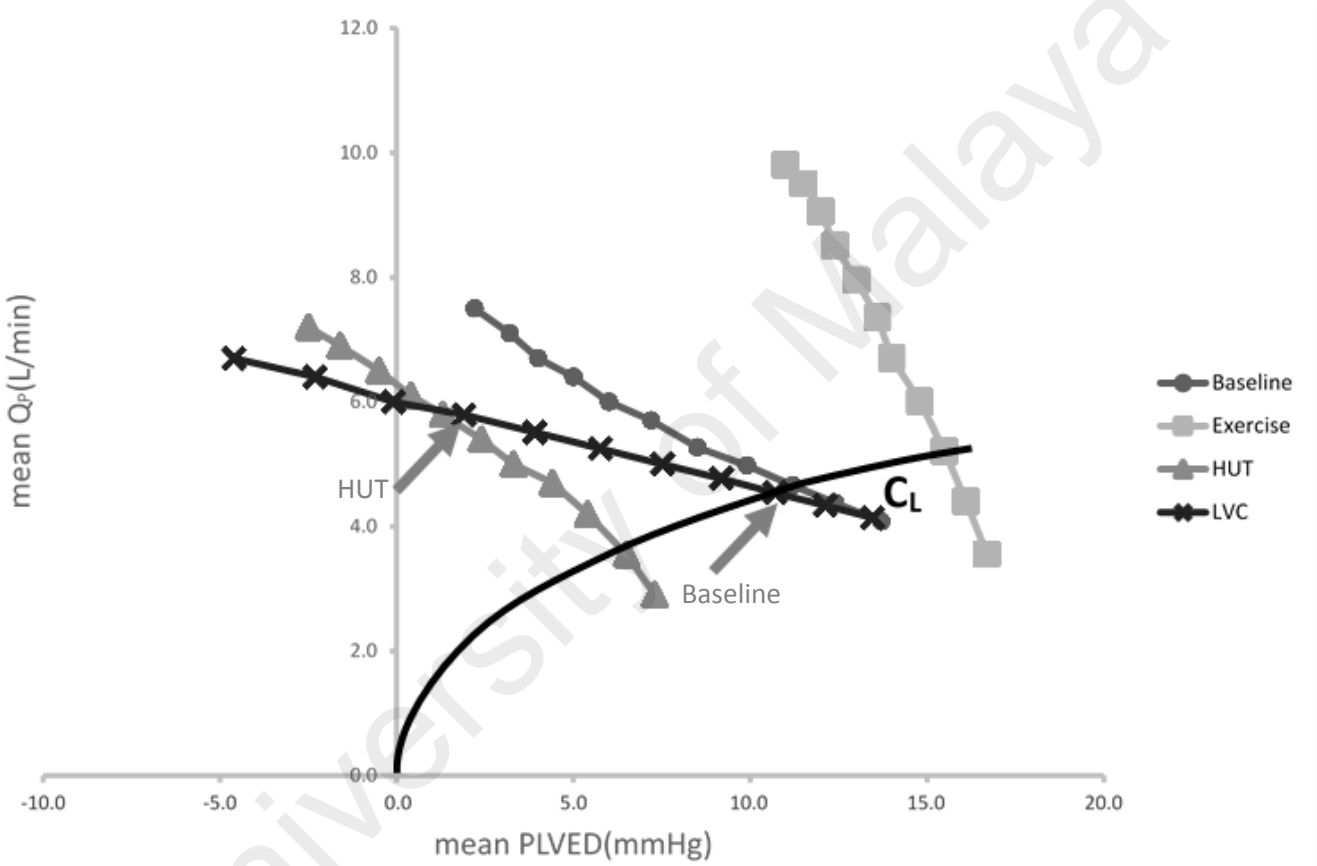

Figure 6.3: System response to variations in mean pump flow ($\overline{\mathbf{Q_P}}$) for baseline and three test conditions. Figure also shows the superimposed control line (C_{Ln}), where the minimum scaling factor (K) that allows the aortic valve to be closed in the baseline condition was chosen. Arrows indicate points where the aortic valve starts to open for baseline and HUT scenarios.

Table 6.1: Gradients for return lines (ratio of mean pump flow to PLVED) for baseline and three test scenarios, i.e. exercise, HUT and reduced LV contractility scenario. During exercise, the aortic valve (AV) remained open throughout the range of speed tested, while in reduced LV contractility scenario (Low LVC), the AV remained close.

System States	Gradient with AV Open (L/min/mmHg)	Gradient with AV Closed (L/min/mmHg)
Baseline	-0.24	-0.32
Exercise	-1.08	---
HUT	-0.62	-0.36
Low LVC	---	-0.14
Mean	-0.65	-0.27

6.2.4 Controller Implementation

Pump speed was measured based on the back electromotive force of the VentrAssist™ motor coils. A proportional-integral and derivative (PID) controller was developed to track the desired pump flow, $\overline{Q_{P_{Ref}}}$, by adjusting the average pump speed. Equation (6.1) defines the PID controller transfer function for tracking, automatically discretized by MATLAB/SIMULINK using a sampling period of 0.0005 seconds.

$$\begin{cases} \mathrm{PID}(S) = \left(K_P + \frac{K_I}{S} + K_D S_l\right) e(S_l) + \bar{\omega}(S_l) \\ e(S) = \overline{Q_{P_{Ref}}}(S_l) - \overline{Q_P}(S_l) \end{cases} \quad (6.1)$$

where $\bar{\omega}$ stands for mean pump rotational speed and S_l is the complex number frequency.

The PID gains were tuned based on Ziegler–Nichols method (Zinober, 1990) to achieve a 5% settling time of 10 s and a 10% maximum overshoot of the final value, in response

to a step change in the mean pump flow set point from 1.80 L/min (corresponding to a pump speed of 1800 rpm, i.e. the minimum operational speed) to the baseline value of 5.15 L/min. The resultant PID controller gains, K_P, K_I and K_D were set to 130, 162.5 and 58.5, respectively, which provided settling and response times of 2.0 s and 4.5 s, with no overshooting.

The speed, pump flow, and PLVED feedback signals were passed through a first-order transfer function to obtain their average values. This filter was selected owing to the simplicity of implementing it in dSpace. The cutoff frequency of the filter was empirically set to 0.25 Hz to abate the short-term variability of the feedback signals without compromising the system bandwidth. To minimize the tracking signal noise, a 1 s moving average filter was also designed and placed after $\overline{Q_{P_{Ref}}}$ and before feeding it to the controller. The moving average filter was selected for its ease and efficiency in removing Gaussian noise. The selected window width was 1 s, based on the normal heart beat of an adult (i.e. 60~100 bpm, corresponds to 1 ~ 1.7 Hz).

6.2.5 Experimental Protocol

Both constant speed operational mode and preload-based controller were subjected to the same assessment protocol. The scaling factor (K) was set to 1.0 for the preload-based controller, while the corresponding speed of the fixed speed control mode was set to 2100 rpm. Each experiment started with the baseline LV failure condition at rest for 120 s to allow the system to settle down, before performing a step change to one of the three test scenarios (exercise, HUT and reduced LVC). Upon transitioning to the new states, the experiments were continued for another 120 s to achieve the post-transition steady state.

To simulate an exercise scenario, 700 mL fluid was shifted from the systemic venous compliance (SVC) chamber into the circulation, emulating the action of the muscle pump in increasing venous return. Heart rate was increased from 60 to 90 bpm, while LVC was

increased from 1040 to 1880 mmHg/s. On the other hand, the systemic vascular resistance (SVR) and pulmonary vascular resistance (PVR) were decreased from 1300 to 600 dynes.s.cm^{-5} and from 110 to 40 dynes.s.cm^{-5} respectively.

To simulate HUT, 300 mL fluid was shifted from the circulation into the systemic venous compliance chamber to emulate blood-pooling effect. The systemic vascular resistance (SVR) and pulmonary vascular resistance (PVR) were increased from 1300 to 1635 dynes.s.cm^{-5} and from 110 to 210 dynes.s.cm^{-5} respectively, to simulate vasoconstriction. Meanwhile, a major reduction in LVC was reproduced by reducing the LV contractility to 2% of its baseline value using the LV electro-pneumatic regulators.

Fluid shifting in the MCL was controlled by adjusting the air pressure in the SVC chamber, where fluid is allowed to move into the SVC by reducing air pressure, while increasing air pressure shifts fluid out of the SVC. The fluid shift was facilitated using manual ball valves. The key MCL parameters used to mimic baseline, exercise, HUT and reduced LVC conditions were listed in Table 6.2.

Table 6.2: Key MCL parameters for mimicking different hemodynamic conditions. C_{lv}, LV end systolic elastance.

Variable	**Baseline**	**Exercise**	**HUT**	**LVC Reduction**
Heart Rate (bpm)	60	90	65	60
SVR (Dynes.s/cm^5)	1300	600	1635	1300
PVR (Dynes.s/cm^5)	110	40	210	110
Circulation fluid shift	---	SVC → RV (700mL)	RV → SVC (300mL)	---
C_{lv} (mmHg/s)	1040	1880	1040	25

For the exercise simulation and LVC scenarios, the change of parameters was immediate and simultaneous. For HUT scenario, changing of all parameters but fluid shifting was performed immediate and concurrently. Although for the posture change, the fluid shifting begun at the same time with other parameter alternation, because of the low dynamic of the mixture, the completion was lengthy but took no more than 20 seconds. For all simulations, we waited for the hemodynamic variables to settle to a steady state condition before transitioning from the baseline into one of the three test conditions. The simulation was then continued for a sufficient period to allow the control modes to achieve a post transition steady state.

6.2.6 Performance Evaluation

The performance of the preload-based and constant speed control methods was compared by observing the changes in mean pump flow, mean cardiac output, mean systemic arterial pressure, and mean left atrial pressure while transitioning from the baseline state to exercise, HUT and reduced LVC scenarios. The preload sensitivity of each controller was also investigated using the formula suggested by Khalil et al. (Khalil, Cohn, Metcalfe, & Frazier, 2008), as shown below:

$$P_S = \frac{\overline{Q_P}_{at} - \overline{Q_P}_{bt}}{\overline{P_{la}}_{at} - \overline{P_{la}}_{bt}} \tag{6.2}$$

where P_S is preload sensitivity (L/min/mmHg), $\overline{Q_P}$ represents the mean pump flow, $\overline{P_{la}}$ is the mean left atrial pressure, "at" represents 'after transition' and "bt" stands for 'before transition'.

6.3 Results

Figure 6.4, Figure 6.5, and Figure 6.6 show the temporal and steady state behaviors of the MAP and $\overline{Q_P}$ to exercise, HUT and reduced LVC respectively, for both controllers. In

addition, the plots also illustrate the relationship between $\overline{Q_P}$ and $PLVED_m$ while going through different perturbations.

As demonstrated in Figure 6.4, three distinct phases were shown while transitioning from the baseline state to exercise: i) an initial phase lasting approximately 5 s, ii) a middle phase lasting around 25 s, and iii) a steady state phase. At the onset of exercise, a drop in SVR and PVR resulted in an initial fall in MAP and rise in $\overline{Q_P}$ despite an increase in heart rate. After a few seconds, fluid was shifted from the systemic venous compliance into the RV, which subsequently activated the Frank-Starling mechanism, causing both left and right ventricular contractility to increase simultaneously. Consequently, MAP and $\overline{Q_P}$ increased gradually before settling to a level higher than their baseline values. Both controllers demonstrated similar hemodynamic transition pattern, with the preload-based controller showing larger fluctuations in the hemodynamic variables, especially $\overline{Q_P}$. Concerning steady state results (Table 6.3), the preload-based controller achieved a higher increase in $\overline{Q_P}$ (7.1 L/min) as compared to the constant speed mode (6.1 L/min). In addition, lower $PLVED_m$ (13.8 mmHg vs. 15.1 mmHg for the constant speed mode) was achieved, indicating less load on the LV. Apart from that, the preload-based controller obtained a higher preload sensitivity (0.56 L/min/mmHg) when compared to the constant speed (0.18 L/min/mmHg).

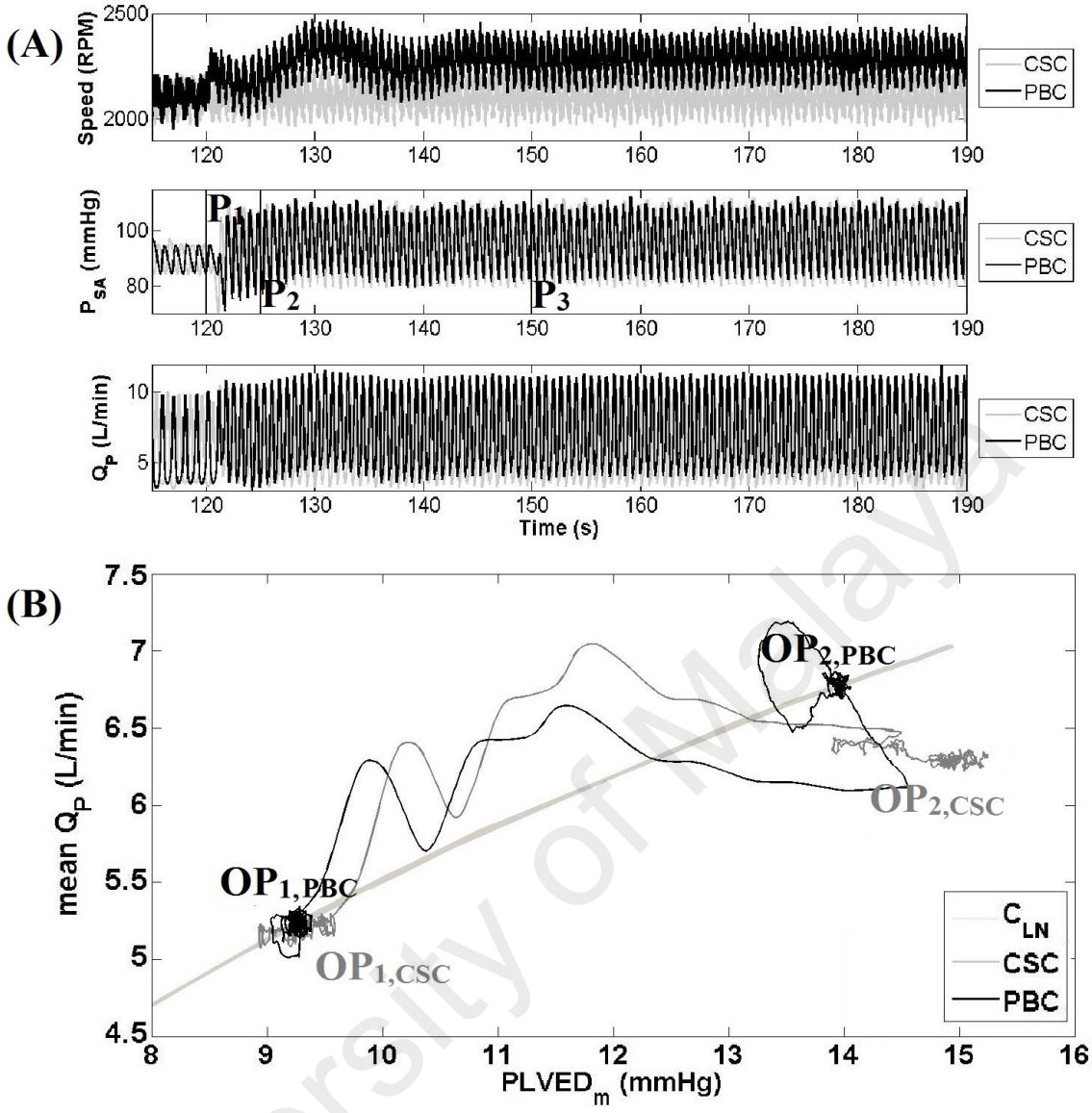

Figure 6.4: (A) Transient and steady state response of the mean arterial pressure and pump flow, and (B) the relationship between mean pump flow and mean PLVED while transitioning from baseline to exercise, for the constant speed mode and preload-based control. P_1, transient phase 1; P_2, transient phase 2; P_3, transient phase 3. The transition started at t=120 s.

Table 6.3: In-vitro hemodynamic data at baseline (rest) and exercise for constant speed mode and preload-based controllers.

		Constant Speed		**Preload**	
Variable	**Unit**	**Baseline**	**Exercise**	**Baseline**	**Exercise**
$\bar{\omega}$	rpm	2100±13	2100±15	2103±18	2295±18
MAP	mmHg	89±0.2	95±0.3	89±0.3	96±0.2
$\overline{P_{LA}}$	mmHg	10.9±0.1	16.3±0.1	10.8±0.1	14.2±0.1
$PLVED_m$	mmHg	9.5±0.1	15.3±0.2	9.3±0.1	13.8±0.4
$\overline{CO}$	L/min	5.2±0.1	10.1±0.1	5.2±0.1	10.4±0.1
$\overline{Q_P}$	L/min	5.2±0.1	6.2±0.1	5.2±0.1	7.1±0.2
Preload-sensitivity	L/min/mmHg	0.18		0.56	

At the onset of HUT, SVR and PVR increased, leading to a rise in MAP and a reduction in $\overline{Q_P}$ (Figure 6.5). As the fluid shifting process was lengthy (around 20 s), the circulation volume was almost constant during the initial stage. As the vacuuming process continued, blood was shifted from the circulation into the SVC, thus reducing the mean circulatory filling pressure, MAP and $\overline{Q_P}$. In terms of steady state results (Table 6.4), mean pump flow was reduced to 3.6 L/min while PLVED fell to 2.7 mmHg for the preload-based control during HUT, in comparison to 4.1 L/min and -0.1 mmHg for the constant speed controller. Thus, it can be concluded that preload-based control was able to reduce $\overline{Q_P}$ adequately to maintain an adequate safety margin against LV suction while constant speed controller could not. Apart from that, the preload-based controller obtained a higher preload sensitivity (0.45 L/min/mmHg) when compared to the constant speed (0.18 L/min/mmHg).

Meanwhile, as illustrated in Figure 6.6, a major reduction in LVC caused a sudden drop in both MAP and $\overline{Q_P}$. As the experiments continued, the preload-based controller was able to gradually increase the MAP and $\overline{Q_P}$ back to its original level by increasing mean pump speed, without a major change in $PLVED_m$. On the contrary, $\overline{Q_P}$ fell to 4.8 L/min while MAP dropped to 86 mmHg for the constant speed operational mode (Table 6.5).

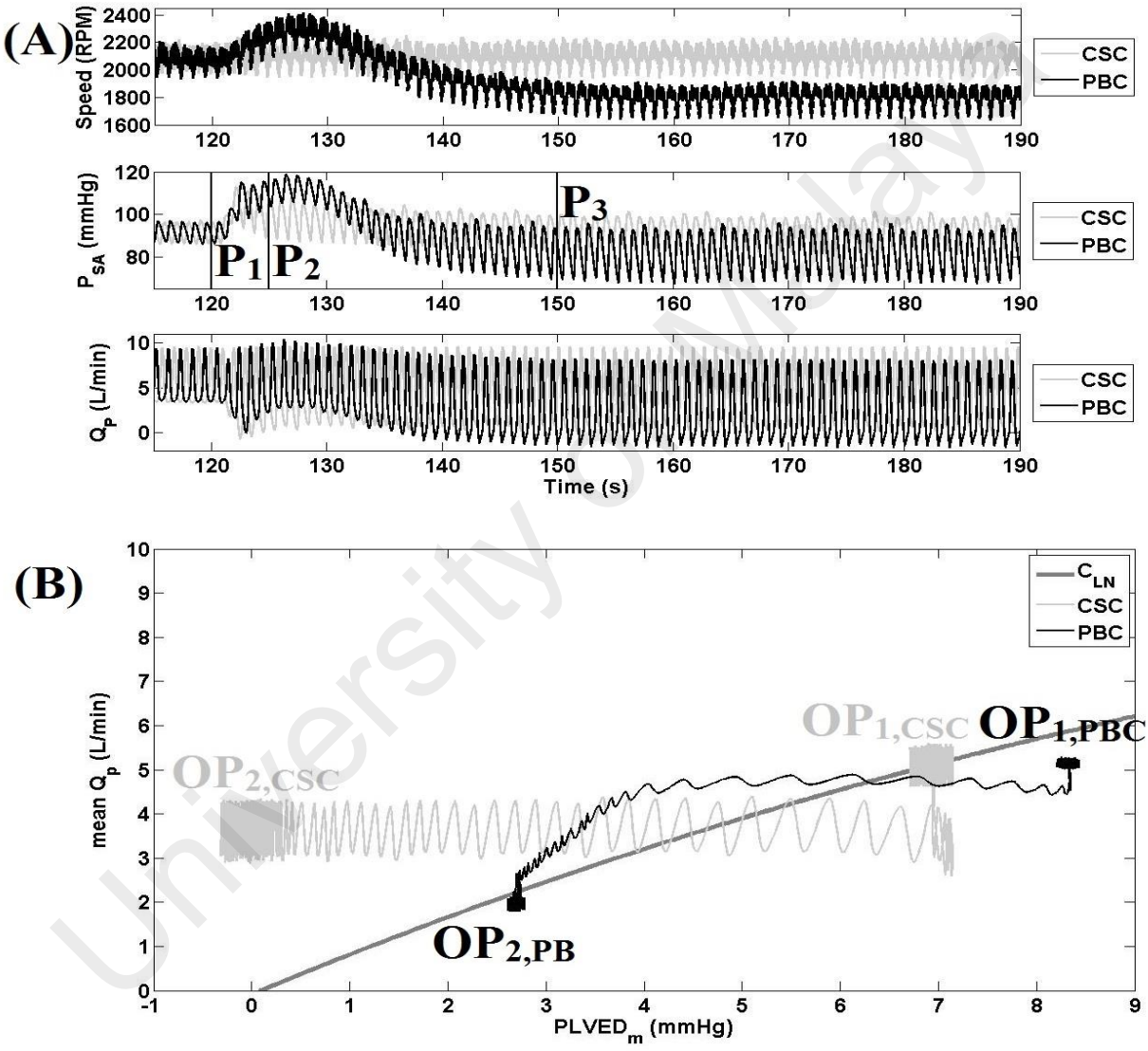

Figure 6.5: **(**A) Transient and steady state response of mean arterial pressure and pump flow, and (B) the relationship between mean pump flows and mean PLVED while transitioning from baseline to 70^0 HUT, for the constant speed mode and preload-based control. P_1, transient phase 1; P_2, transient phase 2; P_3, transient phase 3.The transition started at t=120 s.

Table 6.4: In-vitro hemodynamic data at baseline (rest) and 70° head up tilt (HUT) for constant speed mode and preload-based controllers

		Constant Speed		Preload	
Variable	**Unit**	**Baseline**	**HUT**	**Baseline**	**HUT**
$\bar{\omega}$	rpm	2100±13	2100±20	2096±19	1793±25
MAP	mmHg	91±0.2	92±0.2	92±0.3	81±0.3
$\overline{P_{LA}}$	mmHg	9.2±0.1	1.4±0.0	10.0±0.1	3.2±0.1
$PLVED_m$	mmHg	7.1±0.1	-0.1±0.2	8.3±0.1	2.7±0.1
$\overline{CO}$	L/min	5.2±0.1	4.1±0.1	5.3±0.1	3.6±0.1
$\overline{Q_P}$	L/min	5.1±0.1	3.7±0.2	5.1±0.1	2.0±0.1
Preload-sensitivity	L/min/mmHg	0.18		0.45	

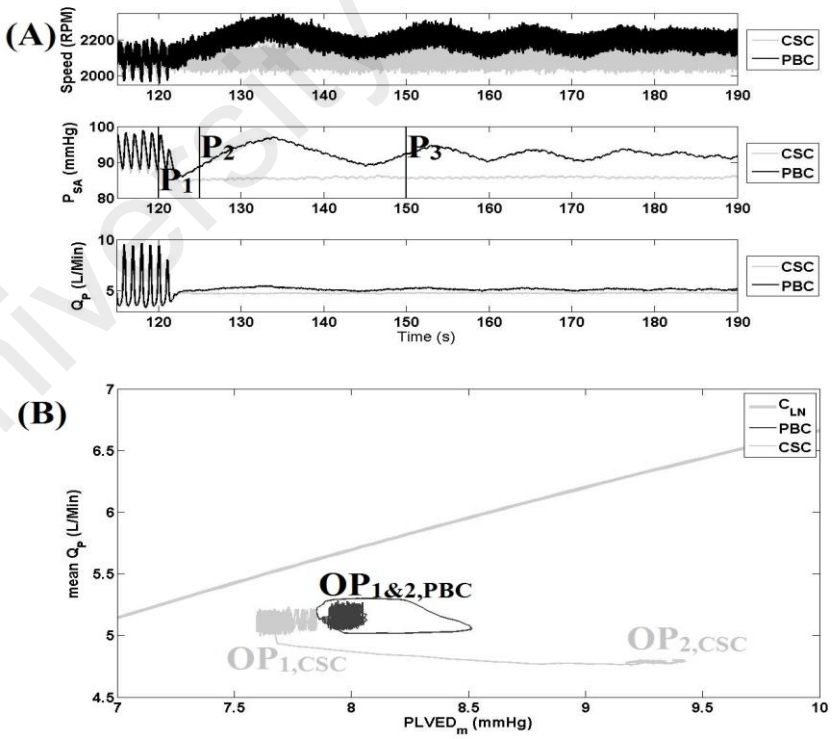

Figure 6.6: (A) Transient and steady state response of mean arterial pressure and pump flow, and (B) the relationship between mean pump flow, and mean PLVED while transitioning from baseline to reduced LV contractility scenario, for the constant speed mode and preload-based control. P_1, transient phase 1; P_2, transient phase 2; P_3, transient phase 3. The transition started at t=120 s.

Table 6.5: In-vitro hemodynamic data at baseline (rest) and reduced LV contractility scenario (LVC) for constant speed mode and preload-based controllers.

		Constant Speed		Preload	
Variable	**Unit**	**Baseline**	**LVC**	**Baseline**	**LVC**
$\bar{\omega}$	rpm	2100±13	2100±1	2096±17	2210±10
MAP	mmHg	92±0.1	86±0.1	92±0.3	92±0.2
$\overline{P_{LA}}$	mmHg	9.2±0.1	9.8±0.1	9.7±0.1	8.6±0.1
$PLVED_m$	mmHg	7.7±0.1	9.2±0.1	8.0±0.1	7.9±0.1
$\overline{CO}$	L/min	5.2±0.1	4.8±0.1	5.3±0.1	5.2±0.1
$\overline{Q_P}$	L/min	5.1±0.1	4.8±0.1	5.1±0.1	5.1±0.1
Preload sensitivity	L/min/mmHg	0.50		0.00	

6.4 Discussion

Apparent deficiencies observed in the fixed-speed operational mode have motivated researchers to develop various physiological responsive controllers. Nicholas R. Gaddum et al. (2014) utilized an adaptive pulsatile control based on the linear relationship between flow and remnant flow pulsatility to imitate the native Starling flow sensitivity (Salamonsen et al., 2012). Although their results demonstrated the strength of pulsatility control over the constant speed mode, there are several limitations associated with their controller. The main issue with the proposed pulsatility controller was that pump pulsatility (flow, current, pressure gradient, or speed) is a consequence of LV contraction while LV preload is one of the determinants of LV contraction. In cases of severe LV failure, LV does not sufficient ability to influence pulsatility and thus the dynamic range of pulsatility indexes is small. More importantly, pulsatility control is not feasible in cases with zero LV contractility.

Schima et al. (2006) described a so-called physiological control for an implantable rotary blood pump. The control proposed controller consists of two main functions. The first function is responsible to ascertain sufficient venous return whilst the second function undertakes controlling the pump. The system gets the pumps speed, motor current, and pump flow that the latter is measured invasively using ultrasound flow probe. The control section then tries to maintain a "desired flow" that already set by the user. Such maintenance is valid until the venous return is sufficient. Cases the venous return is not sufficient the system tries to adjust the speed depending on the pump flow pulsatility and suction. Although the "desired flow" could be set based on the patient's heart rate, however Schima set the flow to high levels that exceeded the patient's demands, the issue highlights the over pumping and draws the patient on the verge of suction. Moreover, Schima derived the venous return based of the pup pulsatility, which could be problematic in cases of severe heart failure(M. A. Bakouri et al., 2014). One limitation of this study is that the method is dependent on a moderate degree of residual LV contractility and will not work in the cases where LV shows low or no contractility at all.

On the contract, Mansouri et al. (2015) proposed a preload-based Starling-like control for implantable rotary blood pumps (IRBPs) using PLVED as the feedback variable. Simulations were conducted using a validated mathematical model. The controller emulates the response of the natural left ventricle to changes in PLVED. He also showed the proposed Starling-like controller outperformed a flow-based pulsatility control in avoiding suction in three common testing scenarios including vigorous exercise, blood loss and a major reduction in the LV contractility.

Compared to constant speed, the Starling-like control was able to synchronize the LV and RV outputs irrespective of variations in venous return (Salamonsen et al., 2012) by emulating the Frank-Starling control mechanism of the natural heart. The preload-based method produced less increase in PLVED during exercise and reduced LV contractility

scenarios (Table 6.3). Thus, utilizing this preload-based method lessens the chances of pulmonary congestion -- an incident that may otherwise lead to long-term right-side circulatory failure (Haddad et al., 2008). With physiological conditions involving a reduction in LV preload such as HUT, the preload-based method was able to maintain adequate distance against LV suction (Table 6.4). There has been evidence that LV suction may cause a significant reduction in RV performance through endocardial damage and septal shift (Salamonsen et al., 2012; Salamonsen, Lim, Moloney, Lovell, & Rosenfeldt, 2015). In cases involving a major reduction in LVC, we observed a preload increment with constant speed mode whilst MAP dropped. The preload-based control responded to such rise in preload by increasing the pump speed and flow, which subsequently returned the preload to its previous value (Table 6.5).

Another aim of this in-vitro study was to characterize the flow sensitivity of the proposed controller to preload and compare it with the conventional constant speed controller. In line with Nicholas R. Gaddum et al. (2014), employing the Frank-Starling controller generated preload sensitivity that is dependent on the body requirements, similar to that for the native heart. Whilst any increase in preload resulted in an increment in the preload sensitivity, preload reduction lowered the sensitivity. This was illustrated in our experimental results (Figure 6.4 (B) vs. Figure 6.5 (B), Table 6.3 vs. Table 6.4), where preloads of 13.8 and 2.7 mmHg during exercise and HUT resulted in sensitivities of 0.56 and 0.45 L/min/mmHg respectively for the preload-based controller. Meanwhile, much lower preload sensitivity 0.18 L/min/mmHg was achieved for the constant speed controller during both scenarios.

Published studies have indicated that employing a fixed-speed operational mode confines the flow sensitivity to preload with the inherent sensitivity of the connecting cannula configuration and resistance (N. R. Gaddum, D. L. Timms, et al., 2012), as well as the LVAD curve gradient (N. R. Gaddum, Fraser, & Timms, 2012). Thus, in case of a major

LVC reduction, substantial flow reduction was observed for the constant speed mode, marked by a preload sensitivity of 0.5 L/min/mmHg (Table 6.5). On the other hand, the preload-based control perfectly maintained $\overline{Q_P}$ and MAP at its baseline level, as reflected by a zero preload sensitivity.

6.5 Limitations and Future Work

The process of adapting curves and changing the scaling factor was initially introduced by Salamonsen et al. (2012) and evaluated by Nicholas R. Gaddum et al. (2014). Although this study focused on using a single preload control line, it is believed that a full controller will be capable of adapting to longer-term changes in the LV function by adjusting the scaling factor. This adjustment to different Frank-Starling curves not only provides inherent protection against LV suction, but also determines the degree of LV unloading.

In cases of low preload sensitivity, a fast-acting controller is ultimately required to apply a change in flow as soon as PLVED changes. In cases the pump flow and/or the head pressure across the pump is estimated an adaptive rule controller as Sliding Mode (M. A. Bakouri et al., 2014) could be used to realize an optimal adaptive control.

6.6 Conclusion

This experimental study clearly established the superiority of the preload-based control over the fixed speed operational mode while transitioning from the baseline state to exercise, HUT, and a major reduction in LVC. The preload-based controller was able to provide a greater flow and cardiac output during exercise as compared to the conventional constant speed controller, with less loading on the heart. In addition, it maintained a better safety margin against LV suction during HUT and MAP during a major reduction in LVC. The preload-based controller achieved a much higher preload-flow sensitivity as compared to the constant speed mode.

CHAPTER 7: CONCLUSIONS AND RECOMMENDATIONS

7.1 Conclusions

Despite extensive efforts in the area of IRBP control, most commercially available IRBPs still operate at a constant speed operational mode adjusted by the physicians, which resulted in a poor sensitivity to changes in the metabolic requirements of the patients. This dissertation attempted to develop and implement a robust preload-based physiological controller that could adapt to the body requirement during various hemodynamic perturbations in the presence of external noise, and without falling into adverse conditions such as suction or pulmonary congestion.

Chapter 3 presented a comparative evaluation of a number of well-established physiologically responsive controllers based on constant set point controlling methods using a validated numerical model, in response to exercise and HUT. Simulation results showed that while an increase in cardiac output during exercise was mainly dominated by an increase in the aortic valve flow, increasing pump speed could further improves total cardiac output through an increase in pump flow, thus reducing elevated filling pressures. Concerning the ability to increase cardiac output during exercise, constant $\overline{P_{la}}$ control outperformed other control modes. However, a fall in MAP was observed upon HUT, which may lead to circulatory instability. Constant $\overline{dP}$ control demonstrated superior performance under both exercise and HUT scenarios, potentially due to the preload and afterload sensitivity of IRBPs. Due to their strong dependency on the pump operating point, PI and $ratio_{PI}$ control performed poorly during exercise and HUT.

In view of the poor performance of the fixed set-point controllers, we have proposed a preload-based Frank-Starling control method, which emulates the Frank-Starling mechanism of the native heart. In this control method, pump flow was regulated using left ventricular end diastolic pressure as the feedback signal. In Chapter 4, the performance of the proposed preload-based control was assessed in comparison with the

constant speed operation and the pulsatility index control using an extensively validated numerical model. Simulation results showed that the preload-based control outperformed both constant speed and pulsatility control modes in handling the transition from a baseline state to exercise, blood loss, and a major reduction in LV contractility. In particular, preload-based control achieved the greatest increase in mean pump flow with minimum loading on the LV during exercise, and maintained the greatest safety margin against LV suction during blood loss. Meanwhile, mean pump flow and PLVED remained relatively constant with a major reduction in LV contractility for the preload-based control, as opposed to the pulsatility control, which demonstrated a substantial drop in mean pump flow and mean arterial pressure.

Chapter 5 describes the implementation of the preload-based controller in vitro using a mock circulatory loop. The flow sensitivity of the preload-based and fixed speed controllers to preload, as well as their steady state and transient response to moderate exercise, 70^0 head-up-tilt, and a major reduction in LV contractility were characterized. Experimental results showed that the preload-based controller was able to provide a greater flow and cardiac output during exercise as compared to the fixed speed controller, with less loading on the heart. In addition, it maintained a better safety margin against LV suction during HUT and MAP during a major reduction in LVC. Concerning preload-flow sensitivity, the preload-based controller achieved a much better preload-flow sensitivity as compared to the fixed speed operational mode.

In the final chapter, a sliding mode controller was developed for the preload-based controller. The transient and steady state performance of the SMC to exercise and blood loss was compared with a proportional-integral-derivative controller using the dynamic cardiovascular numerical model. In addition to the noise-free scenario, the performance of these methods was also evaluated in the presence of noise, where the feedback signal was contaminated with two different levels of Gaussian white noise. Although no

prominent difference in performance existed between the PID and SMC methods in the noise-free condition and at a relatively lower noise level, the PID system faced system instability, substantial hemodynamic deviation, and LV suction during blood loss. In contrast, the response of the SMC was sufficiently rapid and robust against the noisy feedback signals.

7.2 Suggestions for Future Work

7.2.1 Noninvasive estimation of PLVED

In the numerical and experimental studies, the PLVED was obtained directly from the model and measured using a pressure transducer in the MCL at end diastole of each heartbeat. In reality, there is a widespread view that currently available implantable pressure transducers are rendered virtually unusable due to a range of problems. These include limited reliability, drifts in transducers' response over time, and the anatomical distortion they present to pump inlet cannula, resulting in unwanted flow turbulence and associated clotting disorders. For LVAD control purposes, it would be worthwhile to study the correlation between the PLVED and the noninvasive measurements such as speed current and PWM, which would provide a noninvasive and accurate estimation of PLVED. This information can be easily obtained using both the experimental results and the mathematical model.

7.2.2 Adjustments of the scaling factor for the Frank-Starling curves

In this thesis, a single control line was utilized for the preload-based control system. In order to accommodate to longer-term changes in the LV function and metabolic demand, the scaling factor of the control line, which represents the sensitivity of the Frank Starling relationship should be adjusted. This adjustment to different Frank-Starling curves not only provides inherent protection against LV suction, but also determines the degree of LV unloading.

7.2.3 In vivo evaluation of the preload-based controller

The performance of the preload-based controller has been evaluated using both numerical simulations and in vitro mock circulatory experiments. It would be interesting to evaluate the performance of the preload-based control method using in vivo animal experiments, which more closely resembles the human cardiovascular system.

7.2.4 Alternative control strategies

In the present thesis, the performance of both PID and SMC implementation methods has been evaluated for the proposed preload-based controller. More robust control strategies, such as H-infinity control and model predictive control may be explored. In regards to the control objectives, future studies may look into the combination of various control strategies (multi-objective control), as a single control objective may be insufficient for the safe operation of an LVAD.

REFERENCES

Akimoto, T., Yamazaki, K., Litwak, P., Litwak, K. N., Tagusari, O., Mori, T., . . . Umezu, M. (1999). Rotary blood pump flow spontaneously increases during exercise under constant pump speed: Results of a chronic study. *Artificial organs, 23*(8), 797-801.

AlOmari, A.-H., Savkin, A., Ayre, P., Lim, E., Mason, D., Salamonsen, R., . . . Lovell, N. (2011). Non-invasive estimation and control of inlet pressure in an implantable rotary blood pump for heart failure patients. *Physiological measurement, 32*(8), 1035.

AlOmari, A.-H. H., Savkin, A. V., Karantonis, D. M., Lim, E., & Lovell, N. H. (2009). *A dynamical model for pulsatile flow estimation in a left ventricular assist device.* Paper presented at the BIOSIGNALS.

AlOmari, A.-H. H., Savkin, A. V., Stevens, M., Mason, D. G., Timms, D. L., Salamonsen, R. F., & Lovell, N. H. (2013). Developments in control systems for rotary left ventricular assist devices for heart failure patients: A review. *Physiological measurement, 34*(1), R1.

AlOmari, A., Savkin, A., Karantonis, D., Lim, E., & Lovell, N. (2009). Non-invasive estimation of pulsatile flow and differential pressure in an implantable rotary blood pump for heart failure patients. *Physiological measurement, 30*(4), 371.

Arndt, A., Nüsser, P., Graichen, K., Müller, J., & Lampe, B. (2008). Physiological control of a rotary blood pump with selectable therapeutic options: Control of pulsatility gradient. *Artificial organs, 32*(10), 761-771.

Arndt, A., Nüsser, P., & Lampe, B. (2010). Fully autonomous preload‐sensitive control of implantable rotary blood pumps. *Artificial organs, 34*(9), 726-735.

Bakouri, M., Savkin, A., & Alomari, A. (2015). Nonlinear modelling and control of left ventricular assist device. *Electronics Letters, 51*(8), 613-615.

Bakouri, M. A., Salamonsen, R. F., Savkin, A. V., AlOmari, A. H. H., Lim, E., & Lovell, N. H. (2013). A sliding mode‐based starling‐like controller for implantable rotary blood pumps. *Artificial organs*.

Bakouri, M. A., Salamonsen, R. F., Savkin, A. V., AlOmari, A. H. H., Lim, E., & Lovell, N. H. (2014). A sliding mode‐based Starling‐Like controller for implantable rotary blood pumps. *Artificial organs, 38*(7), 587-593.

Bartolini, G., Ferrara, A., & Utkin, V. I. (1995). Adaptive sliding mode control in discrete-time systems. *Automatica, 31*(5), 769-773.

Berne, R. M. (1981). Cardiovascular physiology. *Annual Review of Physiology, 43*(1), 357-358.

Boston, J., Antaki, J., & Simaan, M. (2003). Hierarchical control of heart-assist devices. *Robotics & Automation Magazine, IEEE, 10*(1), 54-64.

Brassard, P., Jensen, A. S., Nordsborg, N., Gustafsson, F., Møller, J. E., Hassager, C., . . . Sander, K. (2011). Central and peripheral blood flow during exercise with a continuous-flow left ventricular assist deviceclinical perspective constant versus increasing pump speed: A pilot study. *Circulation: Heart Failure, 4*(5), 554-560.

Bubnicki, Z. (2005). *Modern Control Theory*: Springer.

Bullister, E., Reich, S., & Sluetz, J. (2002). Physiologic control algorithms for rotary blood pumps using pressure sensor input. *Artificial organs, 26*(11), 931-938. doi: 10.1046/j.1525-1594.2002.07126.x

Choi, S., Antaki, J., Boston, R., & Thomas, D. (2001). A sensorless approach to control of a turbodynamic left ventricular assist system. *Control Systems Technology, IEEE Transactions on, 9*(3), 473-482.

Choi, S., Boston, J. R., & Antaki, J. F. (2005). An investigation of the pump operating characteristics as a novel control index for LVAD control. *Int. J. Control Autom. Syst, 3*, 100-108.

Choi, S., Boston, J. R., & Antaki, J. F. (2007). Hemodynamic controller for left ventricular assist device based on pulsatility ratio. *Artificial organs, 31*(2), 114-125.

Eckberg, D. L., & Sleight, P. (1992). *Human baroreflexes in health and disease*: Oxford University Press.

Elsayed, B. A., Hassan, M., & Mekhilef, S. (2013). Decoupled third-order fuzzy sliding model control for cart-inverted pendulum system. *Appl. Math, 7*(1), 193-201.

Endo, G., Araki, K., Oshikawa, M., Kojima, K., Nakamura, K., Matsuzaki, Y., & Onitsuka, T. (2002). A safe automatic driving method for a continuous flow ventricular assist device based on motor current pulsatility: In-vitro evaluation. *ASAIO Journal, 48*(1), 83-89.

Esmore, D. S., Kaye, D., Salamonsen, R., Buckland, M., Begg, J. R., Negri, J., . . . Rosenfeldt, F. L. (2008). Initial clinical experience with the VentrAssist left ventricular assist device: The pilot trial. *The Journal of heart and lung transplantation, 27*(5), 479-485.

Farrar, D. J., Bourque, K., Dague, C. P., Cotter, C. J., & Poirier, V. L. (2007). Design features, developmental status, and experimental results with the Heartmate III centrifugal left ventricular assist system with a magnetically levitated rotor. *ASAIO Journal, 53*(3), 310-315.

Fu, M., & Xu, L. (2000). Computer simulation of sensorless fuzzy control of a rotary blood pump to assure normal physiology. *ASAIO Journal, 46*(3), 273-278.

Gaddum, N. R., Fraser, J. F., & Timms, D. L. (2012). Increasing the transmitted flow pulse in a rotary left ventricular assist device. *Artif Organs, 36*(10), 859-867. doi: 10.1111/j.1525-1594.2012.01485.x

Gaddum, N. R., Stevens, M., Lim, E., Fraser, J., Lovell, N., Mason, D., . . . Salamonsen, R. (2014). Starling-like flow control of a left ventricular assist device: In-vitro validation. *Artificial organs, 38*(3), E46-E56. doi: 10.1111/aor.12221

Gaddum, N. R., Timms, D. L., Stevens, M., Mason, D., Lovell, N., & Fraser, J. F. (2012). Comparison of preload-sensitive pressure and flow controller strategies for a dual device biventricular support system. *Artif Organs, 36*(3), 256-265. doi: 10.1111/j.1525-1594.2011.01344.x

Gaddum, N. R., Timms, D. L., Stevens, M., Mason, D., Lovell, N., & Fraser, J. F. (2012). Comparison of preload ‐ sensitive pressure and flow controller strategies for a dual device biventricular support system. *Artificial organs, 36*(3), 256-265.

Gao, W., Wang, Y., & Homaifa, A. (1995). Discrete-time variable structure control systems. *Industrial Electronics, IEEE Transactions on, 42*(2), 117-122.

Giridharan, G., Pantalos, G., Koenig, S., Gillars, K., & Skliar, M. (2005). *Achieving physiologic perfusion with ventricular assist devices: comparison of control strategies.* Paper presented at the American Control Conference, 2005. Proceedings of the 2005.

Giridharan, G. A., Pantalos, G. M., Gillars, K. J., Koenig, S. C., & Skliar, M. (2004). Physiologic control of rotary blood pumps: an in vitro study. *ASAIO Journal, 50*(5), 403-409.

Giridharan, G. A., & Skliar, M. (2002). Nonlinear controller for ventricular assist devices. *Artificial organs, 26*(11), 980-984.

Giridharan, G. A., & Skliar, M. (2006). Physiological control of blood pumps using intrinsic pump parameters: A computer simulation study. *Artificial organs, 30*(4), 301-307.

Goodwin, G. C., Graebe, S. F., & Salgado, M. E. (2001). Design via optimal control techniques *Control system design* (pp. 240): Prentice Hall New Jersey.

Gregory, S. D., Stevens, M., Timms, D., & Pearcy, M. (2011). *Replication of the Frank-Starling response in a mock circulation loop.* Paper presented at the Engineering in Medicine and Biology Society, EMBC, 2011 Annual International Conference of the IEEE.

Guyton, A. C. (1963). Circulatory physiology: Cardiac output and its regulation (pp. 237–239). Philadelphia and London: W.B. Saunders Company.

Guyton, A. C. (1965). Circulatory physiology: Cardiac output and its regulation. *The American Journal of the Medical Sciences, 219*(1), 122.

Guyton, A. C., & Hall, J. (1996). Textbook of medical physiology. *Philadelphia: Saunders Company*.

Guyton, A. C., & Hall, J. E. (2005). *Textbook of medical physiology*. Philadelphia: PA: W.B. Saunders Company.

Gwak, K.-W., Kim, H. D., Lee, S.-G., Park, S., & Kim, C.-W. (2015). Sliding mode control for the Frank–Starling response of a piston pump mock ventricle. *Journal of Process Control, 25*(0), 70-77.

Haddad, F., Doyle, R., Murphy, D. J., & Hunt, S. A. (2008). Right ventricular function in cardiovascular disease, part ii pathophysiology, clinical importance, and management of right ventricular failure. *Circulation, 117*(13), 1717-1731.

Hung, J. (1993). *Chattering handling for variable structure control systems.* Paper presented at the Industrial Electronics, Control, and Instrumentation, 1993. Proceedings of the IECON'93., International Conference on.

Jacquet, L., Vancaenegem, O., Pasquet, A., Matte, P., Poncelet, A., Price, J., . . . Noirhomme, P. (2011). Exercise capacity in patients supported with rotary blood pumps is improved by a spontaneous increase of pump flow at constant pump speed and by a rise in native cardiac output. *Artificial organs, 35*(7), 682-690.

Karantonis, D. M., Lovell, N. H., Ayre, P. J., Mason, D. G., & Cloherty, S. L. (2006). Identification and classification of physiologically significant pumping states in an implantable rotary blood pump. *Artificial organs, 30*(9), 671-679.

Khalil, H. A., Cohn, W. E., Metcalfe, R. W., & Frazier, O. H. (2008). Preload sensitivity of the Jarvik 2000 and HeartMate II left ventricular assist devices. *ASAIO Journal, 54*(3), 245-248.

Klabunde, R. (2011). *Cardiovascular physiology concepts*: Lippincott Williams & Wilkins.

Koh, C., Chan, W., Ng, B., & Li, H. (1999). Design and investigation of flow field in a centrifugal blood pump. *ASME-PUBLICATIONS-BED, 42*, 167-168.

Konieczny, G., Opilski, Z., Pustelny, T., Gacek, A., Gibinski, P., & Kustosz, R. (2010). Results of experiments with fiber pressure sensor applied in the polish artificial heart prosthesis. *Acta Physica Polonica, A., 118*(6), 1183.

Lee, J. J., Ahn, C. B., Choi, J., Park, J. W., Song, S. J., & Sun, K. (2011). Development of magnetic bearing system for a new third‐generation blood pump. *Artificial organs, 35*(11), 1082-1094.

Letsou, G. V., Reverdin, S., & Frazier, O. (2013). Thyrotoxicosis-facilitated bridge to recovery with a continuous-flow left ventricular assist device. *European Journal of Cardio-Thoracic Surgery*, ezt106.

Levine, W. S. (1996). *The control handbook*: CRC press.

Lim, E. (2009). *Characterisation of cardiovascular-rotary blood pump interaction.* (Doctor of Philosophy), The University of New South Wales, Sydney, Australia.

Lim, E., Alomari, A., Savkin, A., & Lovell, N. (2009). *Noninvasive deadbeat control of an implantable rotary blood pump: A simulation study.* Paper presented at the Engineering in Medicine and Biology Society, 2009. EMBC 2009. Annual International Conference of the IEEE.

Lim, E., Chan, G. S., Dokos, S., Ng, S. C., Latif, L. A., Vandenberghe, S., . . . Lovell, N. H. (2013). A cardiovascular mathematical model of graded head-up tilt. *PLoS ONE, 8*(10), e77357.

Lim, E., Dokos, S., Cloherty, S. L., Salamonsen, R. F., Mason, D. G., Reizes, J. A., & Lovell, N. H. (2010). Parameter-optimized model of cardiovascular–rotary blood pump interactions. *Biomedical Engineering, IEEE Transactions on, 57*(2), 254-266.

Lim, E., Dokos, S., Salamonsen, R. F., Rosenfeldt, F. L., Ayre, P. J., & Lovell, N. H. (2012a). Effect of parameter variations on the hemodynamic response under rotary blood pump assistance. *Artificial organs, 36*(5), E125-E137.

Lim, E., Dokos, S., Salamonsen, R. F., Rosenfeldt, F. L., Ayre, P. J., & Lovell, N. H. (2012b). Numerical optimization studies of cardiovascular–rotary blood pump interaction. *Artificial organs, 36*(5), E110-E124.

Lim, E., Salamonsen, R. F., Mansouri, M., Gaddum, N., Mason, D. G., Timms, D. L., . . . Lovell, N. H. (2015). Hemodynamic response to exercise and head-up tilt of patients implanted with a rotary blood pump: A computational modeling study. *Artificial organs, 39*(2), E24-E35. doi: 10.1111/aor.12370

Lin, H. C., Lowe, A., & Al-Jumaily, A. (2014). Non-invasive blood pressure measurement algorithm using neural networks. *Artificial Intelligence Research, 3*(2), p16.

Maeda, K., Tsutamoto, T., Wada, A., Hisanaga, T., & Kinoshita, M. (1998). Plasma brain natriuretic peptide as a biochemical marker of high left ventricular end-diastolic pressure in patients with symptomatic left ventricular dysfunction. *American heart journal, 135*(5), 825-832.

Magosso, E., Cavalcanti, S., & Ursino, M. (2002). Theoretical analysis of rest and exercise hemodynamics in patients with total cavopulmonary connection. *American Journal of Physiology-Heart and Circulatory Physiology, 282*(3), H1018-H1034.

Magosso, E., & Ursino, M. (2002). Cardiovascular response to dynamic aerobic exercise: A methematical model. *Medical and Biological Engineering and Computing, 40*(6), 660-674.

Mancini, D., Goldsmith, R., Levin, H., Beniaminovitz, A., Rose, E., Catanese, K., . . . Oz, M. (1998). Comparison of exercise performance in patients with chronic severe heart failure versus left ventricular assist devices. *Circulation, 98*(12), 1178-1183.

Mansouri, M., Salamonsen, R. F., Lim, E., Akmeliawati, R., & Lovell, N. H. (2015). Preload-based Starling-like control for rotary blood pumps: Numerical comparison with pulsatility control and constant speed operation. *PLoS ONE, 10*(4), e0121413. doi: 10.1371/journal.pone.0121413

Markham, D. W., Fu, Q., Palmer, M. D., Drazner, M. H., Meyer, D. M., Bethea, B. T., . . . Levine, B. D. (2013). Sympathetic neural and hemodynamic responses to upright tilt in patients with pulsatile and nonpulsatile left ventricular assist devices. *Circulation: Heart Failure, 6*(2), 293-299.

Mason, D. G., Hilton, A. K., & Salamonsen, R. F. (2008). Reliable suction detection for patients with rotary blood pumps. *ASAIO Journal, 54*(4), 359-366.

Monsees, G. (2002). *Discrete-time sliding mode control*: TU Delft, Delft University of Technology.

Muthiah, K., Gupta, S., Robson, D., Walker, R., Macdonald, P. S., Jansz, P., & Hayward, C. S. (2013). Effect of body position on continuous flow left ventricular assist device flow dynamics. *The Journal of heart and lung transplantation : the official publication of the International Society for Heart Transplantation, 32*(4), S233.

Muthiah, K., Robson, D., Walker, R., Otton, J., Macdonald, P., Keogh, A., . . . Granger, E. (2012). Relationship between heart rate and pump flow in patients implanted with continuous flow left ventricular assist devices (LVAD). *Heart, Lung and Circulation, 21*, S91.

Noon, G. P., & Loebe, M. (2010). Current status of the MicroMed DeBakey Noon ventricular assist device. *Texas Heart Institute Journal, 37*(6), 652.

Park, S. J., Tector, A., Piccioni, W., Raines, E., Gelijns, A., Moskowitz, A., . . . Frazier, O. H. (2005). Left ventricular assist devices as destination therapy: a new look at survival. *The Journal of thoracic and cardiovascular surgery, 129*(1), 9-17.

Pepi, M., Guazzi, M., Maltagliati, A., Berna, G., & Tamborini, G. (2000). Diastolic ventricular interaction in normal and dilated heart during head‐up tilting. *Clinical cardiology, 23*(9), 665-672.

Reesink, K., Dekker, A., Van der Nagel, T., Beghi, C., Leonardi, F., Botti, P., . . . Maessen, J. (2007). Suction due to left ventricular assist: implications for device control and management. *Artificial organs, 31*(7), 542-549.

RevisionWorld. (2015). Human circulatory system. 2015, from http://www.revisionworld.com/a2-level-level-revision/biology/physiology-transport/human-circulatory-system

Sagawa, K., Maughan, L., Suga, H., & Sunagawa, K. (1988). *Cardiac contraction and the pressure-volume relationship* (Vol. 480): Oxford University Press New York.

Saito, I., Ishii, K., Isoyama, T., Ono, T., Nakagawa, H., Shi, W., . . . Abe, Y. (2010). *Preliminary study of physiological control for the undulation pump ventricular assist device.* Paper presented at the Proc. 32nd Annu. Int. Conf. of the IEEE Eng. Med. Biol. Soc.

Salamonsen, R. F., Lim, E., Gaddum, N., AlOmari, A. H. H., Gregory, S. D., Stevens, M., . . . Karunanithi, M. K. (2012). Theoretical foundations of a Starling‐like controller for rotary blood pumps. *Artificial organs, 36*(9), 787-796.

Salamonsen, R. F., Lim, E., Moloney, J., Lovell, N. H., & Rosenfeldt, F. L. (2015). Anatomy and physiology of left ventricular suction induced by rotary blood pumps. *Artificial organs, 39*(8), 681-690.

Salamonsen, R. F., Mason, D. G., & Ayre, P. J. (2011). Response of rotary blood pumps to changes in preload and afterload at a fixed speed setting are unphysiological when compared with the natural heart. *Artificial organs, 35*(3), E47-E53.

Salamonsen, R. F., Pellegrino, V., Fraser, J. F., Hayes, K., Timms, D., Lovell, N. H., & Hayward, C. (2013). Exercise studies in patients with rotary blood pumps: Cause, effects, and implications for starling‐like control of changes in pump flow. *Artificial organs, 37*(8), 695-703.

Schima, H., Vollkron, M., Jantsch, U., Crevenna, R., Roethy, W., Benkowski, R., . . . Wieselthaler, G. (2006). First clinical experience with an automatic control system for rotary blood pumps during ergometry and right-heart catheterization. *The Journal of heart and lung transplantation, 25*(2), 167-173.

Shahnazi, R., Shanechi, H. M., & Pariz, N. (2008). Position control of induction and DC servomotors: a novel adaptive fuzzy PI sliding mode control. *Energy Conversion, IEEE Transactions on, 23*(1), 138-147.

Skogestad, S. (2006). Tuning for smooth PID control with acceptable disturbance rejection. *Industrial & engineering chemistry research, 45*(23), 7817-7822.

Slaughter, M. S., Bartoli, C. R., Sobieski, M. A., Pantalos, G. M., Giridharan, G. A., Dowling, R. D., . . . Koenig, S. C. (2009). Intraoperative evaluation of the HeartMate II flow estimator. *The Journal of heart and lung transplantation, 28*(1), 39-43.

Smith, W. A., Goodin, M., Fu, M., & Xu, L. (1999). System analysis of the flow/pressure response of rotodynamic blood pumps. *Artificial organs, 23*(10), 947-955.

Starling, E., & Visscher, M. (1927). The regulation of the energy output of the heart. *The Journal of physiology, 62*(3), 243-261.

Stevens, M. C. (2014). *Automatic control of dual LVADs as a BiVADs.* (Doctor of Philosophy), The University of Queensland, Brisbane, QLD, AUSTRALIA.

Stevens, M. C., Mason, D. G., Bradley, A. P., Wilson, S., Fraser, J. F., & Timms, D. (2014). Comparison of linear and non-linear control of flow and pressure in a rotary left ventricular assist device. *Medical and Biological Engineering and Computing (Submitted).*

Tagusari, O., Yamazaki, K., Litwak, P., Antaki, J. F., Watach, M., Gordon, L. M., . . . Griffith, B. P. (1998). Effect of pressure‐flow relationship of centrifugal pump on in vivo hemodynamics: A consideration for design. *Artificial organs, 22*(5), 399-404.

Timms, D. (2011). A review of clinical ventricular assist devices. *Medical engineering & physics, 33*(9), 1041-1047.

Timms, D. L., Gregory, S. D., Greatrex, N. A., Pearcy, M. J., Fraser, J. F., & Steinseifer, U. (2011). A compact mock circulation loop for the in vitro testing of cardiovascular devices. *Artificial organs, 35*(4), 384-391.

Troughton, R. W., Ritzema, J., Eigler, N. L., Melton, I. C., Krum, H., Adamson, P. B., . . . Heywood, J. T. (2011). Direct left atrial pressure monitoring in severe heart failure: long-term sensor performance. *Journal of cardiovascular translational research, 4*(1), 3-13.

Ursino, M. (1998). Interaction between carotid baroregulation and the pulsating heart: a mathematical model. *American Journal of Physiology-Heart and Circulatory Physiology, 275*(5), H1733-H1747.

Utkin, V. I. (2013). *Sliding modes in control and optimization*: Springer Science & Business Media.

Vollkron, M., Schima, H., Huber, L., Benkowski, R., Morello, G., & Wieselthaler, G. (2005). Development of a reliable automatic speed control system for rotary blood pumps. *The Journal of heart and lung transplantation, 24*(11), 1878-1885.

Waters, T., Allaire, P., Tao, G., Adams, M., Bearnson, G., Wei, N., . . . Khanwilkar, P. (1999). Motor feedback physiological control for a continuous flow ventricular assist device. *Artificial organs, 23*(6), 480-486.

World Health Organization, W. (2015, January 2015). Malaysia: WHO statistical profile. Retrieved August 02, 2015, from http://www.worldlifeexpectancy.com/malaysia-coronary-heart-disease

Wu, Y., Allaire, P., Tao, G., Wood, H., Olsen, D., & Tribble, C. (2003). An advanced physiological controller design for a left ventricular assist device to prevent left ventricular collapse. *Artificial organs, 27*(10), 926-930.

Wu, Y., Allaire, P. E., Tao, G., Adams, M., Liu, Y., Wood, H., & Olsen, D. B. (2004). A bridge from short‐term to long‐term left ventricular assist device-experimental verification of a physiological controller. *Artificial organs, 28*(10), 927-932.

Wu, Y., Allaire, P. E., Tao, G., & Olsen, D. (2007). Modeling, estimation, and control of human circulatory system with a left ventricular assist device. *Control Systems Technology, IEEE Transactions on, 15*(4), 754-767.

Yamane, T. (2002). The present and future state of nonpulsatile artificial heart technology. *Journal of Artificial Organs, 5*(3), 0149-0155.

Zhou, M.-D., Yang, C., Liu, Z., Cysyk, J. P., & Zheng, S.-Y. (2012). An implantable Fabry-Pérot pressure sensor fabricated on left ventricular assist device for heart failure. *Biomedical microdevices, 14*(1), 235-245.

Ziegler, J. G., & Nichols, N. B. (1942). Optimum settings for automatic controllers. *trans. ASME, 64*(11).

Zinober, A. S. (1990). *Deterministic Nonlinear Control of Uncertain Systems* (Vol. 40): IET.

LIST OF PUBLICATIONS

Lim, E., Salamonsen, R. F., Mansouri, M., Gaddum, N., Mason, D. G., Timms, D. L., . . . Lovell, N. H. (2015). Hemodynamic response to exercise and head-up tilt of patients implanted with a rotary blood pump: A computational modeling study. Artificial Organs, 39(2), E24-E35.

Mansouri, M., Salamonsen, R. F., Lim, E., Akmeliawati, R., & Lovell, N. H. (2015). Preload-based Starling-like control for rotary blood pumps: Numerical comparison with pulsatility control and constant speed operation. PLoS ONE, 10(14).

Mansouri, M., Salamonsen, R., Gregory, S. D., Lim, E., Ng, B. C., Akmeliawati, R., & Lovell, N. H. (2015). Physiological control of rotary blood pumps–speed of response and resistance to noisy feedback signals. Annals of biomedical engineering (submitted).

Mansouri, M., Salamonsen, R., Gregory, S. D., Stevens, M., Lim, E., & Akmeliawati, R. (2015). A preload-based Frank-Starling control of rotary blood pumps: An in-vitro validation. ASAIO Journal (submitted).

Ng, B. C., Lim, E., Salamonsen, R., Gregory, S. D., Stevens, M., Mansouri, M., . . . Wu, Y. (2015). Multiobjective neural predictive control for BiVAD. Artificial Organs(Submitted).